FEDERAL UNIVERSITY OF SANTA CATARINA
CHEMICAL ENGINEERING GRADUATE PROGRAM

Michele Cristina Formolo Garcia

Bacterial nanocellulose biocomposites and hydroxyapatite with cationic substitution by Mg^{2+}, Cu^{2+}, Zn^{2+} and Sr^{2+} for bone regeneration

FLORIANÓPOLIS
2022

Michele Cristina Formolo Garcia

Bacterial nanocellulose biocomposites and hydroxyapatite with cationic substitution by Mg^{2+}, Cu^{2+}, Zn^{2+} and Sr^{2+} for bone regeneration

Doctorate thesis for the degree of Doctor in Chemical Engineering presented to the Chemical Engineering Graduate Program at Federal University of Santa Catarina.

Advisor:
Prof. Dr. Luismar Marques Porto

Co-advisors:
Prof. Dr. Ana Paula Testa Pezzin
Dr. Karina Cesca

Florianópolis
2022

Ficha de identificação da obra elaborada pelo autor,
através do Programa de Geração Automática da Biblioteca Universitária da UFSC.

Garcia, Michele Cristina Formolo
Bacterial nanocellulose biocomposites and hydroxyapatite with cationic substitution by Mg2+, Cu2+, Zn2+ and Sr2+ for bone regeneration / Michele Cristina Formolo Garcia ; orientador, Luismar Marques Porto, coorientadora, Ana Paula Testa Pezzin, coorientadora, Karina Cesca, 2022.
136 p.

Tese (doutorado) - Universidade Federal de Santa Catarina, Centro Tecnológico, Programa de Pós-Graduação em Engenharia Química, Florianópolis, 2022.

Inclui referências.

1. Engenharia Química. 2. Bone tissue remodeling and regeneration. 3. Biocomposites. 4. Bacterial nanocellulose (BNC). 5. Hydroxyapatite (HAp). I. Porto, Luismar Marques. II. Pezzin, Ana Paula Testa. III. Cesca, Karina IV. Universidade Federal de Santa Catarina. Programa de Pós Graduação em Engenharia Química. V. Título.

Michele Cristina Formolo Garcia

BACTERIAL NANOCELLULOSE BIOCOMPOSITES AND HYDROXYAPATITE WITH CATIONIC SUBSTITUTION BY Mg^{2+}, Cu^{2+}, Zn^{2+} AND Sr^{2+} FOR BONE REGENERATION

This thesis was considered adequate for the Doctor in Chemical Engineering degree and was approved in its final form by the Graduate Program in Chemical Engineering at the Federal University of Santa Catarina.

Florianópolis, August 12th 2022.

Documento assinado digitalmente
Debora de Oliveira
Data: 22/10/2022 08:25:05-0300
CPF: ***.453.929-**
Verifique as assinaturas em https://v.ufsc.br

Prof. Débora de Oliveira, Dr.
Coordinator of the Graduate Program in Chemical Engineering

Examination Board:

Documento assinado digitalmente
Luismar Marques Porto
Data: 22/10/2022 08:15:03-0300
CPF: ***.494.909-**
Verifique as assinaturas em https://v.ufsc.br

Prof. Dr. Luismar Marques Porto
Advisor
Federal University of Santa Catarina

Prof. Dr. Ana Paula Testa Pezzin
Co-advisor
University of Joinville Region

Dr .Karina Cesca
Co-advisor
Federal University of Santa Catarina

Prof. Dr Hernane da Silva Barud
São Paulo State University – UNESP, Araraquara

Prof. Dr. Regina Vasconcellos Antônio
Federal University of Santa Catarina

Prof. Dr Agenor Furigo Jr.
Federal University of Santa Catarina

To my dear parentes, who supported me so much to get here.

To my husband, for the unconditional support, who gave me strength and who always believed in me.

To my beloved children, who were patient and understanding with my absences during this journey.

“A mind that opens up to a new idea will never return to its original size.”

Albert Einstein

“New paths, new friendships, new posture, new ideas, new actions, new connections, new opportunities. It is a cycle that must be repeated.”

João Kepler

Acknowledgements

A doctorate is a real journey!!! A journey of learning, growth, friendships, partnerships, and an emotional roller coaster!

But as with any journey, we receive contributions from many people!

So first, I thank God for the amazing people he put in my path!!

And so, I would like to register my special thanks to these wonderful people who were part of this journey!

I think I can start by thanking my advisor Luismar Marques Porto! Professor, you did more than open the doors of a University, your laboratory or guide me on this doctorate journey, you taught me much more than content, and it was 2 subjects!! You taught me to see beyond what is written and opened my mind to go beyond!!

So, I have already taken the opportunity to register here my eternal gratitude to my two scientific mothers and advisors of all my academic journey, Ana Paula Testa Pezzin (here, co-advisor) and Andréa Lima dos Santos Schneider. I would also like to be able to consider him like this, a scientific father. Can I? Because I can say, without a doubt, that I am who I am today, thanks the wonderful examples I received from you!

And in this way, I also thank my co-advisor, Karina Cesca, who helped and guided me; there were many nights and weekends of article corrections and analysis in the laboratory! Thank you very much, Karina!!!

It is also important to note my gratitude to the two institutions that opened the doors for me to develop the entire experimental part of this thesis: Universidade Federal de Santa Catarina and Universidade da Região de Joinville.

To the ICs and Master's students who helped me so much in the laboratory: Elouise Galke, who took on the challenge back at the beginning of the project, and Sandro R. K. Junior, for helping with the analyses. Michele Roberta Fischer was the first student to trust me as a TCC advisor and was my travel partner at the beginning of this journey. To Eduarda Neves Zeni, lab partner, we laughed a lot, and we also cried a lot, many times later, paraphrasing Renato Russo.

But I record here my special thanks to my 2 CIs, which I have as scientific daughters, and without whom this work would not have been possible Bruna Segat and Victória Fonseca Silveira.

To my TCC students: Joana Camila Lopes, Giovanna Cristina Dorabiatto, Karina Siewert, Adriana Mielke, Stefani Regina Zibetti Teixeira, Gabriel Wolff Sfreddo, and more recently Geasi Lucas Martins and Letícia Lotério de Lima for their trust and patience, when I often delivered the corrections of theirs works in the last minutes of the second time because I was also involved in this journey that I now present.

And not to forget anyone, thank you to all the IC and Master's students who went through the Polymeric Materials research group and somehow contributed to this work!!

Priscila F. Franczak, my mentor in the statistical analyses. And the entire DNPrime team for their trust in me, their friendship and their understanding of my absences in the last moments of the document delivery.

To my great friend Maikon Kelbert, brother of the journey, who helped and supported me so much!!

To my parents, who always supported me even when they suffered from my absences! To my brother Douglas Affonso Formolo and my sister-in-law Natalia Paludo Formolo who welcomed me with open arms in their home every time I needed to stay in Florianópolis during the class period. But, a special thanks to my brother Douglas who supported me and gave me strength and was present even from a distance! I am immensely grateful to you, my brother, by blood, soul and journey!

And to the professors Dr. Hernane da Silva Barud, Dr. Regina Antônio Vasconcelos and Dr. Agenor Furigo for accepting the invitation to evaluate this work.

ABSTRACT

The use of biocomposites for guided bone regeneration (GBR) has attracted great interest due to the possibilities of synergistic properties. Bacterial nanocellulose (BNC) is a promising biopolymer due to its high crystallinity, water holding capacity, three-dimensional interconnected porous nanostructure and biocompatibility. While hydroxyapatite (HAp) is the main constituent of the inorganic components of bone tissue, it has excellent biocompatibility, bioactivity and osteoconductivity. Furthermore, incorporating elements such as Mg^{2+} or Sr^{2+} in trace elements can play an essential role in bone growth and repair. This work aimed to study the effect of cationic replacement in BNC biocomposites with HAp and Mg^{2+}, Cu^{2+}, Sr^{2+} and Zn^{2+} apatites for application in guided bone regeneration. For this purpose, BNC membranes were produced using the bacterium *Komagataeibacter hansenii*. After purification, they were functionalized by immersion cycles with hydroxyapatite (BNC/HAp) and copper hybrids (BNC/CuHAp), magnesium (BNC/MgHAp), zinc (BNC/ZnHAp) and strontium (BNC/SrHAp) and bioactivated in simulated body fluid (SFB). The samples obtained were freeze-dried and characterized by Fourier transform infrared spectroscopy with attenuated total reflectance (FTIR/ATR), thermogravimetric analysis (TGA), scanning electron microscopy with energy dispersive spectroscopy (SEM/EDS), X-ray diffraction (XRD) and Raman. The degree of swelling, porosity, antimicrobial properties, cytotoxicity, adhesion and proliferation of osteoblasts and *in vitro* enzymatic degradation assay were determined. The first results for the BNC/MgHAp and BNC/CuHAp biocomposites showed that the formulations maintained good porosity. The FTIR spectra showed the characteristic bands of BNC and bands related to the HPO_4^{2-} group. The TGA analysis showed about 50 to 72% by mass of the mineral phase, demonstrating the formation of biocomposites for all formulations tested. As for the SEM analysis, it was found that the deposition of inorganic material on the nanofibrils of the BNC and the EDS indicated the presence of metallic ions in the composites. The incorporation with Cu^{2+} provided antimicrobial properties to the biocomposite but exerted cytotoxic activity. On the other hand, the biomaterials incorporated with Mg^{2+} did not show antimicrobial activity and did not exert cytotoxicity. New formulations were tested, and a study incorporating Zn^{2+} and Sr^{2+} was also proposed. As for the properties, the new biocomposites presented structural characteristics similar to the previous ones. XRD and Raman analyses showed subtle variations, probably due to the low concentration. The cytotoxicity result showed the best compositions of BNC/MgHAp, BNC/ZnHAp and BNC/SrHAp, and from this point on, the assays with Cu^{2+} were not continued. The cell adhesion assay showed that osteoblast growth was significantly higher at all times analyzed for the biocomposites concerning the BNC/HAp control. Furthermore, the enzymatic biodegradation assay, in vitro, showed that the cellulases could act at pH 8.5 selected in this work as an indicator of the bone regeneration process, demonstrating a potential field of study for the production of these fully bioabsorbable biocomposites.

Keywords: Bone regeneration. Bacterial Nanocellulose. Hydroxyapatite. Biocomposites. Cellulases

RESUMO

O uso de biocompóstitos para regeneração óssea guiada (GBR) tem despertado grande interesse pelas possibilidades de sinergia de propriedades. A nanocelulose bacteriana (BNC) é um biopolímero promissor por sua alta cristalinidade, capacidade de retenção de água, nanoestrutura porosa interconectada tridimensional e biocompatibilidade. Enquanto, a hidroxiapatita (HAp) é o principal constituinte dos componentes inorgânicos do tecido ósseo, possui excelente biocompatibilidade, bioatividade e osteocondutividade. Além disso, a incorporação de alguns elementos como Mg^{2+} ou Sr^{2+} na forma de oligoelementos pode desempenhar um importante papel no crescimento e reparo ósseo. O objetivo deste trabalho foi estudar o efeito da substituição catiônica em biocompósitos de BNC com HAp e apatitas de Mg^{2+}, Cu^{2+}, Sr^{2+} e Zn^{2+}, para aplicação em regeneração óssea guiada. Para tanto, foram produzidas membranas de BNC utilizando a bactéria *Komagataeibacter hansenii*, estas após a purificação foram funcionalizadas por ciclos de imersão com hidroxiapatita (BNC/HAp) e híbridos de cobre (BNC/CuHAp), magnésio (BNC/MgHAp), zinco (BNC/ZnHAp) e estrôncio (BNC/SrHAp) e biotativadas em fluido corporal simulado (SFB). As amostras obtidas foram liofilizadas e caracterizadas por espectroscopia no infravermelho por transformada de Fourier com refletância total atenuada (FTIR/ATR), análise termogravimétrica (TGA), microscopia eletrônica de varredura com espectroscopia por energia dispersiva (SEM/EDS), difração de raios X (DRX) e Raman. Foram determinados o grau de intumescimento, porosidade, propriedades antimicrobianas, citotoxicidade adesão e proliferação de osteoblastos e ensaio de degradação enzimática *in vitro*. Os primeiros resultados para os biocompósitos BNC/MgHAp e BNC/CuHAp demonstraram que as formulações mantiveram boa porosidade. Os espectros de FTIR apresentaram as bandas características da BNC e bandas relacionadas ao grupamento HPO_4^{2-} , a análise de TGA demonstrou a presença de cerca de 50 a 72% em massa da fase mineral, demonstrando a formação dos biocompósitos para todas as formulações testadas. Quanto às análises de MEV, constatou-se a deposição de material inorgânico sobre as nanofibrilas da BNC, o EDS apontou a presença dos íons metálicos nos compósitos. A incorporação com Cu^{2+} proporcionou propriedades antimicrobianas aos biocompósito, mas exerceu atividade citotóxica, por outro lado, os biomateriais incorporados com Mg não apresentaram atividade antimicrobiana, mas também não exerceram citotoxicidade. Novas formulações foram testadas e um estudo com incorporação de Zn^{2+} e Sr^{2+} também foi proposto. Quanto às propriedades, os biocompósitos novos apresentaram características estruturais semelhantes aos anteriores. As análises de DRX e Raman apresentaram variações muito sutis, provavelmente, devido à baixa concentração utilizada. O resultado de citotoxicidade apontou como melhores as composições BNC/MgHAp, BNC/ZnHAp e BNC/SrHAp. O ensaio de adesão celular demonstrou que o crescimento dos osteoblastos foi siginificativamente maior em todos os tempos analisados para os biocompósitos em relação ao controle BNC/HAp. E, o ensaio de biodegradação enzimática, in vitro, demonstrou que as celulases foram capazes de atuar em pH 8,5 selecionado neste trabalho como indicador do processo de regeneração óssea, mostrando um potencial campo de estudo para a produção destes biocompósitos inteiramente bioabsorvíveis.

Palavras-chave: Regeneração óssea. Nanocelulose bacteriana. Hidroxiapatita. Biocompósitos. Celulases.

GRAPHICAL ABSTRACT

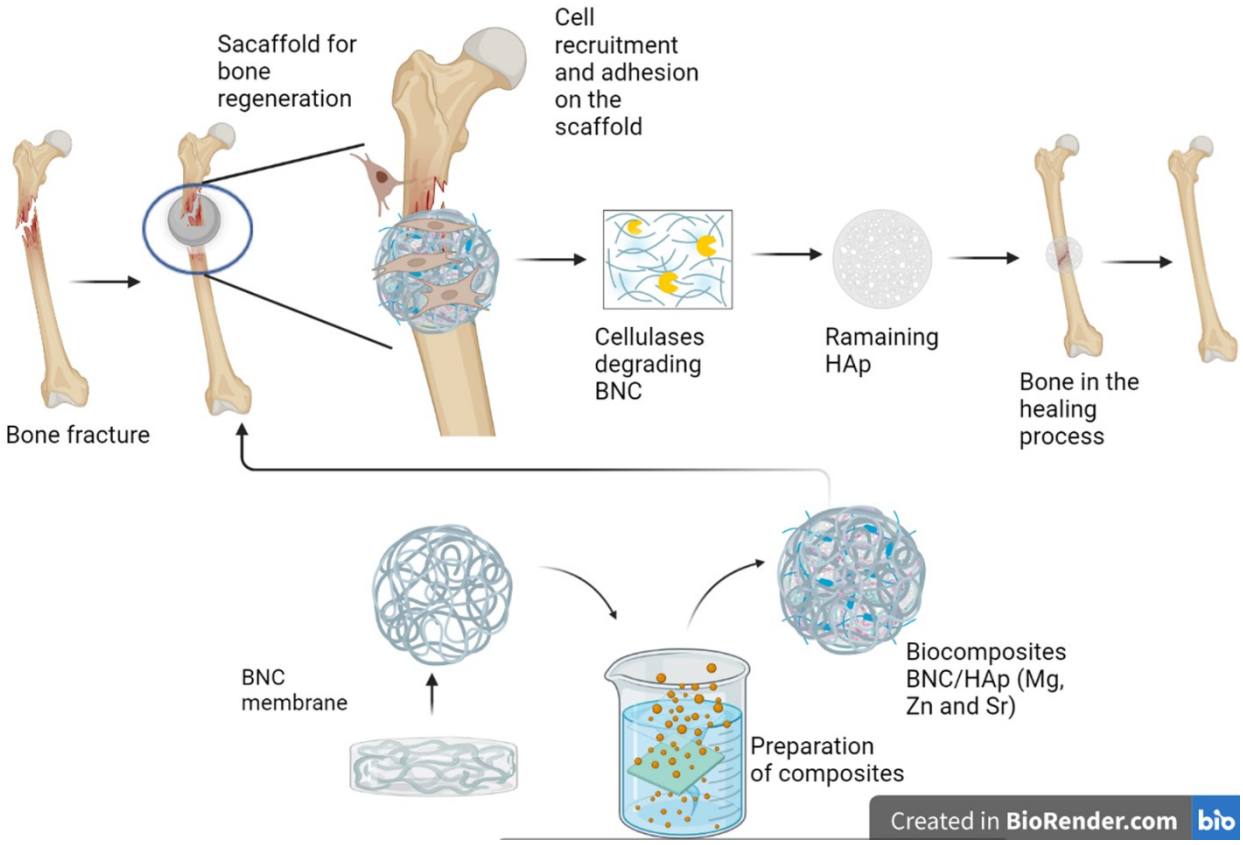

RESUMO ESTENDIDO

BIOCOMPÓSITOS DE NANOCELULOSE BACTERIANA E HIDROXIAPATITA COM SUBSTITUIÇÃO CATIÔNICA POR Mg^{2+}, Cu^{2+}, Zn^{2+} E Sr^{2+} PARA REGENERAÇÃO ÓSSEA

Introdução

Os tratamentos relacionados à lesão e degeneração óssea ainda representam desafio crítico tanto na medicina quanto na odontologia. Este desafio vem estimulando pesquisas crescentes na engenharia de tecidos e medicina regenerativa que buscam constantemente por novas soluções. O conhecimento da composição natural do tecido ósseo como um compósito de hidroxiapatita (HAp) com a matriz orgânica de colágeno tipo I tem direcionado as pesquisas na busca de biocompósitos biomiméticos ideais que induzam ativamente a regeneração óssea nas formas desejadas, além de desempenhar um papel importante como ponto de união em fraturas e outros defeitos ósseos (CAKMAK et al., 2020).

Neste contexto surge a nanocelulose bacteriana (BNC) que apresenta uma morfologia de rede nanofibrilar única, semelhante às fibras colágenas, que mimetizam as propriedades da matriz extracelular e exibem integração tecidual (PIGOSSI et al., 2015). E a HAp, que possui uma estrutura química e cristalina semelhante à apatita óssea natural além de grande biocompatibilidade, alta plasticidade e propriedades mecânicas notáveis, estrutura ultrafina e uma grande área de superfície que é vantajosa para interações célula-biomateriais (NICOARA et al., 2020).

Combinada com técnicas apropriadas e tecnologias inovadoras, a engenharia de tecidos utiliza uma variedade de biomateriais para imitar a estrutura óssea nativa (CAKMAK et al., 2020). E, neste sentido, a união de diferentes biomateriais numa composição híbrida, como os biocompósitos, tem sido explorada, buscando a complementação das propriedades distintas de cada material, originando um biomaterial diferenciado, com melhores propriedades (SHI et al., 2019). Além disso, com o intuito de potencializar os benefícios desta interação, estudos vêm apontando que a incorporação de elementos traço existentes nos ossos, como Na^{+}, Sr^{2+} e Mg^{2+} podem aumentar a osteogênese e a neovascularização (EHRET et al., 2017).

No entanto, a falta de processos bioquímicos que promovam biodegradabilidade da BNC no organismo humano, a torna um biomaterial de

absorção difícil, representando um obstáculo a ser superado para a sua aplicação na engenharia de tecicidos (WANG et al., 2016).

Buscando soluções, algumas pesquisas têm sido desenvolvidas como o uso de pré-oxidação mediada pelo radical 2,2,6,6-tetrametil-1-piperidinoxilo (TEMPO) (NASCIMENTO, 2018 e CHITBANYONG; PISUTPICHED; KHANTAYANUWONG, 2020), ou ainda o estudo de degradação enzimática de celulose regenerada (RCS) com celulases e lisozima (ARAÚJO et al., 2016).

De acordo com Wang et al. (2016), o uso de celulases pode ser uma maneira eficaz de alcançar a degradação corporal completa da celulose e a velocidade de degradação pode ser ajustada sob o progresso controlável da preparação. No entanto, é importante destacar que a celulase é uma enzima produzida, principalmente, a partir de fungos como *Trichoderma sp*, *Aspergillus sp* e *Penicillium sp* e, portanto, sua atividade ótima normalmente encontra-se próxima ao pH 5 (MIAO et al., 2016).

Desta forma, considerando os processos metabólicos de regeneração óssea e, tendo a fosfatase alcalina como principal indicador deste processo, com pH ótimo entre 8,5 e 9,5 (BARBIERI, 2006; MAZORRA; RUBIO; BLASCO, 2002), e, buscando a produção de um biocompósito totalmente bioabsorvível, torna-se necessário estudar a atividade da celulase nestes valores de pH.

Objetivos

O principal objetivo do trabalho consistiu em produzir um biocompósito de nanocelulose bacteriana com apatitas de Mg^{2+}, Cu^{2+}, Sr^{2+} e Zn^{2+} para aplicação como *scaffold* em regeneração óssea guiada (ROG) e, avaliar o efeito desta substituição catiônica sobre as propriedades antimicrobianas, citotoxicidade e adesão celular e a adição de celulases como agente modulador da degradação de BNC.

Metodologia

A primeira etapa do trabalho consistiu na produção e purificação das membranas de BNC pela bactéria *Komagataeibacter hansenii* e posterior funcionalização das mesmas pelo método de ciclos de imersão em soluções de $MgCl_2$ e $CaCl_2$ ou $CuCl_2$ e $CaCl_2$, produzindo apatitas com concentrações de 10%, 30% e 50% de Mg e Cu. Os biocompósitos foram caracterizados para avaliar suas propriedades como porosidade, os principais grupos funcionais foram observados por FTIR, o comportamento térmico característico e teor de resíduos foi mensurado por

TGA, a morfologia da estrutura da BNC e dos cristais foi analisada por MEV, o acessório de EDS foi utilizado para comprovar a presença dos elementos metálicos presentes no biocompósito, o ensaio de propriedades antimicrobianas foi realizado contra as bactérias *Staphylococcus aureus* e *Escherichia coli* pelo método de difusão em disco e o ensaio de citotoxicidade foi conduzido com células de fibroblastos de rato da linhagem L-929, buscando avaliar a influência desta substituição catiônica sobre a viabilidade celular. Todos os ensaios foram comparados com a BNC que neste estudo foi utilizada como controle.

Na segunda parte do trabalho foram produzidos biocompósitos de BNC com apatitas de Mg^{2+}, Cu^{2+}, Sr^{2+} e Zn^{2+} em menores concentrações de 1%, 3% e 5%, que foram novamente caracterizados por MEV/EDS, FTIR, XRD, TGA e ensaio de citotoxicidade com células de fibroblastos de rato da linhagem L-929, buscando selecionar as melhores composições para a aplicação almejada.

Por fim, na terceira parte do trabalho os biocompósitos BNC/HAp, BNC/MgHAp, BNC/CuHAp, BNC/ZnHAp e BNC/SrHAp foram caracterizados por Raman, e então submetidos ao ensaio de adesão celular, no qual a atividade metabólica de osteoblastos da linhagem MC3T3 foi avaliada por 21 dias pelo ensaio MTS, para este ensaio foram selecionados apenas as amostras concentração de 1%, que foram os melhores resultados obtidos no ensaio anterior de citotoxicidade. Paralelamente, um estudo de biodegradação *in vitro*, destes materiais foi conduzido em tampão fosfato pH 7,5 e 8,5 a 37 °C na presença de celulases.

Resultados e Discussão

Os biocompósitos obtidos na primeira etapa já apresentaram uma mudança macroscópica, com variação na coloração relacionada a concentração de Cu^{2+} nas amostras. Também foi observada uma redução no percentual médio de porosidade dos biocompósitos em relação à BNC de cerca de 17%.

A análise de FTIR demonstrou todas as bandas características da BNC e em relação aos biocompósitos, observou-se uma redução da banda entre 3500 e 3200 cm^{-1} referente ao grupo OH. Esta diminuição sugere que as fontes de fosfato de cálcio estão se ligando às hidroxilas da BNC. As bandas em torno de 1030 e 960 cm^{-1}, relacionadas ao HPO_4^{2-} também foram observadas em todos os biocompósitos, confirmando a deposição dos materiais a base de fosfato de cálcio na membrana de

BNC. Outra banda importante observada nos biocompósitos foi em 873 cm^{-1}, relacionada ao íon CO_3^{2-} indicando que parte dos grupos fosfato foram substituídos pelo carbonato. Wan et al., (2011) ressaltaram que a incorporação de CO_3^{2-} gera uma apatita similar àquela situada no osso natural.

Em relação à análise termogravimétrica, a BNC apresentou um comportamento típico, com 3 estágios de perda de massa, sendo os estágios em $T_{máx3}$ de 316 °C o mais proeminente referente a degradação da celulose e em $T_{máx4}$ de 493 °C relacionado aos resíduos carbonáceos, restando apenas um pequeno teor de resíduo de 6,88% após 600 °C. Já os biocompósitos apresentaram 4 estágios de degradação, sendo o 2° estágio, com $T_{máx2}$ em torno de 180 °C, observado apenas nos biocompósitos e que de acordo com Araújo et al. (2016) pode ser atribuído à vaporização da água de cristalização da HAp. Outra informação importante é o teor de resíduos que foi superior a 60% em todos os biocompósitos. Considerando que a análise foi conduzida em atmosfera oxidante, a massa residual pode indicar a presença de material inorgânico o que, de acordo com Saska et al. (2011) confirma a deposição de fosfato na membrana de BNC.

As micrografias obtidas MEV demonstraram as nanofibrilas organizadas randomicamente da BNC. Nos biocompósitos, foi possível observar a deposição dos cristais com formas diferenciadas em função da composição das apatitas sobre as nanofibrilas da BNC. Nos biocompósitos de BNC/MgHAp os cristais apresentaram-se sob a forma de placas irregulares, enquanto nas amostras de BNC/CuHAp os cristais organizaram-se em diversos círculos concêntricos constituindo pequenas e numerosas “rosetas” ao longo das nanofibrilas. A análise de EDS confirmou a presença dos elementos Ca, P, Mg e Cu nas respectivas composições.

No ensaio de propriedades antimicrobianas, não foi observada atividade contra as bactérias testadas em nenhuma das composições de BNC/MgHAp. No entanto, todas as composições de BNC/CuHAp apresentaram uma atividade antimicrobiana similar com halos de inibição de cerca de 12 mm.

O ensaio de viabilidade celular com os fibroblastos L-929 foi avaliado, após o 1º dia de contato, e também foi observado após 3 e 7 dias. Neste caso o resultado foi positivo para as amostras BNC/MgHAp, pois nenhuma das composições afetou a viabilidade das células testadas após o primeiro dia de contato e mesmo após 3 dias o resultado se manteve. No entanto, após 7 dias de contato, as amostras BNC/MgHAp 10% e BNC/MgHAp 50% passaram a afetar a viabilidade das células em cerca de

50%. Apenas a amostra de BNC/MgHAp 30% manteve o mesmo resultado mesmo após 7 dias.

Já as amostras BNC/CuHAp no 1º dia de contato afetaram a viabilidade das células apenas em 10%, o que de acordo com a ISO 10993-5:2009 não seria considerado como comportamento citotóxico. No entanto, após 3 dias, apenas a amostra BNC/CuHAp 30% manteve uma viabilidade celular pouco superior a 70% e após 7 dias, todas as amostras reduziram a viabilidade celular a cerca de 35%.

A partir destes resultados os ensaios foram reestruturados e a composição de todos os biocompósitos foi reduzida para 1%, 3% e 5%. Devido às novas composições, todas as amostras necessitaram ser novamente caracterizadas. Além disso, nesta segunda etapa, foram produzidos biocompósitos de BNC/MgHAp, BNC/CuHAp, BNC/ZnHAp e BNC/SrHAp que foram, a partir deste momento comparados com uma amostra de BNC/HAp que foi considerada como controle.

Os novos biocompósitos apresentaram características estruturais semelhantes aos anteriores, com uma densa camada de cristais que se apresentaram novamente como agregados concêntricos lembrando rosetas que se formaram sobre as nanofibrilas da BNC, o que pode ser observado ao MEV. Porém, as amostras BCN/MgAp 5% e BCN/SrAp 1% apresentaram cristais de forma lamelar. Já as amostras BCN/MgAp 1% e BCN/ZnAp 3% apresentaram algumas deposições de cristais na forma de placas entre os arranjos do tipo roseta. No entanto, as amostras BNC/CuHAp passaram a apresentar um comportamento distinto em relação ao anterior com concentrações mais elevadas. A análise de EDS também foi novamente realizada, mas apenas o Ca e P foram detectados, provavelmente em função da baixa concentração dos cátions na nova formulação.

Como esperado, a análise de FTIR também apresentou espectros semelhantes com redução na intensidade da banda entre 3500 e 3200 cm^{-1} relativa a interação da BNC com os grupamentos fosfato das apatitas, porém, esta alteração foi mais sutil do que nas amostras anteriores com percentuais mais elevados. As bandas entre 1020 e 960 cm^{-1} relativas aos grupos PO_4^{-1} e em 870 cm^{-1} relativas ao grupo CO_3^{-2}, também foram novamente observadas.

Nesta etapa, uma análise de DRX foi realizada buscando observar variações na cristalografia dos biocompósitos que indicasse a presença dos cátions adicionados às apatitas, nas novas formulações. Os difratogramas de DRX apresentaram os 2 picos de difração característicos da BNC em 2 θ ≈ 14,5 ° e 22,6 ° (CASABURI et al.,

2018; SASKA et al., 2011), bem como 2 picos característicos de HAp demonstrados em 2 θ ≈ 26° e 32°, além de outros picos com menor intensidade igualmente característicos de HAp (GRANDE et al., 2009; NAM et al., 2018; WANG et al., 2018) em todas as amostras, destacando-se a incorporação da HAp já observada na análise de FTIR.

Nos biocompósitos de BNC/MgAp, foram observados picos em torno de 2 θ ≈ 27,74° e 34,12° de forma muito sutil, provavelmente devido à baixa concentração utilizada. Giannoulatou et al. (2018) produziram um vidro bioativo de silicato de cálcio e magnésio dopado com íons cobre e atribuíram esses picos à fase cristalina da whitlockita ($Ca_{18}Mg_2H_2(PO_4)_{14}$), que resulta de um processo em que o fosfato de cálcio é substituído por pequenas quantidades de Mg em vez de Ca. Nas amostras NBC/CuAp 1 e 3%, também foram observados, de forma sutil, outros picos em 2θ de 35,57° e 38,67°. Putrakumar et al. (2020), atribuíram esses picos ao aparecimento de uma fase de óxido de cobre. Nas amostras BNC/ZnAp 1 e 3% e BNC/SrAp, a única variação observada foi em relação ao pico em 2 θ ≈ 31,8°. Observou-se também que, em amostras contendo Sr, este pico tornou-se mais nítido e intenso proporcionalmente ao percentual de Sr nas amostras. Wang et al. (2018) produziram *scaffolds* de HAp dopados com Sr e Zn e descobriram que nenhuma nova fase apareceu nos materiais com Sr, mas para os materiais dopados com Zn, foi encontrada a presença de dois novos picos em 31,7° e 34,7°.

Nesta etapa, a análise termogravimétrica foi conduzida até 1000 °C, sendo possível observar a ocorrência de 6 estágios de perda de massa para a BNC/HAp e demais biocompósitos. Os primeiros estágios de degradação térmica foram semelhantes ao observado no estudo anterior, no entanto, um novo estágio muito suave apareceu em torno de 220 °C em quase todas as amostras, atribuído à perda gradual de água posterior (COX et al., 2014). A degradação térmica da BNC manteve-se em $T_{máx}$ em torno de 320 a 330 °C com um quinto estágio, em torno do T_{max5} 412 °C a 452 °C, referente à degradação dos resíduos carbonáceos da BNC (NAINGGOLAN et al., 2013). A sexta etapa ocorreu no $T_{máx6}$ (702 a 856 °C), que, segundo Zhang et al. (2009), está relacionada à perda de massa da apatita carbonatada. Esse resultado também está de acordo com os dados observados por FTIR, que mostrou a decomposição de apatitas não estequiométricas em whitlockita; este evento ocorre acima de 600 °C (COX et al., 2014).

Quanto ao ensaio de citotoxicidade, observou-se que as amostras BNC/MgAp assim como BNC/HAp apresentaram um comportamento semelhante (viabilidade celular ± 75%) independente da concentração, este é um bom resultado para a aplicação desejada. Para as amostras BNC/CuAp, em todas as composições, novamente apresentaram efeito citotóxico, reduzindo a atividade metabólica celular para cerca de 20%. A amostra BNC/ZnAp 1% apresentou o melhor resultado mantendo a atividade metabólica das células em 90%. No entanto, concentrações mais elevadas causaram uma redução intensa da mesma, levando a crer que o efeito citotóxico é dependente da concentração. O biocompósito BNC/SrAp 1% apresentou uma atividade metabólica muito próxima a 90%, e mesmo em concentrações mais elevadas 3 e 5%, os resultados ainda foram superiores a 70%, tornando este biocompósito o melhor resultado para aplicação como material implantável. Segundo (ISO, 2009), se a viabilidade celular for maior que 70% do grupo controle, o material é considerado não citotóxico.

E, finalmente, na terceira etapa do trabalho o ensaio de caracterização por Raman, corroborou os resultados anteriormente apresentados por FTIR com bandas referentes à grupos PO_4 e CO_3^{2-} apresentando-se de forma mais intensa. Não foram observadas novas bandas, mas o deslocamento da banda 960 cm^{-1}, pode estar relacionado à substituição pelos cátions bivalentes.

O ensaio de adesão celular, apresentou um crescimento celular confluente, durante todo o período de análise para todas as amostras, mas é importante destacar que sobre os biocompósitos ocorreram crescimentos significativamente maiores em relação ao padrão BNC/HAp.

O ensaio de biodegradação em presença de celulases mostrou-se promissor. Os resultados de biodegradação avaliados em função de concentração de glicose liberada, apontam que o processo ocorreu de forma mais intensa apenas durante as primeiras 10 h de ensaio. Porém, as imagens obtidas pela análise visual, mostraram que um intenso processo de fragmentação da amostra inicia-se logo após esse período transformando toda a amostra em um pó precipitado. O que foi corroborado pela análise de DRX que apontou que este precipitado apresenta como material dominante a composição de HAp.

Conclusões

Os biocompósitos propostos neste trabalho, mantiveram as características típicas da BNC que a tornam semelhante à matriz extracelular. Além disso a incorporação da HAp com substituição catiônica, foi capaz de estimular o crescimento dos osteoblastos testados de forma mais intensa em relação ao BNC/HAp, comprovando sua característica como oligoelementos importantes ao crescimento celular e caracterizando uma propriedade oestogênica otimizada do material.

E por fim, a adição de celulases, com o objetivo de tornar o biocompósito bioabsorvível, se mostrou bastante promissora. Ainda são necessários estudos mais aprofundados neste sentido, mas os resultados obtidos até aqui apresentam uma importante perspectiva para futuros estudos que vizam a produção de biomateriais com características 4D.

Palavras-chave: Nanocelulose bacteriana, hidroxiapatita, biocompósitos, regeneração óssea.

Referências

ARAÚJO, A. M. DE et al. Regenerated cellulose scaffolds : Preparation , characterization and toxicological evaluation. **Carbohydrate Polymers**, v. 136, p. 892–898, 2016.

BARBIERI, C. M. D. O. **Efeito do fator de crescimento derivado de plaquetas humanas (PDGF) sobre o processo de regeneração óssea em tíbias de ratos**. UNESP - Araraquara, 2006.

CASABURI, A. et al. Carboxymethyl cellulose with tailored degree of substitution obtained from bacterial cellulose. **Food Hydrocolloids**, v. 75, p. 147–156, 2018.

CAKMAK, A. M. et al. 3D Printed Polycaprolactone / Gelatin / Bacterial Cellulose / Hydroxyapatite Composite Scaffold for Bone Tissue Engineering. **Polymers**, v. 12, n. 1962, p. 1–14, 2020.

CHITBANYONG, K.; PISUTPICHED, S.; KHANTAYANUWONG, S. International Journal of Biological Macromolecules TEMPO-oxidized cellulose nano fi bril fi lm from

nano-structured bacterial cellulose derived from the recently developed thermotolerant *Komagataeibacter xylinus* C30 and *Komagataeibacter oboediens*. **International Journal of Biological Macromolecules**, v. 163, p. 1908–1914, 2020.

COX, S. C. et al. Preparation and characterisation of nanophase Sr, Mg, and Zn substituted hydroxyapatite by aqueous precipitation. **Materials Science and Engineering C**, v. 35, n. 1, p. 106–114, 2014.

EHRET, C. et al. Strontium-doped hydroxyapatite polysaccharide materials effect on ectopic bone formation. **PLOS ONE**, v. 12, n. 9, p. e0184663, 14 set. 2017.

GIANNOULATOU, V. et al. Magnesium calcium silicate bioactive glass doped with copper ions; synthesis and in-vitro bioactivity characterization. **Journal of Non-Crystalline Solids**, v. 500, n. January, p. 98–109, 2018.

GRANDE, C. J. et al. Nanocomposites of bacterial cellulose/hydroxyapatite for biomedical applications. **Acta Biomaterialia**, v. 5, n. 5, p. 1605–1615, 2009.

ISO. Biological evaluation of medical devices — Part 5: Tests for in vitro cytotoxicity. **International Journal of Biological Macromolecules**, v. Third edit, p. 1–34, nov. 2009.

MAZORRA, M. T.; RUBIO, J. A.; BLASCO, J. Acid and alkaline phosphatase activities in the clam Scrobicularia plana : kinetic characteristics and effects of heavy metals. **Comparative Biochemistry and Physiology Part B: Biochemistry and Molecular Biology**, v. 131, p. 241–249, 2002.

MIAO, X. et al. Application and characterization of magnetic chitosan microspheres for enhanced immobilization of cellulase. **Biocatalysis and Biotransformation**, v. 34, n. 6, p. 272–282, 2016.

NAINGGOLAN, H. et al. Mechanical and thermal properties of bacterial-cellulose-fibre-reinforced Mater-Bi® bionanocomposite. **Beilstein Journal of Nanotechnology**, v. 4, n. 1, p. 325–329, 2013.

NAM, P. T. et al. Synthesis, characterization and antimicrobial activity of copper doped hydroxyapatite. **Vietnam Journal of Chemistry**, v. 56, n. 6, p. 672–678, 2018.

NASCIMENTO, E. S. D. **Filmes nanocompósitos à base de celulose bacteriana e nanocristais de celulose**. [Tese] Fortaleza, Universidade Federal do Ceará, 2018.

NICOARA, A. I. et al. *In situ* and *ex situ* designed hydroxyapatite : bacterial cellulose materials with biomedical applications. **Materials**, v. 13, n. 4793, p. 1–17, 2020.

PIGOSSI, S. C. et al. Bacterial cellulose-hydroxyapatite composites with osteogenic growth peptide (OGP) or pentapeptide OGP on bone regeneration in critical-size calvarial defect model. **Society For Biomaterials**, p. 3397–3406, 2015.

PUTRAKUMAR, B. et al. High performance and sustainable copper-modified hydroxyapatite catalysts for catalytic transfer hydrogenation of furfural. **Catalysts**, v. 10, n. 9, p. 1–17, 2020.

SASKA, S. et al. Bacterial cellulose-hydroxyapatite nanocomposites for bone regeneration. **International Journal of Biomaterials**, v. 2011, p. 1–8, 2011.

SHI, R. et al. Current advances for bone regeneration based on tissue engineering strategies. **Front. Med.**, v. 13, n. 2, p. 160–188, 2019.

WAN, Y. et al. Preparation and mineralization of three-dimensional carbon nano fi bers from bacterial cellulose as potential scaffolds for bone tissue engineering. **Surface & Coatings Technology**, v. 205, n. 8–9, p. 2938–2946, 2011.

WANG, B. et al. *In vitro* biodegradability of bacterial cellulose by cellulase in simulated body fluid and compatibility in vivo. **Cellulose**, v. 23, n. 5, p. 3187–3198, 2016.

WANG, Q. et al. Experimental and simulation studies of strontium/zinc-codoped hydroxyapatite porous scaffolds with excellent osteoinductivity and antibacterial activity. **Applied Surface Science**, v. 462, n. August, p. 118–126, 2018.

ZHANG, S. et al. Characterisation of hydroxyapatite / bacterial cellulose. **Polymers & Polymer Composites**, v. 17, n. 6, p. 353–358, 2009.

LIST OF FIGURES

LIST OF TABLES

List of acronyms, symbols and abbreviations

3D	Three-dimensional
ALP	Alkaline phosphatase
Ang1	Angiopoietin-1
Ang2	Angiopoietin-2
RA	Relative enzyme activity
ATCC	American culture collection
ATR	Azul de tripan
BG	β-glucosidase
BNC	Bacterial Nanocellulose
BMP	Bone morphogenetic proteins
CaP	Calcium phosphate
CBH	Cellobiohydrolases
CMC	Carboxymethylcellulose
DMEM	Dulbecco's modified Eagle's medium
DNS	3,5-dinitrosalicylic acid
ECM	Extracellular Matrix
EG	Endoglucanase
ERK	Extracellularly regulated kinases
FGF	Fibroblast growth factor
FTIR / ATR	Fourier transform infrared spectroscopy with attenuated total reflectance
GBR	Guided Bone Regeneration
GF	Growth factor
GTR	Guided Tissue Regeneration
HAp	Hydroxyapatite
hBMSC	Stromal cells derived from human bone marrow
SP (%)	Swelling percentage
IGF	Insulin-like growth factor
IL1	interleukin-1
LCME	Central Laboratory of Electronic Microscopy at UFSC
LRS	Lotus root starch

MH	Mueller Hinton Cultivation Medium
MTS	3-(4,5-dimethylthiazol-2-yl)-5-(3-carboxymethoxyphenyl)-2-(4-sulfophenyl)-2H-tetrazolium
m_1	swollen mass of BNC
m_2	dry mass of BNC after lyophilization
MO	Optical microscopy
PBS	Saline Phosphate Buffer
PDGF	Platelet-derived growth factor
RCS	Regenerated cellulose
SEM-EDS	Scanning electron microscopy with energy dispersive spectroscopy
SBF	Simulated body fluid
TCP	Tricalcium phosphate
TEMPO	2,2,6,6-tetrametil-1-piperidinoxilo
TNFα	Fator de necrose tumoral α
TGA	Thermogravimetric Analysis
Tie2	Tyrosine kinase
U	Enzyme activity unit
VEGF	Vascular endothelial growth factor
XRD	X-ray diffraction
ε (%)	Porosity
λ	Wave-length

CONTENTS

1 INTRODUCTION AND MOTIVATION

Bone defects can be caused by disabling degenerative diseases such as osteoporosis, osteomyelitis and osteogenesis imperfecta or even caused by trauma such as traffic accidents or even surgical resection and can generate severe complications in the neuromuscular system affecting the quality of life of millions of people worldwide (PINA et al., 2017).

Clinical therapies for bone regeneration involve autologous bone, allograft, heterologous demineralized bone, or bone substitutes. Although autografts represent an excellent option, thanks to their osteoconductivity, osteoinductivity and non-immunogenicity, their use is limited by the scarcity of donors and the morbidity of the donor bank. In addition, the allograft carries the risk of immunological problems and disease transmission (LANGROUDI; SARAVANI; NOURI, 2017).

Thus, tissue engineering has been seeking the development of biomaterials with different combinations to mimic the affected tissue in the best possible way, relating these biomaterials to factors that stimulate the growth and development of cells at the site.

In this context, scaffolds for bone regeneration emerged to mimic the natural extracellular matrix of bone (ECM), providing a basic structure and microenvironment for the growth of bone tissue with excellent biocompatibility, adaptable biodegradability, osteoconductivity and minimal immunogenic responses (SHI et al., 2019).

Bacterial nanocellulose (BNC) membranes have been explored as suitable matrices for this application due to their structure composed of three-dimensional (3D) nanofibril networks similar to the extracellular matrix, composed of linear polysaccharides polymer with β-(1,4) glycosidic bonds. With a highly porous and hydrophilic structure, they also have good mechanical properties, high levels of crystallinity and excellent biocompatibility. These characteristics are as advantageous for regenerating organs such as skin, bones, cartilage, nerves, heart and blood vessels (AN et al., 2017a; RECOUVREUX et al., 2011).

Hydroxyapatite (HAp) has also been extensively investigated in this regard. It is the main constituent of inorganic components in the natural bone due to its excellent

biocompatibility, bioactivity and osteoconductivity. Studies have shown that HAp promotes adhesion and proliferation of osteoblasts cultured in vitro (TU et al., 2017).

Hybrid materials obtained from the interaction of NBC with HAp have shown promise for use in tissue engineering. The properties of BNC combined with the properties of HAp promote several benefits to bone tissue (LUZ, 2016). However, to maximize the benefits of this interaction, studies have shown that incorporating trace elements existing in bones, such as Na^{+}, Sr^{2+} and Mg^{2+}, can increase osteogenesis and neovascularization (EHRET et al., 2017).

It is also important to note that the human body does not naturally express cellulase enzymes capable of degrading cellulose (ARAÚJO et al., 2016).

In this context, this work aims to study the effect of cationic substitution in cell culture of biomaterials based on BNC functionalized with HAp and Mg^{2+}, Cu^{2+}, Sr^{2+} and Zn^{2+} apatites for application in guided bone regeneration. It is also intended to characterize the material produced and evaluate the biomaterial's structural modulation by the addition of cellulases *in vitro.*

Thus, this research aims to answer the following questions:

(i) Can replacing Ca^{2+} with other bivalent metals favor essential aspects of the guided bone regeneration process?

(ii) will the biomaterial formed have better characteristics than those currently available?

(iii) is the addition of cellulases capable of promoting material with modulable biodegradation?

In the attempt to answer these questions, the following analyzes will be proposed for each of the proposed levels:

- ✓ Analysis of cytotoxicity and cell adhesion;
- ✓ material characterization analyses such as Fourier transform infrared spectroscopy with attenuated total reflectance (FTIR/ATR), thermogravimetry analysis (TGA), scanning electron microscopy with energy dispersive spectroscopy (SEM-EDS), X-rays (XRD), degree of swelling, porosity and ion release after immersion in simulated body fluid (SFB);
- ✓ *in vitro* degradation assays of the biomaterial with cellulase incorporation.

1.1 Aim of this work

To study the effect of cationic substitution in BNC-HAp biocompposites by Mg^{2+}, Cu^{2+}, Sr^{2+} and Zn^{2+} for application in bone regeneration.

1.1.1 Specific aims

• Produce BNC biocomposites containing calcium phosphate (HAp) by incorporating Mg, Cu, Sr and Zn apatites into BNC membranes by the batch adsorption technique, varying the metal ion concentration;
• Characterize the biomaterials in order to determine the physicochemical characteristics related to the interaction of ions with the BNC fibers;
• Evaluate the effect of this structural modification on cell viability of fibroblasts;
• Evaluate the adhesion and proliferation of osteoblastic cells;
• Determine the antibacterial potential of the biomaterials formed;
• Evaluate the structural modulation of the biomaterial by the effect of the addition of cellulases *in vitro*.

1.2 Structure of the thesis

This thesis is divided into Chapters, whose key points are provided below:
In the current Chapter (1), a general contextualization is displayed alongside the aim of this work.
Chapter 2 will present a theoretical survey regarding the state of the art in which this thesis fits.
Chapters 3 and 4, are presented the experimental results. Chapter 3 is the first submitted experimental work. The steps of preparation and characterization of bacterial nanocellulose and biocomposites produced from NBC with HAp partially substituted only by cations Mg and Cu are described. This first test was carried out with a higher percentage of substitute cations, seeking to combine antimicrobial and osteogenic properties.

The results obtained from this study showed us some new paths. Thus, in chapter 4, we present the second experimental work submitted with the cationic substitution by 4 elements, Mg, Cu, Zn and Sr, in lower concentrations.
Chapter 5 presents some results obtained during the thesis but did not form part of a publication.
Chapter 6 summarizes the main conclusions of this doctorate, highlighting the contributions derived from it and presents perspectives for future work.

1.3 References

AN, S.-J. et al. Preparation and Characterization of Resorbable Bacterial Cellulose Membranes Treated by Electron Beam Irradiation for Guided Bone Regeneration. **International Journal of Molecular Sciences**, v. 18, n. 11, p. 2236, 2017.

ARAÚJO, A. M. DE et al. Regenerated cellulose scaffolds : Preparation , characterization and toxicological evaluation. **Carbohydrate Polymers j**, v. 136, p. 892–898, 2016.

EHRET, C. et al. Strontium-doped hydroxyapatite polysaccharide materials effect on ectopic bone formation. **PLOS ONE**, v. 12, n. 9, p. e0184663, 14 set. 2017.

LANGROUDI, M. M.; SARAVANI, M.; NOURI, A. Surfactant-assisted synthesis of polyvinylpyrrolidone-hydroxyapatite composites as a bone filler. **Journal of Applied Biomaterials & Functional Materials**, v. 15, n. 4, p. e-334-e340, 2017.

LUZ, E. P. C. G. **Desenvolvimento de materiais híbridos à base de Celulose Bacteriana e/ou Hidroxiapatita dopados com estrôncio**. Fortazeza, Universidade Federal do Ceará, 2016.

PINA, S. et al. Biofunctional Ionic-Doped Calcium Phosphates: Silk Fibroin Composites for Bone Tissue Engineering Scaffolding. **Cells Tissues Organs**, v. 204, n. 3–4, p. 150–163, 2017.

RECOUVREUX, D. O. S. et al. Novel three-dimensional cocoon-like hydrogels for soft tissue regeneration. **Materials Science and Engineering: C**, v. 31, n. 2, p. 151–157, 2011.

SHI, R. et al. Current advances for bone regeneration based on tissue engineering

strategies. **Front. Med.**, v. 13, n. 2, p. 160–188, 2019.

TU, Y. et al. Fabrication of nano-hydroxyapatite/chitosan membrane with asymmetric structure and its applications in guided bone regeneration. **Bio-Medical Materials and Engineering**, v. 28, n. 3, p. 223–233, 2017.

2 STATE OF ART

2.1 The Bone Tissue

Bone tissue constitutes a heterogeneous matrix formed by associating a mineral and an organic phase (LUZ, 2016). In this tissue, according to Junqueira and Carneiro (2017), the bone tissue cells belong to two different lineages: (1) the cells of the osteoblastic lineage, formed by osteoblasts and osteocytes, are derived from osteoprogenitor cells of mesenchymal origin and (2) cells of the osteoclastic lineage are osteoclasts, originating from monocytes produced in the hematopoietic marrow.

Osteoblasts are mononucleated cells responsible for secreting collagen and non-collagenous proteins, bone matrix proteoglycans, and metalloproteinases that regulate growth factors, forming a framework that allows the deposition of mineral salts and consequent mineralization and also releasing cytokines that regulate osteoclastic development (CARVALHO, 2010) while osteoclasts are responsible for bone resorption, forming excavations where the action of proteolytic enzymes occurs, acidifying the environment and promoting demineralization of the bone matrix (JUNQUEIRA and CARNEIRO 2017).

Osteocytes are located in cavities or gaps within the bone matrix. From these gaps, canaliculi are formed that go to other gaps, thus making the diffusion of nutrients possible thanks to the communication between the osteocytes. Osteocytes play a crucial role in maintaining the integrity of the bone matrix (BARBIERI, 2006) and (CARVALHO, 2010).

Macroscopically, the bone is divided into cortical and spongy (Figure 2.1). Cortical bone is dense and present in the axis of long bones. The collagen matrix is organized in the form of concentric lamellae, usually around a central vascular channel constituting the Haversian system. The central channels, containing nerves and blood vessels, communicate with each other and with the bone marrow cavity through Volkmann's channels. The outer bone surface is covered by a membrane called the

periosteum and the inner surface by the endosteum. Both nourish the bone and serve as a source of osteoblasts for osteogenesis (ISOLA, 2012).

Figure 2.1: Illustrative image of a bone, demonstrating two conformations of bone tissue: compact bone, which in long bones is called cortical, and spongy bone.

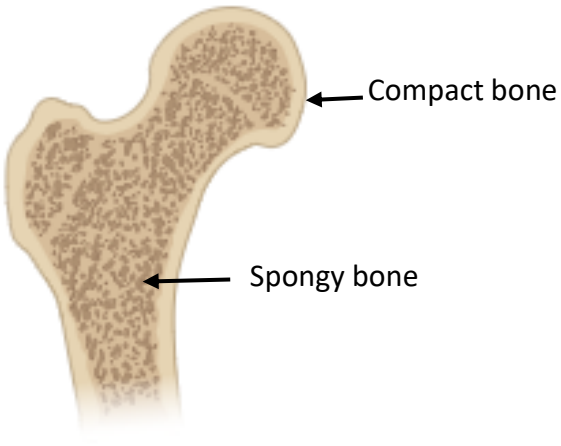

* Created in Biorender.com

Based on the structural organization, bone is said to be lamellar or tissue. The first is a mature form of bone composed of cortical and cancellous bones. Lamellar bones are slow-depositing bones with aggregated and well-organized arrangements of collagen. In contrast, woven bones deposit rapidly during intramembranous ossification or fracture healing and are distinguished by their loosely packed and randomly arranged collagen fibers, lower mineral density, and high water content (RATH et al., 2000).

The organic matrix consists of collagen, predominantly proteoglycans and adhesive glycoproteins, and the inorganic matrix is formed by phosphate (PO_4), calcium (Ca) ions and in low amounts of magnesium (Mg), potassium (K), sodium (Na), among others. The junction between PO_4 and Ca forms hydroxyapatite (HAp) crystals that associate with collagen fibers (LUZ, 2016).

Other examples of non-collagenous molecules present in this tissue are osteocalcin, which contains carboxyglutamic acid–α residues in its molecule that

promote calcium-binding, favoring bone mineralization or crystal growth regulation. Osteopontin participates in bone mineralization by containing calcium-binding sites, osteoblastos, and osteoclasts adhesion to the bone matrix. Among the acidic glycoproteins found in bone tissue, osteonectin stands out, which is considered the most abundant non-collagenous protein in bone and manifests in osteoprogenitor cells, osteoblasts, and newly formed bone osteocytes. It is related to bone mineralization, but its function is not clearly defined (CARVALHO, 2010).

Bone maturity can be defined as completing of crucial structural development and mineralization and attained of optimal mechanical strength. The maturation process involves many different molecular and biochemical changes in the bone that lead to optimal physical and biomechanical properties. These changes can occur in collagen fiber diameter, crosslinking content, and deposition of more lamellar-like bones (RATH et al., 2000).

2.1.1 Bone tissue remodeling and regeneration

The remodeling cycle occurs in a highly regulated and stereotyped fashion, with five overlapping steps of activation, resorption, reversal, formation, and termination occurring over 120 to 200 days in cortical and trabecular bone. Osteocytes orchestrate bone remodeling by regulating osteoclast and osteoblast differentiation and, therefore, bone resorption and formation. Thus, new bone formation can be divided into two parts: (1) osteoblasts synthesize and secrete an osteoid matrix rich in type 1 collagen, and (2) osteoblasts play a role in regulating osteoid mineralization (KENKRE; BASSETT, 2018).

In the formation phase, where the recruited osteoblasts are activated and synthesize the organic matrix, it will mineralize and end the cycle. This process has been evaluated by determining biochemical markers, with alkaline phosphatase being a good marker of bone formation and acid phosphatase, resistant tartrate, a good marker of bone resorption (BARBIERI, 2006).

While bone regeneration is a multi-step process involving migration, proliferation, differentiation and activation of various cell types. Bone formation occurs through two distinct processes: intramembranous ossification, where mesenchymal cells differentiate directly into bone-forming osteoblasts, which occurs during the development of some bones of the skull and face; and endochondral ossification, where bone formation occurs via intermediary cartilage present in the development of long bones and vertebrae (BARBIERI, 2006) and (CARVALHO, 2010).

One of the main conditions necessary for bone repair to be consolidated is the presence of adequate vascularization, which according to Shi et al. (2019), is a crucial factor in satisfying the nutritional supplement and waste removal during bone tissue regeneration. Contact with the extracellular matrix (ECM) is also essential since it is considered a physiological storehouse of several growth factors (GFs) (UEBERSAX; MERKLE; MEINEL, 2009), such as insulin-like growth factor (IGF), platelet-derived growth factor (PDGF) and fibroblast growth factor (FGF), as well as bone proteins morphogenetic proteins (BMP, bone morphogenetic proteins) that are directly related to the differentiation and development of osteoblasts. This deposit osteoid matrix becomes a mineralized structure when kept immobile during the healing process. They are located on the bone surface, promoting deposition of the osteoid matrix and can ultimately differentiate into osteocytes (CARVALHO, 2010).

There are many variables regarding the self-healing capacity of different tissues after damage. This ability is mainly related to the potential of a tissue to attract or induce the proliferation of tissue-specific cells, prevent the invasion of non-specific cells and even the loss of the original tissue and its associated functions. In addition to variations between tissues, self-regeneration decreases with age, regardless of tissue type (UEBERSAX; MERKLE; MEINEL, 2009).

Osteogenesis is critical for maintaining a healthy and fully functional skeletal system and is strongly associated with average blood vessel growth during endochondral bone formation (Figure 2.2). Blood vessels mediate the transport of circulating cells, oxygen, nutrients and waste and provide angiogenic and angiocrine signals controlling organ growth and homeostasis. Therefore, normal vascular formation plays a vital role in the physiological and pathological processes of the skeletal system (HUANG et al., 2018).

Figure 2.2: Formation of a long bone from a cartilaginous model demonstrating the importance of the participation of the vascular system.

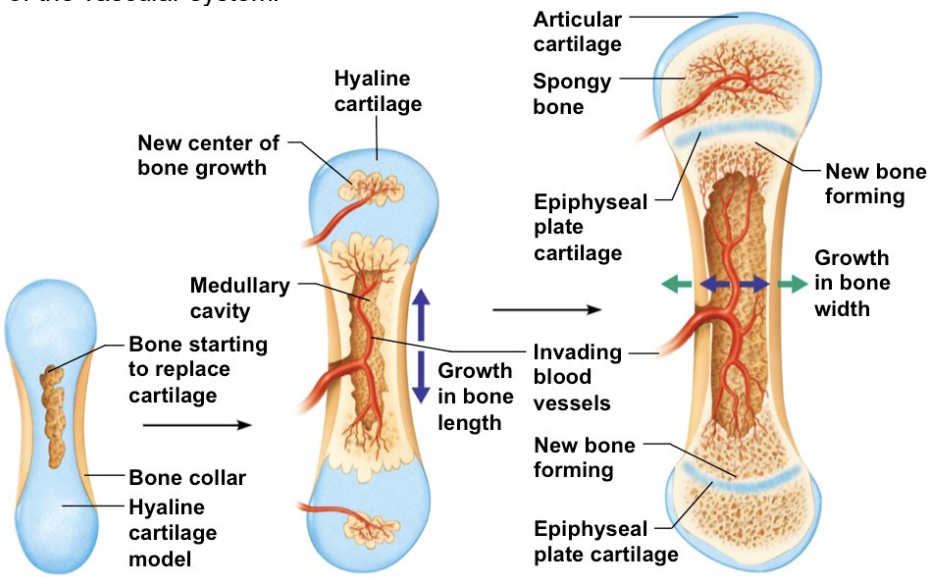

Source: Google images.

2.1.2 Cell signaling and bone metabolism

Mature osteoblasts express high levels of bone tissue-specific alkaline phosphatase (ALP) [phosphate-monoester phosphohydrolase (EC 3.1.3.1), a key enzyme involved in bone formation and osteoid mineralization. This osteoblastic differentiation marker is a metalloenzyme anchored to the plasma membrane and the vesicles secreted from the matrix. ALP is a phosphomonoesterase whose catalytic activity depends on a multimeric configuration, requires Mg^{2+} as a cofactor, and includes two Zn^{2+} ions per monomer to stabilize its tertiary structure (FERNÁNDEZ et al., 2014).

In bone metabolism, alkaline phosphatase is related to the mineralization capacity of osteoblasts, acting to control the concentration of mineralization inhibitors such as inorganic pyrophosphates through an increase in the local concentration of phosphate ions, removing phosphate from other proteins and or possibly acting as an ion carrier. It is found in human serum and tissues that form bones, kidneys, liver,

intestine, and placenta. The two predominant forms in circulation are the liver and bone. This marker detects significant increases in bone metabolism, especially in Paget's disease, advanced bone metastases, and fracture healing. Fracture of a long bone causes an increase in serum alkaline phosphatase activity, as with surgical repair or surgical manipulation of the bone (BARBIERI, 2006) and (VIMALRAJ, 2020).

2.2 Guided Bone Regeneration (GBR)

The development of the guided bone regeneration (GBR) technique brings hope to solve these problems, having as a fundamental principle the creation of an isolated space using a barrier membrane to prevent the invasion of fast-growing fibrous tissue and other soft tissues from migrating to the bone defects, thus allowing time for populations of osteogenic cells from the host bone to inhabit the defective bone (TU et al., 2017).

The creation of an isolated anatomical site to promote healing was first introduced 50 years ago, when cellulose acetate filters were used experimentally to regenerate nerves and tendons. In the mid-1980s, the principle of Guided Tissue Regeneration (GTR) was introduced, according to which regeneration of a specific type of tissue is achieved when cells capable of regenerating the specific type of lost tissue can fill the defect during the healing (RETZEPI; DONOS, 2010).

Tissue engineering has the principle of inducing tissue regeneration in a temporary three-dimensional environment (3D) or “scaffold”, which must mimic the nanostructure and properties of natural bone. As matrix degradation during new tissue formation is preferable, biocompatibility becomes an essential scaffold feature (KARADZIC et al., 2015).

The scaffold must also mimic the natural bone extracellular matrix (ECM), which provides a basic structure and corrects the microenvironment for bone tissue growth. Several essential features are required among the different types of third-generation scaffolds, such as 3D biomimetic structure, excellent biocompatibility, porosity, bioactivity, adaptable biodegradability, pre-vascularized structure osteoconductivity, and lower immunogenic responses (SHI et al., 2019).

Osteoconductivity is the ability of a material to stimulate and support the formation of new bone tissue on its surface and is related to the bioactivity that can be promoted by a thin layer of carbonated HAp capable of adsorbing proteins for cell attachment and proliferation. A chemical composition such as the release of ions and phosphates and pore architecture is also associated with this characteristic, providing growth of the mineral layer and space for infiltration of the neotissue (FRASSICA and GRUNLAN, 2020).

Interconnectivity also provides a basic microstructure for natural cell migration, growth and nutrient distribution. Another desirable feature is controlled degradation after implantation; the degradation rate must be as close to the rate of tissue growth to maintain stable mechanical properties in the tissue structure composite during regeneration (SHI et al., 2019).

The ability to control pore size is also essential in fabricating scaffolds for bone regeneration (200–500 μm) (DI LUCA et al., 2016). The structure of pores, as well as their size, shape, volume and interconnectivity, is fundamental as it is directly linked to proliferation, migration, differentiation, vascularization and better spatial organization for cell growth and ECM formation (SHI et al., 2019).

Therefore, knowledge of biology, engineering and materials science is needed to create substitutes that can reduce the known disadvantages of traditional grafts (SHI et al., 2019).

Materials play an essential role in this process. The combination of inorganic compounds, such as calcium phosphates (CaPs) and biopolymers, has attracted much attention in the fields of tissue engineering and GBR due to the mechanical improvement of the mixture compared to their single-phase (PINA et al., 2017) and mainly for stimulating the adhesion and proliferation of osteoblasts (TU et al., 2017).

2.3 Biomaterials as bone substitutes

Many recent attempts have focused on developing materials with mechanical and biological properties suitable for replacing natural bone tissue (LANGROUDI; SARAVANI; NOURI, 2017). Ideal bone repair materials should be able to guide

osteoblast proliferation and differentiation, stimulate endothelial cell angiogenesis and resist bacterial infection (LIU et al., 2016). In addition, it must also be biocompatible, absorbable and replaced by new tissue formation.

Calcium phosphates (including HAp) have been the most used material for bone regeneration due to their similarity to the inorganic phase of native bone tissue and their ability to recruit and stimulate MSCs while simultaneously initiating angiogenic and chemotactic responses. Bonding as polymers, in the form of composites, has also been explored for better control over pore morphology and toughness. Furthermore, recently, bioglasses and bioceramics have been used after modifications via doping of elements (e.g., F^{-}, Cl^{-}, Na^{+} and Mg^{2+}) to reduce brittleness, delay resorption rates, stimulate osteogenic differentiation or suppress inflammation (FRASSICA and GRUNLAN, 2020).

Synthetic polymer scaffolds have been extensively studied in the tissue engineering field for decades due to the level of control over crucial chemical and physical properties, e.g., degradation rate, pore morphology, chemical functionality, modulus, etc. (FRASSICA and GRUNLAN, 2020). In particular, natural polymers have received substantial attention as molding materials for medical applications (SHI et al.,2019).

The use of biopolymers for GBR is attractive due to the possibility of processing them into three-dimensional structures, with BNC being one of the most promising biopolymers. However, despite its biocompatibility, its use alone is limited by significant drawbacks, such as poor mechanical properties. Studies propose compounds based on biopolymers reinforced with inorganic particles to improve the structure's mechanical properties (LANGROUDI; SARAVANI; NOURI, 2017); this gives rise to hybrid materials, which have been widely explored, as they are multifunctional materials with complementary properties (LUZ, 2016).

Studies show that natural composites and synthetic biomaterials have a high osteogenic potential. Bones contain hydroxyapatite and collagen porous compounds, so scaffolds must be porous compounds with ceramic and polymer phases. The dual composition aims to complement the distinct properties of each material, giving rise to a differentiated biomaterial with more refined properties. It should minimize the

problems faced with single porous polymers (low compressive strength) or with porous hydroxyapatite ceramics (mechanically fragile and brittle) (KARADZIC et al., 2015).

The development of BNC-based composites with biocompatible materials is a commonly used protocol. Various biomaterials, such as collagen, gelatin, chitosan, and starch, have been explored. In addition, as hydroxyapatite (HAp) is an essential bioactive component present in bones, facilitating the differentiation and growth of cells in this tissue, BNC/HAp compounds have also been extensively studied for applications in GBR (WU et al., 2019).

2.3.1 Bacterial nanocellulose (BNC)

Bacterial nanocellulose is a polysaccharide secreted by several bacterial species, among which bacteria of the genus *Gluconacetobacter* (formerly *Acetobacter* and recently renamed *Komagataeibacter*) stand out (DU et al., 2016). Macroscopically, BNC it is characterized as a hydrogel due to its high water content, while microscopically, it has an ultrafine three-dimensional network of nanofibrils (3D) (WU et al., 2019).

BNC is a fibril backbone consisting of the β(1-4) glucan chain with molecular formula $(C_6H_{10}O_5)_n$. The glucan chains are held together by inter and intramolecular hydrogen bonds (Figure 2.3). The fibrous network of BNC is composed of well-organized three-dimensional nanofibers, resulting in hydrogel sheets with high surface area and porosity. During the synthesis process, the protofibrils of the glucose chain are secreted through the bacterial cell wall, forming cellulose ribbons structured as nanofibrils. These ribbons build the network structure of the BNC in the form of a web with a highly porous matrix due to the intense presence of hydroxyl groups on its surface. It is characterized by having high hydrophilicity, biodegradability and chemical modification capacity

BNC presents characteristics such as high purity, high crystallinity and porosity, high water retention capacity, excellent biocompatibility and mechanical behavior comparable to other complex and synthetically produced polymers and fibers.

These are suggested as some of the essential characteristics for the regeneration of the body organs (AN et al., 2017; BALDIKOVA et al., 2017; RECOUVREUX et al., 2011).

Figure 2.2: BNC structure showing intra and intermolecular hydrogen bonds.

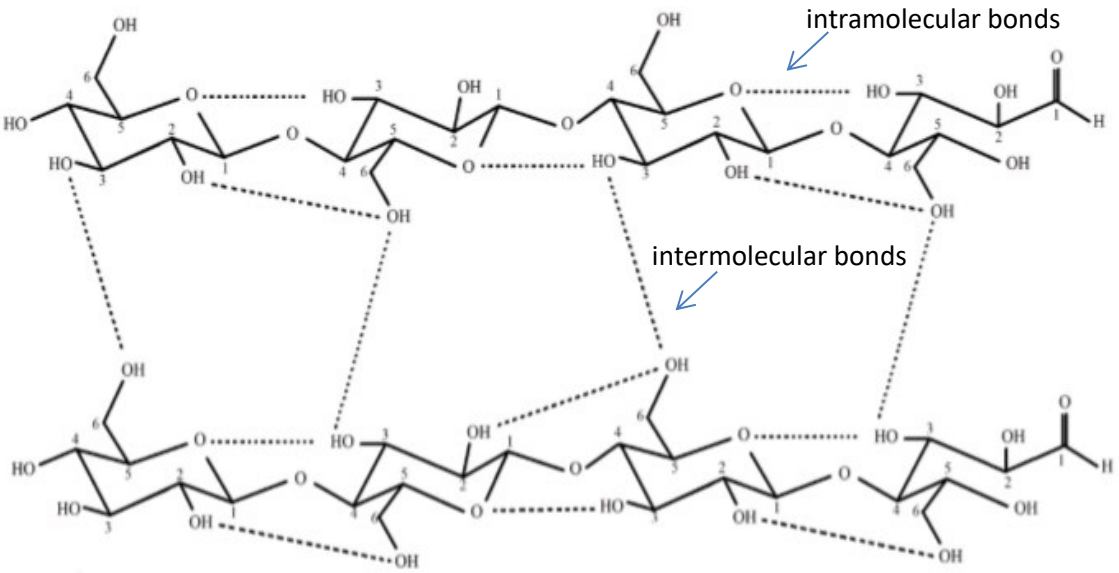

Source: Adapted from ESA; TASIRIN; RAHMAN, 2014.

In recent years, there has been a growing interest in using BNC in medical applications, especially in exploring new porous biomaterials which can be used in tissue engineering (ARAÚJO et al., 2016). With numerous applications (Figure 2.4) in various fields, including skin tissue repair, tissue engineering potential structure, wound healing applications, immobilization, papermaking, cosmetics, dye bleaching and as a thickening and stabilizing agent in the food industry (BALDIKOVA et al., 2017).

According to Saska et al. (2011), BNC/HAp biocomposites were used for GBR in critical and non-critical sized bone defects, in periodontal lesions and as a resorbent barrier membrane occluding fibroblast cells and fibrous connective tissue in bone

defects, the results revealed that the membranes BNC promote effective bone formation at the site, in addition to being a low-cost treatment.

Figure 2.3: Image demonstrating the versatility of BNC applications.

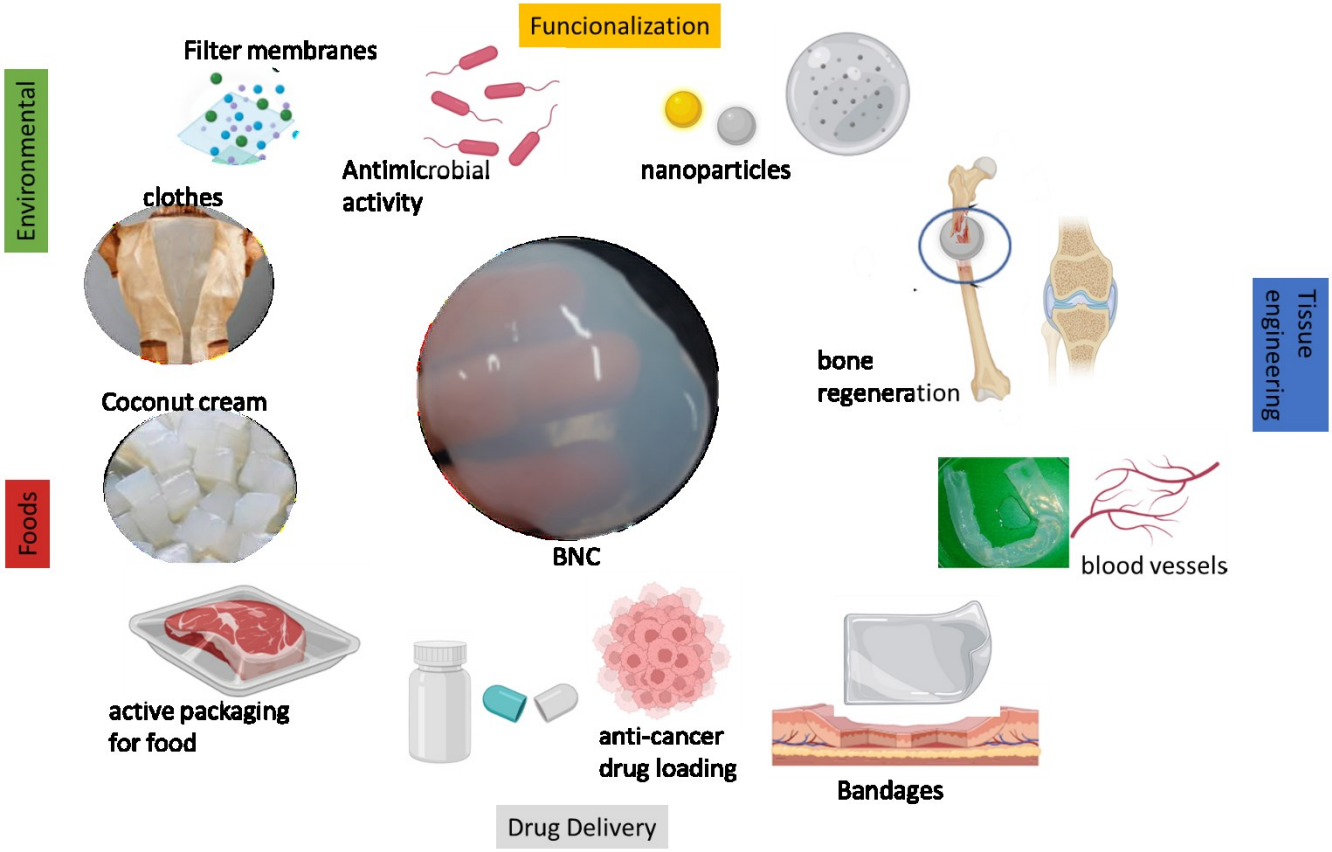

* Created with Biorender.com

2.3.2 Hydroxyapatite (HAp)

Materials based on calcium phosphates, including HAp, due to their similarity to native bone tissue, have been the most used materials for bone regeneration. They promote remineralization processes, recruit and stimulate MSCs, and initiate angiogenic and chemotactic responses (FRASSICA and GRUNLAN, 2020). It also has

an ultrafine structure and a large surface area that is advantageous for cell–biomaterial interactions with the advantages of excellent biocompatibility, high plasticity, and remarkable mechanical properties, for this has been widely studied in applications for bone engineering (NICOARA et al., 2020). In addition, it is bioabsorbable and can undergo cellular degradation without producing toxic byproducts (WUBNEH et al., 2018).

Calcium phosphates are classified by their Ca/P ratio, ranging from 0.5 to 2.0. Compounds with higher Ca/P ratios are less soluble under neutral conditions and have lower degradation rates, while materials with high phosphorus content are more reactive. Hydroxyapatite (HAp) is a critical and essential part of the bone (OLIVEIRA et al., 2019). It consists of double salt of tricalcium phosphate and calcium hydroxide in its pure form. However, biological apatites differ from pure HAp in composition, crystal size, morphology and stoichiometry. The Ca/P ratio of pure HAp is 1.67, but biological apatites are generally non-stoichiometric (1.59 for enamel, 1.67 for dentin, and 1.65 for bone) (BEZERRA, 2011).

The biological importance of HAp is related to facilitating the multiplication of fibroblasts, osteoblasts and other bone cells. Its compatibility with bone tissue is due to its superficial chemical similarity with the bone itself, the ability to exchange ions with the physiological environment, tending to implant-bone balance. The chemical composition of biological HAp varies throughout life. It can be formed by other ions such as carbonate or grouping other elements such as Sr, Si, Mg, and others (LUZ, 2016).

Fang et al., (2009) showed that the developed HAp/BNC scaffolds were biocompatible and could promote cell proliferation and differentiation in vitro using human bone marrow-derived stromal cells (hBMSC) and are therefore considered good candidates for guided bone regeneration.

2.3.3 Biocomposites

Studies show that natural composites and synthetic biomaterials have a high osteogenic potential. Bones consist of a porous compound of hydroxyapatite and

collagen, so scaffolds must be porous compounds with ceramic and polymer phases. The hybrid composition aims to complement the distinct properties of each material, creating a differentiated biomaterial with better properties, also seeking to minimize the problems faced with using a unique and porous polymer matrix, such as low compressive strength or with hydroxyapatite ceramics. porous that alone are mechanically fragile (SHI et al., 2019).

Nanostructures such as nanoparticles or nanofibers were designed to intensify the mechanical properties of load-bearing scaffolds to mimic natural bone. Nanocomposites have been applied to produce osteoinductive structures by increasing surface area and volume proportions, improving surface roughness and changing nano-topography. In *in vitro* studies, it was observed that these nanostructured scaffolds could influence stem cell behavior, such as cell adhesion, viability, proliferation and osteogenic differentiation, stimulating bone regeneration (SHI et al., 2019).

The association of HAp and BNC results in a nanostructured hydrogel biocomposite, an excellent matrix for incorporating other compounds. In recent years, BNC has shown promising results for tissue repair. In addition, biocomposites based on BNC and HAp are considered osteoconductive (PIGOSSI et al., 2015).

Zimmermann et al. (2011) worked with BNC and HAp membranes and demonstrated that the increase in HAp crystals was favored by the density of BNC fibers, making them more porous. This porosity, in turn, is well seen for tissue engineering as it benefits the migration and multiplication of cells, making bone tissue regeneration possible.

2.3.4 The addition of metals to biocomposites as trace elements

Bone tissue is naturally a composite, composed not only of calcium phosphate but also other elements such as Na^{+}, Mg^{2+} or Sr^{2+} in the form of trace elements. These trace elements play a vital role in bone growth and repair. They can control

degradation, increase materials' mechanical strength, and upregulate their bioactive properties, such as osteoconduction (EHRET et al., 2017).

One cation that can replace calcium in the HAp structure, Sr^{2+}, has attracted significant interest due to its beneficial effect on bone formation. *In vitro* studies have shown that Sr^{2+} has a dual effect on bone cells: it increases osteoblast-mediated bone formation and decreases osteoclastic bone resorption. Allied to this, it has beneficial effects on bone mass, bone quality, and bone strength, observed in animal models of metabolic bone disease and patients with osteoporosis. However, the strontium content of bone can vary depending on its turnover and anatomical location. For example, more significant amounts of strontium are found in cancellous bone than in cortical bone. In osteoblasts, Sr^{2+} stimulates cell proliferation and differentiation by activating the calcium-sensitive receptor of the Wnt/β-catenin pathway (FERNÁNDEZ et al., 2014) (EHRET et al., 2016).

Studies with osteoblastic cells (MC3T3E1) showed that Sr^{2+} could increase the production of type 1 collagen, the specific activity of ALP and the expression of intracellular markers such as extracellularly regulated kinases (ERK) and β-catenin while decreasing the secretion of cytokines inflammatory TNFα and IL1. Sr^{2+} incorporated into the mineral network can directly interact with bone ALP expressed by osteoblasts and present in secreted matrix vesicles, potentially influencing the osteoid mineralization process (FERNÁNDEZ et al., 2014).

The substitution of calcium ions for strontium ions is favored because both are alkaline earth metals. The structure of HAp allows substituting up to 100% of the Ca^{2+} ions by Sr^{2+} ions. However, this substitution must be controlled since *in vivo* studies have shown that the metal's effects depend on the dose used. When used at low doses (4 mmol Sr/kg/day), strontium reduces bone resorption and bone formation, resulting in increased bone mass in rats. The presence of Sr^{2+} increases the number of osteoblasts, cells responsible for producing the organic part of the bone matrix. It decreases the number and activity of osteoclasts responsible for bone destruction, thus decreasing in bone resorption (BEZERRA, 2011).

Another essential trace element is Zn, which plays a vital role in the normal development and growth of the skeletal system thanks to its favorable rate of degradation and biocompatibility, especially for orthopedic applications. About 30% of

the total Zn in the body is stored in bone tissue. Zn deficiency impairs the development of the skeletal system and is associated with the pathogenesis of osteoporosis. Zn stimulates bone formation and improves the osteogenic response in osteoblasts, increasing cell proliferation, gene expression related to osteogenesis and extracellular matrix synthesis. Thus, many studies have introduced Zn into biomaterials intending to improve their bone formation capacity and show more significant osteoinductive potential (YU et al., 2017).

Zinc is essential in regulating hydroxyapatite crystallization, collagen synthesis and osteoblasts' cellular invasion of the cartilage matrix. This invasion requires the activity of collagen matrix metalloproteinases, particularly collagenase-3, which contain Zn at their active sites. The fact that intracellular Zn fluxes are associated with apoptosis in growth plate chondrocytes suggests that Zn may play a role in endochondral ossification and its participation in vascular invasion and hydroxyapatite crystallization. Zinc is also associated with changes in gene transcription that accompany the ossification process (DIBNER et al., 2007).

When compared to Mg and Fe, Zn has a degradation rate more compatible with tissue healing. Furthermore, the Zn ion plays a significant role in cellular metabolic activity and bone growth functions, and this is an additional beneficial feature of implants that release Zn during degradation. Indeed, evidence has shown that Zn^{-} based medical implants exhibited good biocompatibility in various animal models, including abdominal aortas from rabbits and rats and femurs from rats and mice (SU et al., 2019).

Zinc (Zn^{2+}) is present in human bones in low amounts (between 126-276 µg/g). Zn^{+2} stimulates bone growth and mineralization. Its presence in apatite at calcium sites decreases the inflammation reaction induced by phagocytosis of HAp powders (BEZERRA, 2011).

One of the most studied substituents is magnesium, the fourth most abundant cation in human bone (0.44 – 1.23% mass). It is essential for the correct fixation of calcium in the body. Its lack can cause decalcification in the bones (osteoporosis). The presence of Mg^{2+} in the structure of HAp significantly affects its crystallization, destabilizing its structure and favoring the formation of β - tricalcium phosphate (β-TCP) (BEZERRA, 2011).

Several studies have investigated the effect of enriching the surface of a biomaterial such as hydroxyapatite with Mg ions and suggest a biochemical role for magnesium in the bone system. It is even a cofactor for many enzymes. The level of Mg in the extracellular fluid varies between 0.7 and 1.05 $mmol \cdot L^{-1}$, with homeostasis maintained by the kidneys and intestine. Preliminary observations indicate that magnesium promotes calcium phosphate precipitation in an *in vitro* environment, a feature that can be exploited to induce or enhance osteoconductivity (STAIGER et al., 2006).

Copper is a trace element that plays a vital role in the immune system, restoring regular bone resorption rate in bone metabolism and increasing collagen fiber deposition, being attractive in bone engineering. Both osteoinduction and osteoclast activity is affected by Cu deficiency, which also stimulates endothelial cell proliferation and increases angiogenesis, an important physiological event in bone regeneration (LIU et al., 2016). It is also present in the amorphous mineral of the matrix vesicles, preventing its premature crystallization and playing an essential role in the cross-linking of collagen and elastin, which gives bone its tensile strength and elasticity (DIBNER et al., 2007).

It is important to highlight that in healthy tissues, especially cartilage, copper is essential in synthesizing cellular enzymes, such as superoxide dismutase, cytochrome oxidase and lysyl oxidase. In particular, lysyl oxidase, a copper-dependent enzyme, plays a key role in collagen cross-linking and cartilage formation. In addition, copper has been shown to have a positive effect on osteogenesis (LIN et al., 2019).

Using bone implants has also been associated with the risk of bacterial colonization of the materials. Although antibiotic-laden materials are well accepted for treating an established infection, their role in preventing infection remains controversial because of bacterial drug use, resistance, efficacy, and cost issues. Choosing a bone implant with a high bacteriostatic activity helps to slow or limit the growth of any remaining bacteria, even after treating infected bone defects (WEI; DING, 2017).

In this way, the activity of the Cu element stands out again, as it plays a fundamental role in maintaining physiological homeostasis and antibiosis in our body, thus being an important element for cellular and humoral immunity (LIN et al., 2019).

Surface modification of dental and orthopedic implants is critical to improving the clinical performance of medical devices. Coating implants with increased osteogenesis and reduced bacterial adhesion have attracted much interest. Thus, numerous attempts based on a simple design for the functionalization of bone implants have been made to individually endow osteogenesis or antibacterial capacity. However, it is difficult to simultaneously achieve the requirements to inhibit bacterial adhesion and promote osteogenic cell functions on implant surfaces since the concentrations necessary to achieve a desired antimicrobial effect are usually cytotoxic (WEI; DING, 2017).

Nevertheless, Wei and Ding (2017) hypothesized that chitosan, gelatin, collagen and silicate-based materials could effectively improve antibacterial activity and maintain osteogenesis. The aim was to produce higher early-stage antimicrobial concentrations at the implant site, thereby reducing the duration of infection treatment and providing bioactive scaffolds for cell growth. Thus, we studied the effectiveness of the two compounds with different concentrations in eliminating Gram-positive (*S. aureus*) and Gram-negative (*E. coli*) bacteria and maintaining osteogenesis of osteoblastic cells (MG63) using an implant coated with Ag was used as control.

2.4 Biomaterials in three dimensions

To mimic ECM, the 3D scaffolds must be able to serve as a substrate to interact with cells, support newly formed tissues, provide nutrients and promote cell invasion (WU et al., 2019). This way, strategies have been developed to design 3D scaffolds capable of delivering multiple growth factors in a controlled manner, preferably with different release kinetics. (BASMANAV; KOSE; HASIRCI, 2008).

However, the ECM is a hierarchical structure whose components and processes are defined at various spatial and temporal scales, from nanometers and nanoseconds to meters and hours. Cells are sensitive to chemical and topographical patterns at the micro and nanoscale. At the nanoscale, the structure of the ECM consists of a natural network of nanofibers. This network provides mechanical support and instructive cues to guide the behavior of cells that induce them to form complex

tissues such as skin, heart, liver, and kidney, among others. The ability to create materials that resemble this intricate network of functional nanofibers is a reality that uses nanoscale engineering methods to create cellular environments (ROCHA; PORTO; RAMBO, 2014).

BNC has been attracting significant attention for its wide range of biomedical and tissue engineering applications (RECOUVREUX et al., 2011; PIGOSSI et al., 2015; FAVI et al., 2016; NICOARA et al., 2020; MAIA et al., 2021). Because it is a polysaccharide produced by bacteria in the form of nanofibrils arranged in a random arrangement, which gives it a highly porous 3D architecture, in addition to having high biocompatibility, high water content and high binding affinity with other substances, which resembles it ECM, BNC is considered an excellent 3D matrix for cell and tissue growth (ROCHA; PORTO; RAMBO, 2014).

However, Wu et al. (2019) recently proposed that because the nanofibril network is very dense, BNC has some limitations in meeting the complex biological requirements of tissue engineering. The authors studied different strategies seeking to improve these properties by modifying the surface of BNC by lotus root starch (LRS), building a three-dimensional (3D) architecture by modeling agarose porogen and deposition of hydroxyapatite (HAp) on the same BNC substrate (*in situ*). They obtained a hierarchical nanoporous structure with a pore size of 300–500 μm, which showed effective cell growth with successful 3D chondrocyte distribution with significantly higher cell viability and total cell number after 14 days of culture. Furthermore, the alkaline phosphatase activity (ALP) test showed significantly higher ALP activity in approximately 50% and 100% increments, respectively, in pBC/LRS-M/HAp when compared to the control scaffold (BNC).

Another critical point to highlight is that the human body does not naturally have cellulase enzymes capable of degrading cellulose. Due to this and seeking to obtain the *in vivo* reabsorption of cellulose, Araújo et al. (2016) studied the *in vitro* enzymatic degradation of regenerated cellulose scaffolds (RCS) using two different enzymes produced by *Trichomona reesei*, cellulases and lysozyme. The results obtained in the enzymatic degradation assay revealed that lysozyme showed a milder catalytic action when compared to cellulase. However, both enzymes were efficient in the degradation of RCS.

2.5 The fourth dimension in biomaterials

In 2014, Skylar Tibbits, director of the Self-Assembly Lab at the Massachusetts Institute of Technology (MIT), first demonstrated four-dimensional (4D) printing as a technology that prints multi-materials with the ability to transform over time. This technology was quickly applied to the field of tissue engineering (WAN et al., 2020).

Although the 4D concept has emerged linked to 3D printing, the fourth dimension (4D), in this sense, is defined as “time”. By considering transformations over time as an additional aspect, it is possible to create more intelligent and relevant devices, mainly in biomedical applications (LIU et al., 2019). Thus, biomaterials produced by other techniques with modulation of biodegradation responsive to body changes could be considered biomaterials with 4D properties.

Regenerative medicine and personalized medicine have increasingly stimulated the development of intelligent biomaterials that respond to environmental stimuli that can change their structure or properties from different physical, chemical, mechanical and biological signals (AMUKARIMI et al., 2022).

According to Liu et al. (2019) and Amukarimi et al. (2022), this is possible by manipulating the characteristics of materials that can be significantly transformed over time by external stimuli, such as temperature, liquid, light, magnetism, electric field, pH, ion concentrations, glucose concentration and enzymes.

Given this, the production of biomaterials with 4D properties emerges as an essential concept that emphasizes the need to consider the dynamic processes of tissue healing and regeneration within the human body when designing biomedical devices (LIU et al., 2019).

2.6 Cellulases

Cellulases are classified as hydrolytic enzymes capable of hydrolyzing cellulose β(1-4) glycosidic bonds (BEHERA et al., 2017). They are produced by various microorganisms, but mainly fungi. The most frequently used for the production of cellulases are cellulolytic fungal strains such as *Aspergillus sp*, *Humicola sp*,

Penicillium sp and *Trichoderma sp*. These biocatalysts have numerous practical applications in many fields of industry and agriculture (ZDARTA et al., 2017).

The complete hydrolysis of cellulose to glucose requires the synergistic action of at least three enzymes: endoglucanases (EG endo-1,4-β-D-glucanase, EC 3.2.1.4) preferentially attack amorphous regions, randomly cleaving the internal bonds of glycan chains, thus providing reducing or non-reducing cellooligosaccharide ends for cellobiohydrolases (CBH or exoglucanase, 1,4-β-D-glucan-cellobiohydrolase, EC 3.2.1.91) to attack (Figure 2.4). CBH hydrolyzes these chain ends, producing cellobiose as the main product. Finally, β-glucosidase (BG cellobiase, β-D-glucosideglucan hydrolase, EC 3.2.1.21) further hydrolyzes cellobiose to glucose and releases glucose from the non-reducing ends of soluble cellooligosaccharides. There is a high degree of synergy between cellobiohydrolases (exoglucanases) and endoglucanases, which is necessary for the efficient hydrolysis of cellulose. The products of endoglucanases and cellobiohydrolases, cellodextranes and cellobiose, respectively, are inhibitors of enzyme activity. Thus, efficient hydrolysis of cellulose requires the presence of β-glycosidases that cleave the final glycosidic bonds that produce glucose as the end product (BEHERA et al., 2017).

The data and studies cited to demonstrate that cellulases have excellent potential as an enzyme capable of promoting the degradation of BNC.

Figure 2.4: Schematic representation of enzymatic hydrolysis of cellulose.

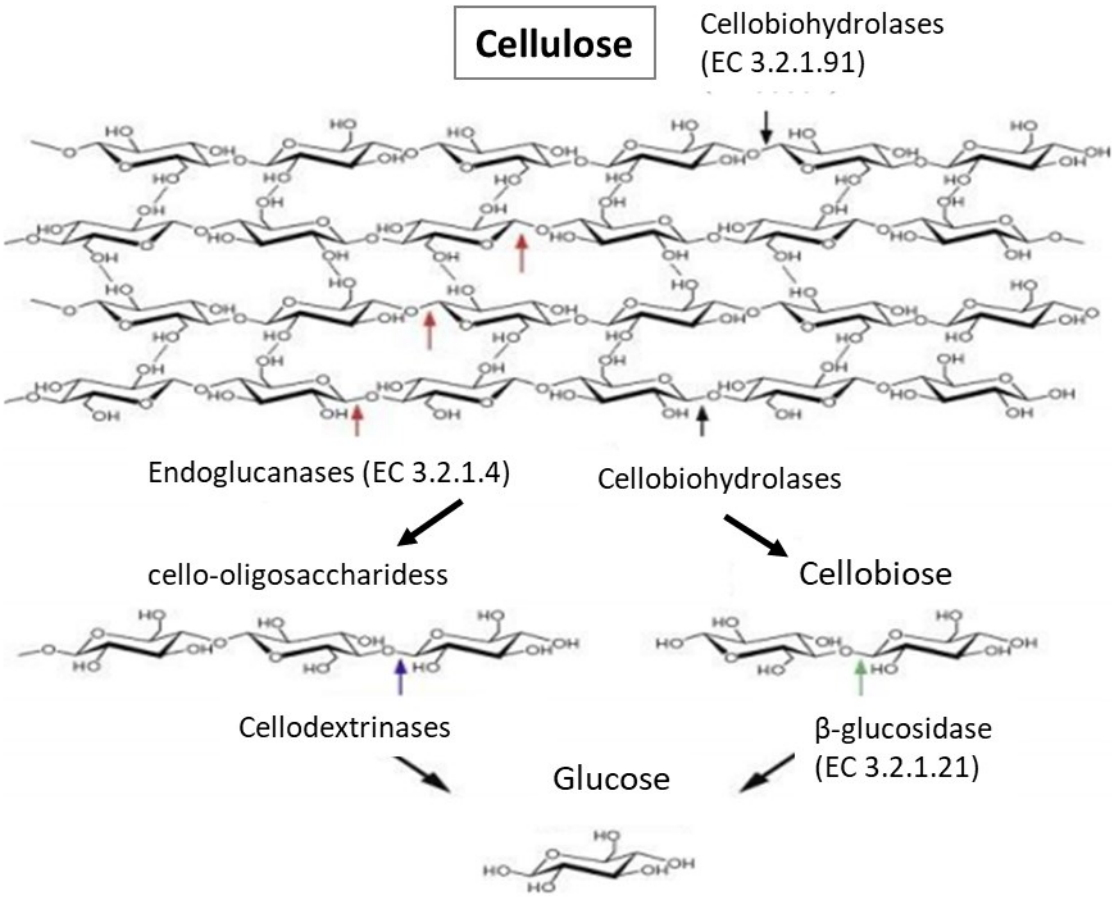

Source: (VILELA, 2013).

2.7 References

AMUKARIMI, S. et al. Smart biomaterials: From 3D printing to 4D bioprinting. **Methods**, v. 205, p. 191 – 199, 2022.

AN, S.-J. et al. Preparation and characterization of resorbable bacterial cellulose membranes treated by electron beam irradiation for guided bone regeneration. **International Journal of Molecular Sciences**, v. 18, n. 11, p. 2236, 2017.

ARAÚJO, A. M. de et al. Regenerated cellulose scaffolds : Preparation, characterization and toxicological evaluation. **Carbohydrate Polymers j**, v. 136, p. 892–898, 2016.

BALDIKOVA, E. et al. Magnetically modified bacterial cellulose: A promising carrier for immobilization of affinity ligands, enzymes, and cells. **Materials Science &**

Engineering C, v. 71, p. 214–221, 2017.

BARBIERI, C. M. D. O. **Efeito do fator de crescimento derivado de plaquetas humanas (pdgf) sobre o processo de regeneração óssea em tíbias de ratos**. Araraquara - UNESP, 2006.

BASMANAV, F. B.; KOSE, G. T.; HASIRCI, V. Biomaterials sequential growth factor delivery from complexed microspheres for bone tissue engineering. **Biomaterials**, v. 29, p. 4195–4204, 2008.

BEHERA, B. C. et al. Microbial cellulases – Diversity & biotechnology with reference to mangrove environment : A review. **Journal of Genetic Engineering and Biotechnology**, v. 15, n. 1, p. 197–210, 2017.

BEZERRA, P. G. P. **Degradação *in vitro* de grânulos bifásicos de fosfato de cálcio dopados com estrôncio**. [Dissertação de Mestrado] Rio de Janeiro, Universidade Federal do Rio de Janeiro, 2011.

CARVALHO, A. C. A. DE. **Reparo ósseo de defeito crítico em calvária de rato com microesferas de hidroxiapatita e selante de fibrina**. Salvador, Universidade Federal da Bahia, 2010.

DIBNER, J. J. et al. Metabolic challenges and early bone development. **The Journal of Applied Poultry Research**, v. 16, n. 1, p. 126–137, 2007.

DI LUCA, A.; OSTROWSKA, B.; LORENZO-MOLDERO, I.; LEPEDDA, A.; SWIESZKOWSKI, W.; VAN BLITTERSWIJK, C.; MORONI, L. Gradients in pore size enhance the osteogenic differentiation of human mesenchymal stromal cells in three-dimensional scaffolds. **Sci. Rep**. v.6, p. 22898e, 2016.

DU, J. et al. Structure of the cellulose synthase complex of *Gluconacetobacter hansenii* at 23.4 Å resolution. **PLOS ONE**, v. 11, n. 5, p. e0155886, 2016.

EHRET, C. et al. Strontium-doped hydroxyapatite polysaccharide materials effect on ectopic bone formation. **PLOS ONE**, v. 12, n. 9, p. e0184663, 2017.

ESA, F.; TASIRIN, S. M.; RAHMAN, N. A. Overview of bacterial cellulose production and application. **Agriculture and Agricultural Science Procedia**, v. 2, p. 113–119, 2014.

FANG, B. et al. Proliferation and osteoblastic differentiation of human bone marrow stromal cells on hydroxyapatite/bacterial cellulose nanocomposite scaffolds. **Tissue Engineering Part A**, v. 15, n. 5, p. 1091–1098, 2009.

FAVI, M. P et al., Preparation and characterization of biodegradable nano hydroxyapatite–bacterial cellulose composites with well defined honeycomb pore arrays for bone tissue engineering applications. **Cellulose**, v. 23, p. 1263 –1282, 2016.

FERNÁNDEZ, J. M. et al. Strontium ranelate stimulates the activity of bone-specific alkaline phosphatase: interaction with Zn^{2+} and Mg^{2+}. **BioMetals**, v. 27, n. 3, p. 601–607, 2014.

FRASSICA, M. T. and GRUNLAN, M.A. Perspectives on synthetic materials to guide tissue regeneration for osteochondral defect repair. **ASC Biomater. Sci. Eng.** v. 6, n. 8, p.4324-4336, 2020.

HUANG, S. et al. Role and regulation of growth plate vascularization during coupling with osteogenesis in tibial dyschondroplasia of chickens. **Scientific Reports**, n. February, p. 1–15, 2018.

ISOLA, J. G. M. P. & P. C. M. D. Bone structure and regeneration - Literature review. **Revista Científica Eletrônica de Medicina Veterinária**, n. 18, p. 12, 2012.

JUNQUEIRA, L.C., CARNEIRO, J. **Histologia básica**. 13.ed. Rio de Janeiro: Editora Guanabara Koogan, 2017.

KARADZIC, I. et al. Effects of novel hydroxyapatite-based 3D biomaterials on proliferation and osteoblastic differentiation of mesenchymal stem cells. **Journal of Biomedical Materials Research A**, v. 103A, n. 1, p. 350–357, 2015.

KENKRE, J. S.; BASSETT, J. H. D. The bone remodelling cycle. **Annals of Clinical Biochemistry**, v. 0, n. 0, p. 1–20, 2018.

LANGROUDI, M. M.; SARAVANI, M.; NOURI, A. Surfactant-assisted synthesis of polyvinylpyrrolidone-hydroxyapatite composites as a bone filler. **Journal of Applied Biomaterials & Functional Materials**, v. 15, n. 4, p. e334 - e340, 2017.

LIN, R.; DENG, C.; LI, X.; LIU, Y.; ZHANG, M.; QIN, C.; YAO, Q.; WANG, L.; WU, C. Copper-incorporated bioactive glass-ceramics inducing anti-inflammatory phenotype and regeneration of cartilage/bone interface. **Theranostics**, v.9, n. 21, p. 6300– 6313, 2019.

LIU, C. et al. Biodegradable Mg-Cu alloys with enhanced osteogenesis, angiogenesis, and long-lasting antibacterial effects. **Scientific Reports**, v. 6, n. 1, p. 27374, 2016.

LIU, Y. S. et al. 4D printing and stimuli-responsive materials in biomedical applications. **Acta Biomaterialia**, v. 92, p. 19 - 36, 2019.

LUZ, E. P. C. G. **Desenvolvimento de materiais híbridos à base de celulose bacteriana e/ou hidroxiapatita dopados com estrôncio.** [Dissertação de Mestrado] Fortaleza, Universidade Federal do Ceará, 2016.

MAIA, M. T. et al. Advances in Bacterial Cellulose/Strontium Apatite Composites for Bone Applications. **Polymer Reviews**, v. 61, n. 4, p. 736-764, 2021.

NICOARA, A. I. et al. *In situ* and *ex situ* designed hydroxyapatite: bacterial cellulose materials with biomedical applications. **Materials**. v.13, n. 21, p.4793e, 2020.

OLIVEIRA, M. J. C. DE et al. Calcium phosphate submicrometric fibers produced by solution blow spinning. **Materials Research**, v. 22, n. 3, p. 1–8, 2019.

PIGOSS, S. C. et al. Bacterial cellulose-hydroxyapatite composites with osteogenic growth peptide (OGP) or pentapeptide OGP on bone regeneration in critical-size calvarial defect model. **J Biomed Mater Res Part A**, v. 103, p. 3397–3406, 2015.

PINA, S. et al. Biofunctional Ionic-Doped Calcium Phosphates: Silk Fibroin Composites for Bone Tissue Engineering Scaffolding. **Cells Tissues Organs**, v. 204, n. 3–4, p. 150–163, 2017.

RATH, N. C. et al. Factors regulating bone maturity and strength in Poultry 1. **Poultry Science**, v. 79, n. 7, p. 1024–1032, 2000.

RECOUVREUX, D. O. S. et al. Novel three-dimensional cocoon-like hydrogels for soft tissue regeneration. **Materials Science and Engineering: C**, v. 31, n. 2, p. 151–157, mar. 2011.

RETZEPI, M.; DONOS, N. Guided bone regeneration: biological principle and therapeutic applications. **Clinical Oral Implants Research**, v. 21, n. 6, p. 567–576, 19 mar. 2010.

ROCHA, E. L.; PORTO, L. M.; RAMBO, C. R. Nanotechnology meets 3D *in vitro* models : Tissue engineered tumors and cancer therapies. v. 34, p. 270–279, 2014.

SASKA, S. et al. Bacterial cellulose-hydroxyapatite nanocomposites for bone regeneration. **International Journal of Biomaterials**, v. 2011, p. 1–8, 2011.

SHI, R. et al. Current advances for bone regeneration based on tissue engineering strategies. **Front. Med.**, v. 13, n. 2, p. 160–188, 2019.

STAIGER, M. P. et al. Magnesium and its alloys as orthopedic biomaterials: A review. **Biomaterials**, v. 27, n. 9, p. 1728–1734, 2006.

SU, Y. et al. Interfacial zinc phosphate is the key to controlling biocompatibility of

metallic zinc implants. **Advanced Science**, v. 6, p. 1–12, 2019.

TU, Y. et al. Fabrication of nano-hydroxyapatite/chitosan membrane with asymmetric structure and its applications in guided bone regeneration. **Bio-Medical Materials and Engineering**, v. 28, n. 3, p. 223–233, 2017.

UEBERSAX, L.; MERKLE, H. P.; MEINEL, L. Biopolymer-Based growth factor delivery for tissue repair : from natural concepts to engineered systems. **Tissue Engineering: Part B**, v. 15, n. 3, p. 263–289, 2009.

VILELA, E. D. DE S. **Análise da produção de celulases e beta glicosidase produzidas por *Streptomyces sp.*** [Dissertação de Mestrado]. Universidade Federal de Goiás, 2013.

VIMALRAJ ,S. Alkaline phosphatase: Structure, expression and its function in bone mineralization. **Gene**, v. 754, p. 144855e, 2020.

WAN, Z. et al. Four-dimensional bioprinting: current developments and applications in bone tissue engineering. **Acta Biomateialia**, v 101, p 26 - 42, 2020.

WEI, C.; DING, S. Dual-functional bone implants with antibacterial ability and osteogenic activity. **Journal of Materials Chemistry B**, v. 5, p. 1943–1953, 2017.

WU, J. et al. Simultaneous 3D cell distribution and bioactivity enhancement of bacterial cellulose (BC) scaffold for articular cartilage tissue engineering. **Cellulose**, v. 26, n. 4, p. 2513–2528, 2019.

WUBNEH, A. et al. Current state of fabrication technologies and materials for bone tissue engineering. **Acta Biomaterialia**, v. 80, p. 1 - 30, 2018.

YU, W. et al. Evaluation of zinc-doped mesoporous hydroxyapatite microspheres for the construction of a novel biomimetic scaffold optimized for bone augmentation. **International Journal of Nanomedicine**, v. 12, p. 2293–2306, 2017.

ZDARTA, J. et al. Immobilization of cellulase on a functional inorganic – organic hybrid support : stability and kinetic study. **Catalysts Article**, v. 7, n. 12, p. 374, 2017.

ZIMMERMANN, K. A. et al. Biomimetic design of a bacterial cellulose/hydroxyapatite nanocomposite for bone healing applications. **Materials Science and Engineering C**, v. 31, n. 1, p. 43–49, 2011.

3 **CHAPTER:** Based on the article submitted to the journal Macromolecular Symposia.

Evaluation of potential biomaterials with osteogenic properties and antimicrobial activity

Bacterial nanocellulose (BNC) membranes have high water holding capacity, interconnected porous nanostructures and excellent biocompatibility. The functionalization of these, with sources of calcium phosphate and metal ions, can stimulate osteogenesis and also prevent infections. This study aims to synthesize and characterize BNC membranes, functionalize them with copper and magnesium apatites, and perform antimicrobial and cytotoxic assays. Membranes were synthesized for 8 days in Mannitol Medium. The functionalization of apatites occurred through successive immersion cycles. The biocomposites were characterized by porosity analysis, Fourier transforms infrared spectroscopy (FTIR), scanning electron microscopy (SEM), thermogravimetric analysis (TGA), antimicrobial and cytotoxicity assays. The FTIR and SEM results showed phosphate groups were incorporated into the BNC. The TGA analysis also indicated the incorporation of the inorganic phase. The membrane functionalization with Cu improved the antimicrobial properties of the biomaterial; however, the biomaterials incorporated with Mg had a less harmful behavior on cell viability, proving to be more suitable for implantable materials.

Keywords: Bacterial nanocellulose, apatites, biocomposites, osteogenesis, antimicrobial properties.

3.1 Introduction

More and more people have been facing health problems related to bone defects resulting from trauma, tumors, infections and degenerative diseases (MAIA et al., 2021; ZOU et al., 2019). The healing process of bone fractures is considered a regenerative and biologically complex process (PEREIRA et al., 2020). Autologous bone grafts have been pointed out as the primary solution (ZOU et al., 2019). However, there may be a risk of infections, the need for a second surgery for removal, and chronic pain; another option is an allograft. However, this carries the risk of transmission of infectious diseases and rejection (FILIPPI et al., 2020).

In this context, guided bone regeneration (GBR) appears as an alternative to stimulate and guide bone regeneration. Luz et al. (2020) considered one of the most

effective and reliable methods to promote bone restructuring. This technique is widely used in periodontal, alveolar, and implant surgery (FLORJANSKI et al., 2019; GUO et al., 2020; LIAN et al., 2020; LUZ et al., 2018).

The membrane used for GRO needs to be biocompatible, safe, non-allergenic, non-toxic, and mechanically stable. On top of that, it has an appropriate degradation rate that allows bone reconstruction and is preferably capable of integrating into tissues, transferring nutrients and increasing tissue adhesion (FLORJANSKI et al., 2019). For this reason, different biomaterials have been studied, such as collagen, chitosan and bacterial nanocellulose (BNC) membranes and synthetic biomaterials such as ceramics, composites, and metals, which function correctly as a physical barrier in this technique. BNC membranes stand out as biomaterial with excellent characteristics for osteogenic applications among the natural polymers studied (MAIA et al., 2021).

BNC is an extracellular polysaccharide produced by some bacterial genera, such as *Acetobacter*, *Komagataeibacter*, *Rhizobium*, and *Salmonella* (RANGASWAMY; VANITHA; HUNGUND, 2015), especially the species of *Komagataeibacter* (RYNGAJŁŁO et al., 2019). With randomly arranged nanofibrils, many hydroxyls constitute a porous matrix capable of retaining a significant water content, behaving like a hydrogel similar to the extracellular matrix. Its surface allows the adsorption of metallic ions or metallic nanoparticles (ARAÚJO et al., 2018). It has low rejection and inflammatory reaction due to its excellent biocompatibility, good permeability, hygroscopicity, and flexibility, allowing its wide use in tissue engineering as a scaffold (PANG et al., 2020). However, BNC alone does not have all the properties necessary to act as a device for a bone implant. In this context, the incorporation of hydroxyapatite in the BNC matrix is studied, as this bioceramic provides bone binding and biocompatibility properties (MAIA et al., 2021).

Hydroxyapatite (HAp) is the main inorganic compound of teeth and bones, and because it is bioceramic, it has excellent biocompatibility (SIMON et al., 2019), non-toxic and high osteoconductivity (CHOCHOLATA; KULDA; BABUSKA, 2019). The chemical similarity of HAp to naturally existing bone matrix, coupled with its bioactive material, makes it highly attractive for use in bone regeneration and implantation (SIMON et al., 2019; TORGBO; SUKYAI, 2019).

The biocomposite of bacterial nanocellulose and hydroxyapatite (BNC/HAp) is formed by the porous membrane reinforced with HAp crystals. This structure allows this material to promote vascularization and trigger the fixation and proliferation of bone cells at the defect site (MAIA et al., 2021). In addition, since the HAp particles are physically attached to the cellulose fibers, these particles do not migrate to neighboring areas, preventing damage that could be caused to the surrounding soft tissues (HUTCHENS et al., 2006; LUZ et al., 2018). However, this composite does not have antimicrobial activity, so some metal ions can be added to improve the properties of this material (MAIA et al., 2021), such as cerium, copper, silver, and zinc (NAM et al., 2018) and magnesium.

Copper (Cu) is an essential micronutrient involved in the immune system and has bacteriostatic and antibacterial effects, modifying cell permeability and eventually leading to bacterial cell death (HIDALGO-ROBATTO et al., 2018). In addition, it can stimulate angiogenic properties, assist in the regulation of bone resorption rate and increase the deposition of collagen fibers, attributing several functionalities when incorporated into HAp (AI et al., 2020; HIDALGO-ROBATTO et al., 2018).

Magnesium (Mg) is also an essential trace element; it acts in bone resorption processes and stimulates the proliferation of osteoblasts (GOPI; SHINYJOY; KAVITHA, 2014). In addition, the degradation product (Mg^{2+}) is a standard component of the human body and has antitumor and antibacterial characteristics, reducing the risk of infections and the need for further surgeries (SABET; JABBARI; SEDIGHI, 2018; XU et al., 2019). Using Mg-functionalized HAp is essential in developing bone substitutes because Mg^{2+} combined with natural calcium phosphate helps the spontaneous formation of bone bonding *in vivo* (PREDOI et al., 2019), which can alter the metabolism mineral, resulting in the modification of the dissolution rate of the crystals and the biodegradation of the related materials (VRANCEANU et al., 2020).

In this context, this work aimed to synthesize and characterize BNC membranes functionalized with copper and magnesium apatites, seeking to produce a biocomposite for application in GBR and evaluate its antimicrobial activity and cytotoxicity.

3.2 Methodology

3.2.1 Materials

The culture medium used in this work consisted of mannitol (Kinetics), bacteriological peptone (Himedia), yeast extract (Kasvi), citric acid (Audaz) and disodium phosphate (Synth). NaOH (Scientific Exodus) was used for the purification of the BNC membrane and the preparation of apatites $CaCl_2$ (Dynamic), $MgCl_2$ (Dynamic) and $CuCl_2$ (Dynamic).

3.2.2 Membrane production

The bacterium *Komagataeibacter hansenii* ATCC 23769 was used for the biosynthesis of BNC membranes. The culture medium used was the Mannitol Medium (MM), consisting of (g L^{-1}): 20 g mannitol, 5 g peptone, 5 g yeast extract, and 2.7 g disodium phosphate. The cells were activated in an Erlenmeyer flask (500 mL) containing 200 mL of medium and incubated at 30 °C under static conditions for two days. After this period, the pre-inoculum was transferred to the culture medium at a 20% (v/v) rate with an optical density equal to 1 (λ = 600 nm). This step was carried out in 250 mL Erlenmeyer flasks with 50 mL of culture medium at 30 °C and static condition for 9 days to form BNC membranes.

3.2.3 Membrane purification

Aiming purifies the BNC formed on the surface of the liquid culture; the membranes were removed, washed with distilled water, and treated with a 0.1 M NaOH solution at 80°C for 60 min to remove bacterial cells and other impurities. After that, the membranes were washed with distilled water until reaching pH 7, sterilized, and stored in a refrigerator (TEIXEIRA et al., 2019).

3.2.4 Production of biocomposites

The biocomposites functionalized with Mg and Cu were produced according to the methodology described (HUTCHENS et al., 2006). The BNC membranes, never dried, were immersed in $MgCl_2$ and $CuCl_2$ solutions in different proportions concerning the $CaCl_2$ solution for 24 h under agitation in an orbital shaker at 26 °C and 85 RPM. Subsequently, the membranes were washed with distilled water to remove residues from the previous step and then immersed in a Na_2HPO_4 solution for another 24 h. Three immersion cycles were performed in each solution (Figure 3.1). The biocomposites formed were BNC/MgHAp and BNC/CuHAp.

Figure 3.1: Scheme demonstrating the concentration of solutions used in immersion cycles for the formation of biocomposites.

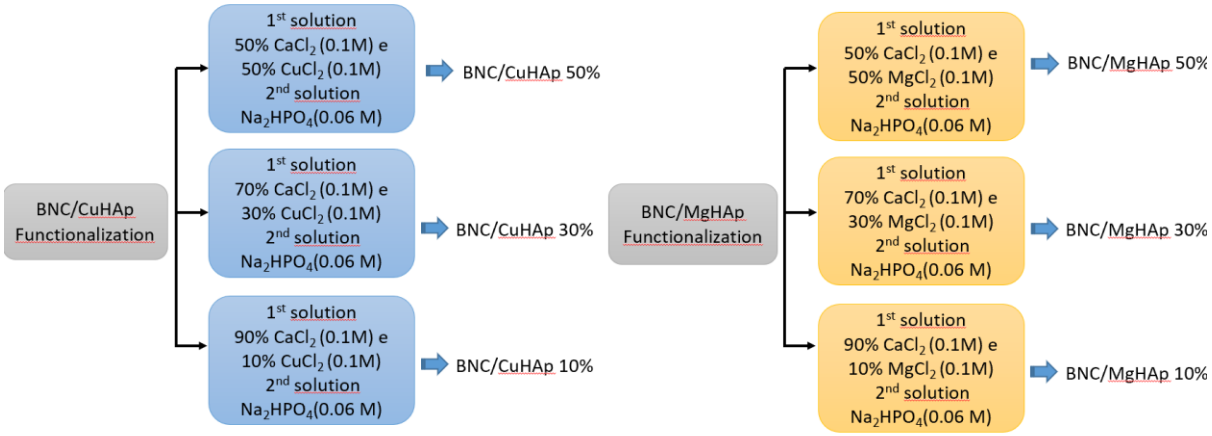

3.2.5 Characterization techniques

BNC membranes and biocomposites were lyophilized (Terroni, LT) and then characterized by porosity techniques, Fourier transform infrared spectroscopy with attenuated total reflectance enhancement (FTIR/ATR), scanning electron microscopy with energy dispersive spectroscopy (SEM/EDS) and thermogravimetric analysis (TGA).

3.2.5.1 Determination of porosity

The samples were weighed previously wet and after drying by lyophilization for 24 hours. According to Zeng and Ruckenstein (1996), the porosity of biomaterials was determined through Equation 1.

$$\varepsilon\,(\%) = \frac{(m_1 - m_2)/\rho_{\text{water}}}{v} \times 100 \qquad (1)$$

Where ε is the porosity of the membrane, m_1 and m_2 are the masses (g) of the wet and dry membrane, respectively, ρ_{water} is the specific mass of water obtained at 20 ºC, which is equivalent to 0.9982 g/cm^3, and v is the volume (cm^3), calculated using Equation 2.

$$v = \frac{\pi \times D^2 \times h}{4} \qquad (2)$$

Where D represents the diameter (cm), and h refers to the thickness (cm) of the membrane.

The samples were analyzed in triplicate and submitted to analysis of variance (ANOVA) using the OriginPro® 8.5 software.

3.2.5.2 Fourier transform infrared spectroscopy with attenuated total reflectance (FTIR/ATR)

Thirty-two scans were performed per sample from 4000 to 500 cm^{-1}, resolution of 4 cm^{-1}, using the attenuated total reflectance module (ATR) in a spectrometer (Perkin-Elmer, Frontier).

3.2.5.3 Scanning electron microscopy with energy dispersive spectroscopy (SEM/EDS)

The samples were fixed on metallic supports and covered with gold. The equipment used was a scanning electron microscope (JEOL, model JSM-6390LV). An

electron beam bombarded the samples, and the X-rays emitted from the samples were detected by a silicon solid-state detector device for a point elemental analysis of the sample.

3.2.5.4 Thermogravimetric analysis (TGA)

The TG and DTG curves were obtained using the TGA-Q50/TA Instruments. The samples were heated from 25°C to 600°C at a 10°C/min rate under an oxidizing atmosphere.

3.2.6 Antimicrobial properties assay

The antimicrobial properties assay was performed using the disk diffusion technique of Bauer et al. (1966), using Müeller Hinton (MH) medium with the microorganisms *Staphylococcus aureus* and *Escherichia coli* (species of gram-positive and gram-negative bacteria, respectively) activated for 24 h at 37ºC, in brain heart infusion (BHI) broth. Cell concentration was determined on the Mac Farland scale (according to 0.5 tube of the Mac Farland scale, turvation standard) standardizing the absorbance at 0.28.

Inoculation was performed with a swab to allow the formation of a microbial mat in the Petri dishes. Then, discs of the produced biocomposites (identifying them with the percentage of incorporation element). One disc of pure BNC in each plate as a control (BR) was placed on the inoculated cells and incubated at 37 °C for 24 h. The analysis was carried out in duplicate.

3.2.7 Cytotoxicity analysis

Mouse fibroblast cells (L929) were maintained in Dulbecco's Modified Eagle's Medium (DMEM) medium supplied with 10% FBS and 1% antibiotics. Cells were cultured in an incubator with 5% CO_2 at 37 °C and 95% humidified air during the *in vitro* tests. In vitro cytotoxicity of the sample was performed in L929 cells through the direct contact method (Aguilar et al., 2021). The L929 cells were seeded in 24-well culture plates, containing 100 µL of medium, with $4.0 \cdot 10^4$ cells/well (Corning Life

Sciences). After 24 h, samples were added (one 0.5 mm diameter disk per well, previously sterilized), the test was conducted in triplicate. Cells were incubated for 24 h at 37 °C and 5% CO_2. After each cultivation time, the culture medium and samples were removed. Then, the cells were washed with PBS, and cell viability was measured using an MTS assay. Then, the remaining medium was transferred into 96 well plates to measure optical density at a wavelength of 490 nm using a spectrophotometer (Molecular Devices). The metabolic activity was calculated concerning the sample control.

3.3 Results and Discussion

3.3.1 Synthesis of the BNC membrane

The BNC membrane was formed after eight days of cultivating the bacterium *Komagataeibacter hansenii*, with a thickness varying between 2 and 3.5 mm (Figure 3.2A). After purification, the membranes had a gelatinous appearance in the form of a translucent hydrogel (Figure 3.2B). On the other hand, lyophilization brought a spongy characteristic to the membrane (Figure 3.2C).

Figure 3.2: Bacterial nanocellulose membranes: A) biosynthesis, B) after purification, and C) after lyophilization.

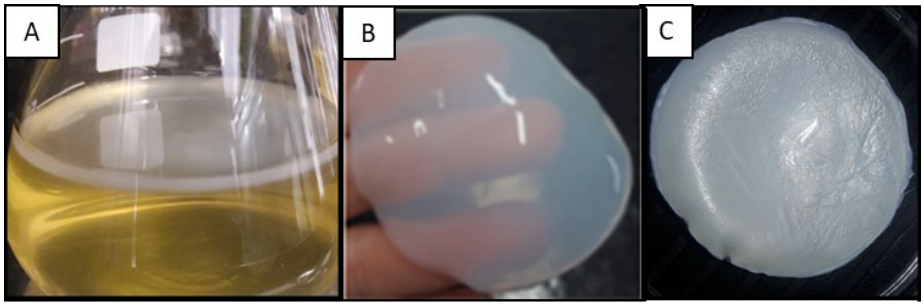

3.3.2 Production of biocomposites

The biocomposites were produced by immersion cycles in hybrid solutions containing $CaCl_2$ and $MgCl_2$ or $CuCl_2$ and Na_2HPO_4. The biocomposites formed

showed a change in color according to the percentage of the incorporated element (Mg or Cu) (Figure 3.3), and from then on, they were called BNC/CuHAp and BNC/MgHAp.

Figure 3.3: Image of the biocomposites formed at different concentrations: A) BNC/MgHAp 50%; B) BNC/MgHAp 30%; C) BNC/MgHAp 10%; D) BNC/CuHAp 50%; F) BNC/CuHAp 30%; G) BNC/CuHAp 10%.

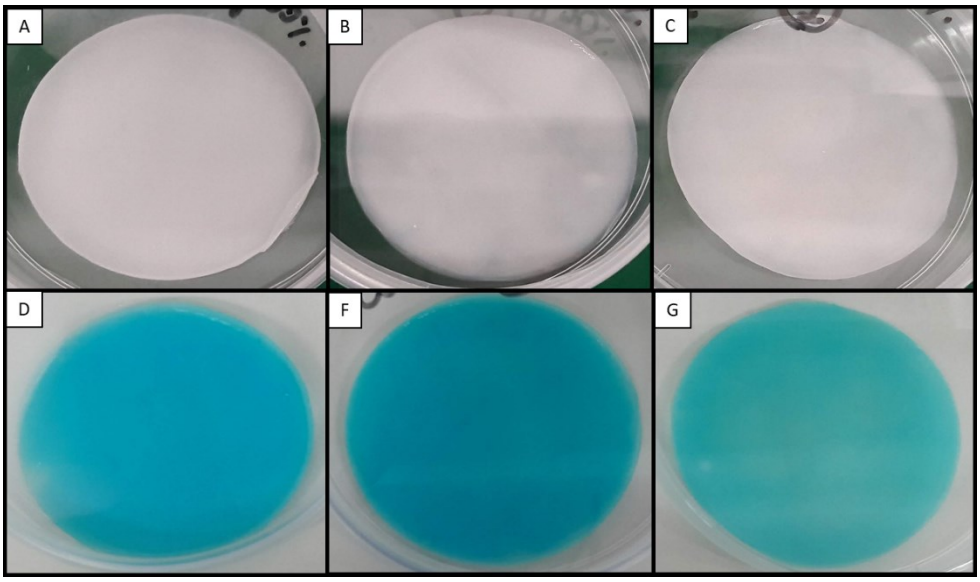

The biocomposites obtained were lyophilized to maintain pore integrity and provide an environment conducive to the migration and cell adhesion of this material when implanted. According to Kim et al. (2015), the greater the porosity, the better the permeability of the material, which will facilitate vascularization, its gas exchange and the transport of nutrients to the cells, thus increasing the possibility of successful tissue regeneration.

3.3.3 Characterization techniques

3.3.3.1 Determination of porosity

Determining the porosity of the biomaterials helps interpret the data obtained in the subsequent tests since the pores favor the adsorption phenomena (LUZ, 2016).

BNC has a highly porous structure (96%) (Table 3.1), and incorporating inorganic material can affect this characteristic. According to Jin et al. (2012), the pore

size of the matrix decreases with increasing hydroxyapatite mass, and eventually, accumulations may occur in the pore structure. However, the biocomposites formed from the BNC by the immersion technique would be expected to maintain good porosity.

Table 3.1: Porosity of the tested biomaterials.

% of incorporation	m_u	m_s	ε (%)	m_u	m_s	ε (%)	Average	Standard deviation
BNC	8.84	0.08	96.97	8.76	0.07	95.21	96.09	±0.88
BNC/Cu HAp 50%	7.71	0.40	86.38	7.25	0.39	80.96	83.67	±2.71
BNC/CuHAp 30%	4.60	0.29	76.37	5.87	0.32	78.61	77.49	±1.12
BNC/CuHAp 10%	5.64	0.30	75.64	7.41	0.36	83.28	79.46	±3.82
BNC/MgHAp 50%	6.71	0.30	87.31	7.11	0.31	80.37	83.84	±3.47
BNC/MgHAp 30%	5.05	0.28	84.58	6.50	0.35	87.23	85.91	±1.32
BNC/MgHAp 10%	6.14	0.35	81.96	8.30	0.42	79.78	80.87	±1.09

The concentration of metal ions did not significantly influence the porosity values. However, Figures 3.4A and 3.4B show an average reduction of 15% in the average porosity percentage of the biocomposites concerning BNC, suggesting the deposition of inorganic material.

Figure 3.4: Average percentage of porosity of the biocomposites: in A) BNC/MgHAp and in B) BNC/CuHAp.

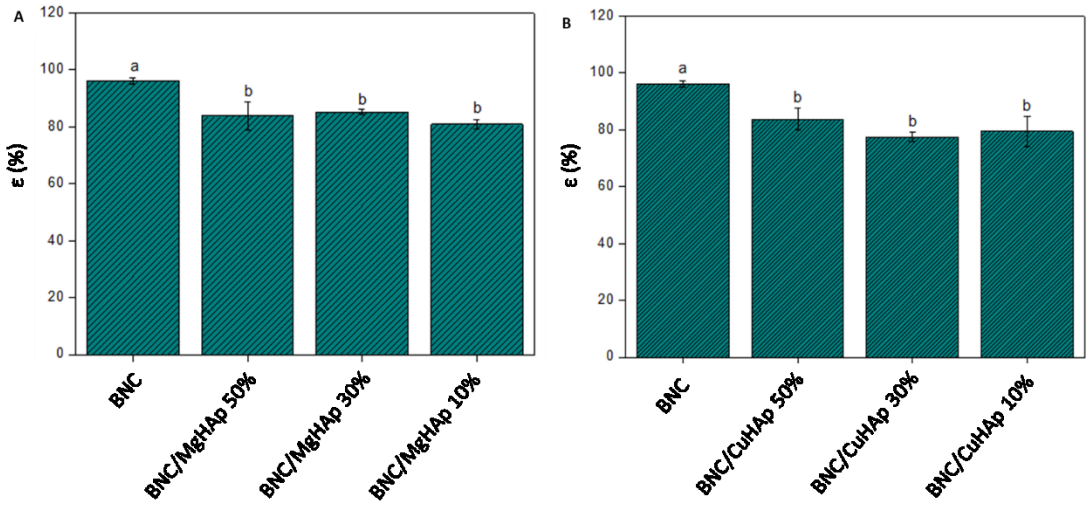

This result suggests that metallic apatite deposition occurred superficially and inside the BNC. The biocomposites still maintained a high percentage of average porosity (± 80%).

Luz (2016), in his study with BNC/CaHA/Sr and BNC/SrAp biocomposites, also observed an average porosity of 72% and 83%, respectively. The author attributed this difference to the methodology used to obtain the materials. In the first case, the sample was obtained as BNC/CaHA and doped with Sr in more immersion cycles. In contrast, there was only cationic substitution in the immersion solutions in the second case, as in this study.

This characteristic is essential for implantable biomaterials because it helps anchor cells and contributes to distributing nutrients and growth or differentiation factors to cells.

3.3.3.2 Fourier transform infrared spectroscopy with sttenuated total reflectance (FTIR/ATR)

The FTIR spectrum (Figure 3.5) characteristic of pure BNC is marked by bands in the region of 3345 cm^{-1}, which according to He et al. (2012), is characteristic of the stretching of the hydroxyl groups present in BNC. In addition, the CH stretching and asymmetric stretching at 2897 cm^{-1}, CH_2 deformation at 1427 cm^{-1}, OH deformation at 1315 and 1359 cm^{-1}, as well as the antisymmetric bridge of the C-O-C stretch at 1109 and 1162 cm^{-1} and the band in the region of 1056 cm^{-1} related to the vibrations of the C-O stretch are characteristic of BNC (Table 3.2). Another exciting band located around 400 to 700 cm^{-1}, is characteristic of the torsion of the OH groups.

The bands at 1030 cm^{-1} and 962 cm^{-1}, related to PO_4, were observed in all biomaterials formed (Figure 3.5), although only one of the two bands was observed in some cases (Table 3.2). According to Hutchens et al. (2006), these two bands may represent the elongation mode of the phosphate group vibration, which can overlap the BNC membrane groups at wavelengths between 1000 and 1100 cm^{-1}.

Figure 3.5: FTIR spectra obtained for BNC membranes and BNC/MgHAp and BNC/CuHAp biocomposites.

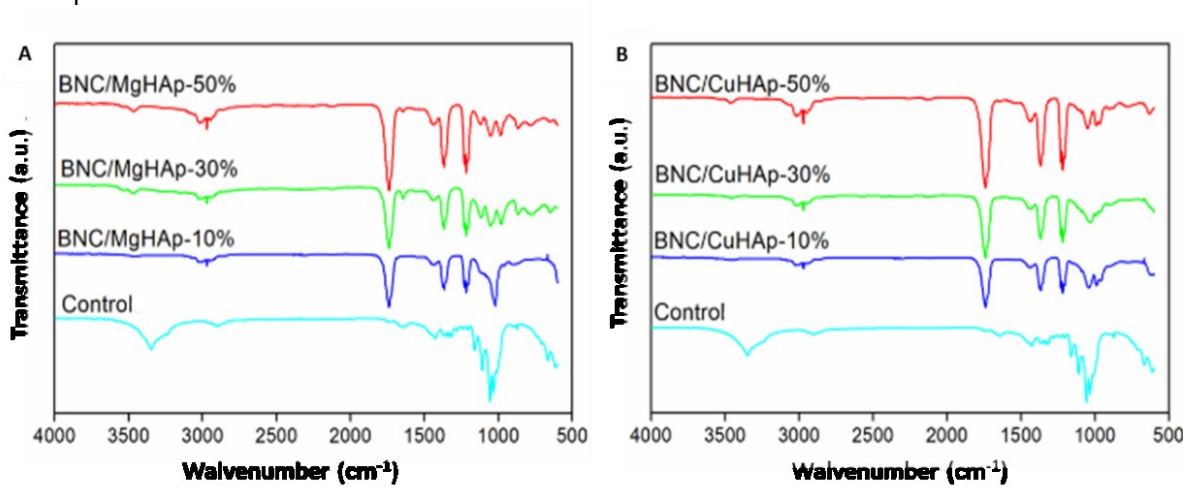

Table 3.2: Peaks observed in the FT-IR/ATR analysis for the biocomposites of BNC/HAp, BNC/CuAp and BNC/MgAp.

Vibrational frequencies	BNC	BNC/ HAp	BNC/ CuHAp 50%	BNC/ CuHAp 30%	BNC/ CuHAp 10%	BNC/ MgHAp 50%	BNC/ MgHAp 30%	BNC/ MgHAp 10%	Literature
OH stretching	3348	3375	3462	3355	3457	3468	3464	3460	(HUANG et al., 2015)
CH stretching of CH_2 and CH_3 groups	2998	---	2949	2931	2933	2933	2934	2933	(AN et al., 2017)
Water OH bending	1648	1620	1644	1624	1645	1648	1645	1643	(HUANG et al., 2015)
H-C-H deformation	1428	1427	1437	1436	1427	1436	1435	1437	(HUANG et al., 2017)
Antisymmetric bridge C–O–C stretching	1161	1161	1155	---	1154	1119	1117	---	(HUANG et al., 2017)
C–O strecthing	1110		1111	1092	1092	1092	---	1110	(HUANG et al., 2017)
C–O C-C strecthing	1057	---	1050	---	1043	1053	1054	---	(HUANG et al., 2017)
Asymmetric stretching vibration of P–O bond	---	1021	--- 966	1030 963	--- 963	--- 961	--- 980	1022 964	(FAVI et al., 2016; HUANG et al., 2015)
Stretching mode of CO_3^{2-}		880	875	878	878	871	871	876	(BOYD et al., 2015b)

Another band at 873 cm^{-1} was observed in the analyzed samples, corresponding to the carbonate ion (CO_3^{2-}), indicating that part of the phosphate group incorporated into the BNC was replaced by carbonate. It is suggested that this substitution was due to the carbon dioxide present in the air since the analyzes were carried out under atmospheric conditions. Wan et al. (2011) considered that the composition and structure of the incorporated carbonate produce an apatite similar to that found in natural bone. Table 1 also describes other peaks referring to BNC and biocomposites.

3.3.3.3 Thermogravimetric analysis (TGA)

Figure 3.6 shows the TG and DTG curves obtained for BNC and Mg and Cu apatites. According to Wan et al. (2011), the behavior obtained for the BNC corresponds to the typical gravimetric curve of bacterial nanocellulose. Pure BNC presented the first stage of mass loss of 1.77%, which refers to the loss of water present in the sample. The second stage took place at a T_{max} of 316 ºC (Table 3.3), and in this stage, the highest percentage of mass loss of the sample occurred, equivalent to 74.38%, which is related to the degradation of cellulose. The last stage of degradation for the BNC sample showed a mass loss of 17.19%, occurred at a T_{max} of 494 ºC and was related to carbonaceous residues' degradation (BARUD et al., 2011; LIMA et al., 2015).

The stages of thermal degradation observed in the curves of Figure 3.6 was extracted and displayed in Table 3.3, which presents the data on the maximum temperature of degradation (T_{max}) and the percentage of mass loss for each stage of degradation.

The samples of BNC/MgHAp50%, BNC/MgHAp30%, BNC/MgHAp10% and BNC/CuHAp10% showed an additional stage of mass loss of 6.6%, 7.1%, 1.6% and 2.0%, respectively, with T_{max2} around 180 ºC. Araújo *et al.* (2016) attributed the water's vaporization to the crystallization of HAp.

Figure 3.6: TG (A and C) and DTG (B and C) curves for BNC and BNC/MgHAp and BNC/CuHAp biocomposites.

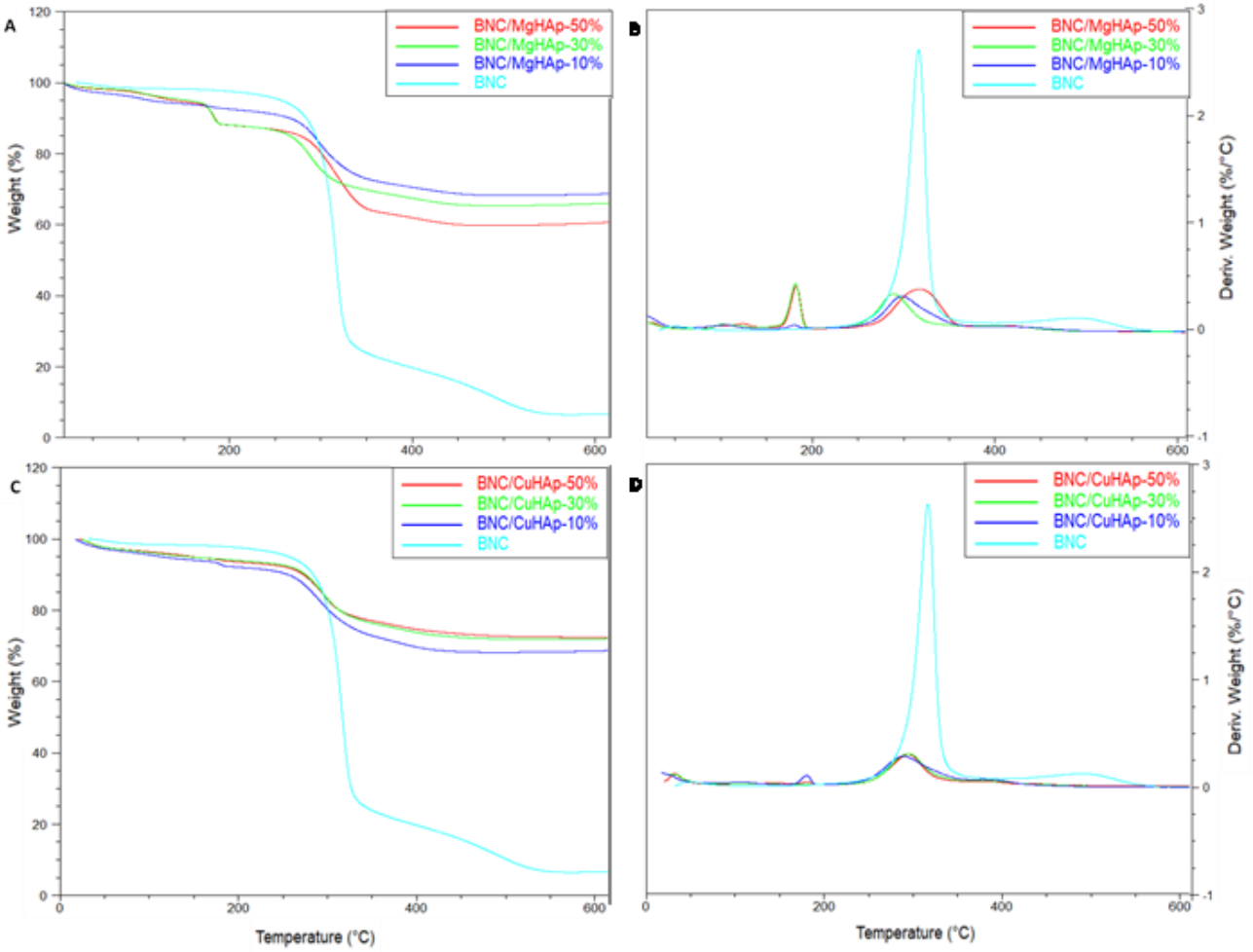

The T_{max3} presented by BNC was 316 ºC, while for biocomposite, was around 290 ºC (Table 3.3). According to Saska et al. (2011), this can be associated with broken hydrogen bonds to form apatites. Another feature that stands out is the high percentage of residue at the end of the test; which for all biocomposites produced presented a value greater than 60%. This result can be attributed to the inorganic material in the sample because the analysis was performed in an oxidizing atmosphere (BARUD et al., 2011), which, according to Saska et al. (2011), confirms the incorporation of the desired phosphate sources on the BNC membrane. In this context, it is interesting to note that the lower the concentration of Mg or Cu added, the higher

the percentage of residue, which may represent a possible competition between these elements e the Ca, during the immersion cycles.

Table 3.3: Maximum degradation temperature (T_{max}) and percentage of mass loss data, obtained from the TG and DTG curves of the BNC and BNC/CuHAp, and BNC/MgHAp samples.

Sample	Mass loss $_1$ (%)	Mass loss $_2$ (%)	Tmáx$_2$ (°C)	Mass loss $_3$ (%)	Tmáx$_3$ (°C)	Mass loss $_4$ (%)	Tmáx$_4$ (°C)	Residue (%)
BNC	1.8	-	-	74.4	316.5	17.2	493.9	6.58
BNC/ MgHAp50%	5.3	6.6	182.4	23.6	316.4	4.4	368.4	60.45
BNC/ MgHAp30%	4.8	7.1	181.6	17.8	288.7	4.7	473.9	65.91
BNC/ MgHAp10%	5.9	1.6	180.5	19.5	297.9	4.7	374.1	68.58
BNC/ CuHAp50%	4.0	-	-	16.9	294.7	5.6	417.4	72.33
BNC/ CuHAp30%	5.2	-	-	16.9	294.0	5.8	354.1	72.01
BNC/ CuHAp10%	5.9	2.0	180.4	17.3	288.1	6.5	394.0	68.56

3.3.3.4 Scanning electron microscopy with energy dispersive spectroscopy (SEM/EDS)

In Figure 3.7A, it is possible to observe the morphology of the BNC obtained by SEM, with nanofibers randomly arranged in a three-dimensional structure, forming a highly porous structure. This condition allows the migration of osteogenic cells and assists in bone regeneration and tissue healing (LUZ, 2016; TU et al., 2017).

In the BNC/MgHAp biocomposites with 10%, 30% and 50% M (Figure 3.7B - D), the phosphate crystals formed were in the form of plates deposited on the BNC nanofibril network but with low interaction with them.

The energy scattering X-ray spectroscopy (EDS) result confirmed the presence of calcium, magnesium and phosphorus elements (Figure 3.7H).

Figure 3.7: Micrographs of the surface of the membrane of BNC (A) and of the biocomposites incorporated with Mg: B) BNC/MgHAp50%; C) BNC/MgHAp30%; D) BNC/MgHAp10%; E) BNC/CuHAp 50%; F) BNC/CuHAp 30% and G) BNC/CuHAp 10%. In (H) and (I) are presented the EDS of surfaces of samples with Mg and Cu.

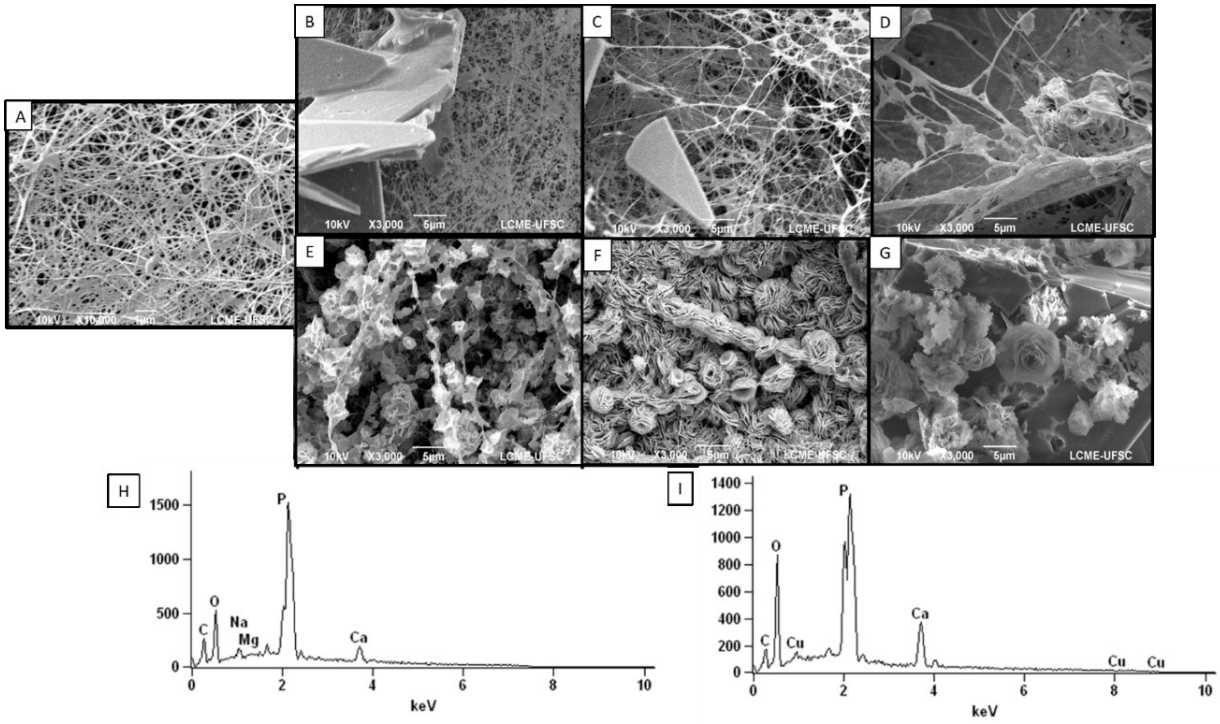

According to Neto (2015), the formation of HAp depends on the diffusion and adsorption of OH^-, Ca^{2+} and PO_4^{3-} ions. Thus, at more acidic pH, the adsorption of OH^- ions is limited, and the most common morphological growth presents the phosphate crystals in the form of plaques. They observed that when the synthesis of HAp was carried out at pH 6, the formation of brushite and monetite was obtained. In this work, BNC was immersed in solutions of $CuCl_2$, $MgCl_2$ and $CaCl_2$ with pH between 4 and 5 and Na_2HPO_4 at pH 8, which may have enabled the formation of apatite precursor phases.

The morphology of the BNC/CuHAp biocomposites can be seen in Figures 3.7E-G. The energy scattering X-ray spectroscopy (EDS) result also confirmed the presence of calcium, copper and phosphorus elements (Figure 3.7I). In images 3.7E and F, it is possible to observe the nanofibrils of the BNC but with the deposition of the inorganic material with lamellar crystalline form or rosettes referring to the compositions BNC/CuHAp 30% and 50%. Interestingly, in the 3.7F image, the

biomaterial with 30% Cu showed a denser crystalline formation, covering the entire surface of the BNC. While in the BNC/CuHAp10% sample (Figure 3.7F), there was a second flat crystalline form in addition to the already described as lamellar or rosettes.

In immersion cycles, Hutchens et al. (2006) produced different Ca-deficient HAp BNC (CdHAp) compositions. The authors observed the formation of crystallites with a needle or lamellar morphology that resembles the "rosette" structure, highlighting the similarity with the structures of apatite found in physiological bone. They found that this "rosette" structure implies that apatite was nucleated from a distinct location on the BNC nanofibrils. Furthermore, at higher concentrations of CdHAp, the particles appeared to have a larger and rougher texture, indicating that the molecules of CdHAp provided secondary nucleation sites for additional apatite formation. This characteristic was also observed in the 3.7F image of this work (BNC/CuAp30%). They also observed that the distinct arrangement of the BNC nanofibers appears to have guided the growth of apatite in clusters, which can also be seen in images 3.7E and F.

3.3.4 Antimicrobial properties

For implantable biomaterials, it is essential to take care of infections caused by the association of bacteria on the biomaterial's surface. Thus, inhibiting bacterial adhesion to the biomaterial is considered a critical step for preventing infections caused by implants (HETRICK; SCHOENFISCH, 2006).

Hidalgo-Robatto *et al.* (2018) state that the microorganisms that can most cause infections in implants of biomaterials are *Staphylococcus aureus* and *Staphylococcus epidermidis* (Gram-positive), *Pseudomonas aeruginosa*, and *Escherichia coli* (Gram-negative).

Figure 3.8 shows the result of the antimicrobial susceptibility test with the BNC/MgHAp and BNC/CuHAp biocomposites after 24 h of incubation at 30 ºC with the microorganisms *Escherichia coli* and *Staphylococcus aureus*. The absence of inhibition halos in the samples containing Mg indicates that these samples did not show an antimicrobial effect. On the other hand, all compositions of BNC/CuHAp

biocomposites showed inhibition halos that varied between 11 and 13 mm in diameter (Table 3.4).

Figure 3.8: Antimicrobial susceptibility test of the BNC/MgHAp and BNC/CuHAp biocomposites against the microorganisms *Escherichia coli* and *Staphylococcus aureus*.

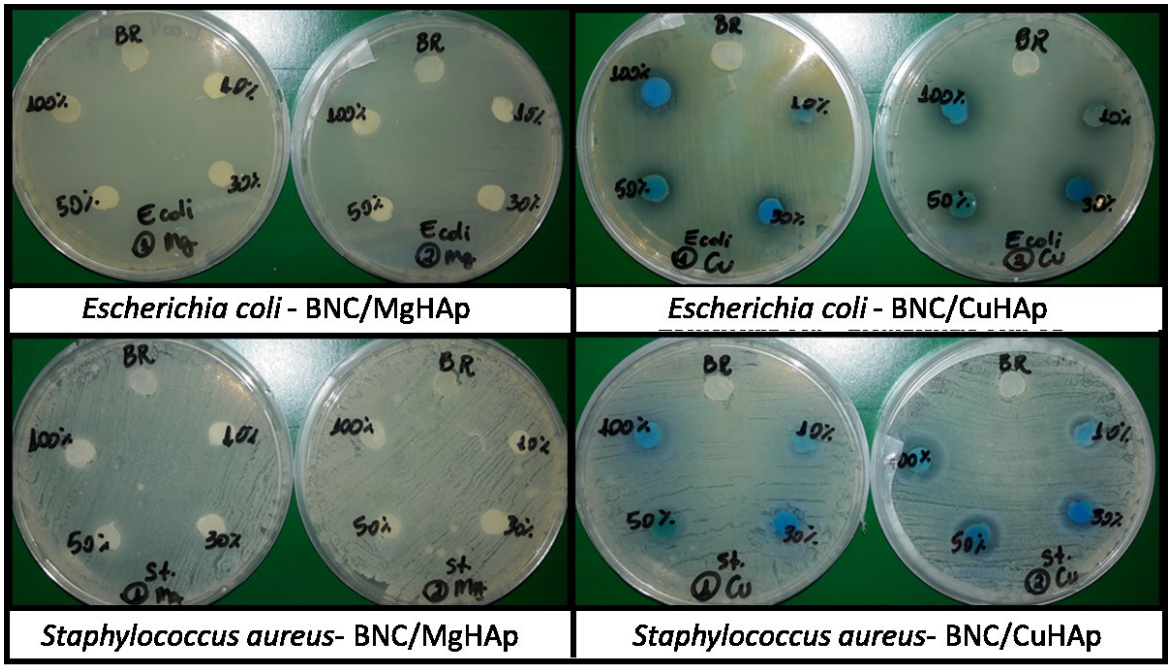

Mg is essential for life, playing critical roles as an enzyme cofactor and being involved in cell signaling and stabilizing cellular components. However, new information has emerged about the antibacterial effect of magnesium. Studies raised and reported by Demishtein, Reifen and Shemesh (2019) propose that magnesium affects cell membrane permeabilization, making bacteria more sensitive. The authors present a survey of different effects on different microorganisms, further highlighting the potential to affect the formation of microbial biofilms. However, in this study, no antimicrobial effect of Mg was observed on the microorganisms tested in any of the concentrations used.

On the other hand, Cu showed greater antibacterial activity, as seen in the formation of inhibition halos for *E. coli* and *S. aureus* bacteria (Figure 3.8 and Table 3.4). Liu et al. (2016) performed a study with Cu-Mg metal alloys for guided bone regeneration. They observed that the greater the degree of Cu release, the greater the

antibacterial capacity. Araújo et al. (2018) point out that the Cu(II) ion can act on microorganisms by different mechanisms, breaking the plasma membrane, blocking biochemical pathways, forming complexes with proteins and even causing DNA damage.

Table 3.4: Diameter (mm) of the inhibition halo for the antimicrobial susceptibility test to biomaterials.

	Inhibition halo (mm)	
Sample	***E. coli***	***S. aureus***
BNC/MgHAp50%	**-**	**-**
BNC/MgHAp30%	**-**	**-**
BNC/MgHAp10%	**-**	**-**
BNC/Cu HAp50%	11.5 ± 0.5	12.5 ± 0.5
BNC/CuHAp30%	13.0 ± 1.0	11.0 ± 1.0
BNC/CuHAp10%	11.0 ± 1.0	11.5 ± 0.5

3.3.5 Cytotoxicity analysis

A preliminary cytotoxicity assay is one of the critical assessments of the biological properties of biomaterials before in vivo assessment (LIN et al., 2015). According to ISO 10993-5:2009 (ISO/EN10993-5, 2009), if the cell viability is greater than 70% compared to the control group, the material is considered non-cytotoxic.

The cell viability results of the MTS tests, evaluating the cytotoxicity of the BNC/MgHAp and BNC/CuHAp biocomposites during the incubation period of 1, 3 and 7 days, are presented in Table 3.5.

The biocomposites containing Cu (BNC/CuHAp) showed a slightly negative effect on the first analysis day, reducing the cellular metabolic activity to 90%, but

remaining above 70%. In contrast, the biomaterials containing Mg (BNC/MgHAp) practically showed no change in the control group.

Table 3.5: Cell viability resulting from the cytotoxicity analysis of the biomaterials produced.

Sample	1 day Cell viability (%)	Standard deviation	3 days Cell viability (%)	Standard deviation	7 days Cell viability (%)	Standard deviation
BNC	100.00	0.02	100.00	0.02	100.00	0.18
BNC/MgHAp50%	100.27	0.02	101.72	0.01	55.41	0.03
BNC/MgHAp30%	100.27	0.02	103.25	0.02	100.56	0.15
BNC/MgHAp10%	101.47	0.01	108.32	0.01	52.46	0.06
BNC/CuHAp50%	90.14	0.01	50.00	0.06	35.93	0.02
BNC/CuHAp30%	90.60	0.02	77.27	0.12	35.53	0.01
BNC/CuHAp10%	90.40	0.02	45.07	0.19	37.73	0.01

After 3 days of testing, the Cu samples showed a cytotoxic effect, except for the BNC/CuHAp30% sample, which remained at 77.27%. In contrast, all samples with Mg maintained the same behavior presented at the beginning of the experiment, remaining similar to the control group.

After 7 days, all BNC/CuHAp samples confirmed a negative effect on cell viability dropping to about 35%. The samples containing BNC/MgHAp started to show a more diversified behavior; the sample BNC/MgHAp30% maintained the same behavior from the beginning to the end of the assay, while the samples BNC/MgHAp 10% and 50% began to exert a negative effect on cells showing a reduction of about 50% on cellular activity. Thus, the biomaterials functionalized with Mg presented the best performance for the incubation times. Although they did not present an antimicrobial effect, they are better adjusted as an implantable material.

Shanmugam e Gopal (2014) studied the cytotoxic and antimicrobial behavior in hydroxyapatite samples with different concentrations of bismuth and silver in their composition. They observed a correlation between the antimicrobial effect and

cytotoxicity, noting that toxicity increased with increasing concentration in their assays. In this work, the concentrations of Cu and Mg in the biocomposites did not present a concentration-dependent cytotoxic effect. Considering the desired activity, the biocomposites containing Mg had the lowest negative effect on cellular metabolism.

3.4 Conclusion

The BNC membranes presented an excelente template for inserting metallic apatites, offering good porosity and available hydroxyls to make the bonds. The FTIR/ATR, SEM/EDS and TG assays confirmed the presence of phosphate sources in the biocomposites. Incorporating Cu into the apatites promoted the antimicrobial action against *E. coli* and *S. aureus*. However, at the concentrations tested, this element was cytotoxic to fibroblast cells (L929). The biomaterials incorporated with Mg did not show antimicrobial activity; however, they showed a lower cytotoxic effect, especially for BNC/MgHAp30% samples. Among the biocomposites produced, only those incorporated with Mg presented the best implantable materials. Nevertheless, further analysis is still needed to propose a biomaterial with favorable characteristics for application in guided bone regeneration.

3.5 Acknowledgements

The authors are grateful for the financial support of FAPESC and FAP/UNIVILLE for the project and the Central Laboratory of Electron Microscopy Analysis (LCME-UFSC) for the analyses.

3.6 References

Al, F. et al. Hydroxyapatite scaffolds containing copper for bone tissue engineering. **Journal of Sol-Gel Science and Technology**, v. 95, n. 1, p. 168–179, 2020.

AN, S. J. et al. Preparation and characterization of resorbable bacterial cellulose membranes treated by electron beam irradiation for guided bone regeneration. **International Journal of Molecular Sciences**, 2017.

ARAÚJO, I. M. S. et al. Hydrothermal synthesis of bacterial cellulose–copper oxide nanocomposites and evaluation of their antimicrobial activity. **Carbohydrate Polymers**, 2018.

ARAÚJO, P. M. A. G. et al. Avaliação das propriedades estruturais, morfologicas, térmicas e magnéticas da hidroxiapatita para aplicação no tratamento da osteomielite. **In:** 60º Congresso Brasileiro de Cerâmica. Águas de Lindóia, 2016.

BARUD, H. S. et al. Antimicrobial bacterial cellulose-silver nanoparticles composite membranes. **Web of Science**, v. 2011, p. 8, jan. 2011.

BAUER, A. W. et al. Antibiotic susceptibility testing by a standardized single disk method. **American Journal of Clinical Pathology**, v. 45, n. 4_ts, p. 493–496, 1966.

BOYD, A. R. et al. Strontium-substituted hydroxyapatite coatings deposited via a co-deposition sputter technique. **Materials science & engineering. C, Materials for biological applications**, v. 46, p. 290–300, 2015.

CHOCHOLATA, P.; KULDA, V.; BABUSKA, V. Fabrication of scaffolds for bone-tissue regeneration. **Materials**, v. 12, n. 4, 2019.

DEMISHTEIN, K; REIFEN, R.; SHEMESH, M. Antimicrobial properties of Magnesium open opportunities to develop healthier food. **Nutrients**, v. 11, n. 10, p.2363e, 2019.

FAVI, P. M. et al. Preparation and characterization of biodegradable nano hydroxyapatite–bacterial cellulose composites with well-defined honeycomb pore arrays for bone tissue engineering applications. **Cellulose**, v. 23, n. 2, p. 1263–1282, 2016.

FILIPPI, M. et al. Natural polymeric scaffolds in bone regeneration. **Frontiers in Bioengineering and Biotechnology**, v. 8, 2020.

FLORJANSKI, W. et al. Modifications of polymeric membranes used in guided tissue and bone regeneration. **Polymers**, v. 11, n. 5, p. 1–11, 2019.

GOPI, D.; SHINYJOY, E.; KAVITHA, L. Synthesis and spectral characterization of

silver/magnesium co-substituted hydroxyapatite for biomedical applications. **Spectrochimica Acta - Part A: Molecular and Biomolecular Spectroscopy**, 2014.

GUO, H. et al. A pure zinc membrane with degradability and osteogenesis promotion for guided bone regeneration: *In vitro* and *in vivo* studies. **Acta Biomaterialia**, v. 106, p. 396–409, 2020.

HE, M. et al. Structure and properties of hydroxyapatite/cellulose nanocomposite films. **Carbohydrate Polymers**, v. 87, n. 4, p. 2512–2518, 2012.

HETRICK, E. M.; SCHOENFISCH, M. H. Reducing implant-related infections: Active release strategies. **Chemical Society Reviews**, v. 35, n. 9, p. 780–789, 2006.

HIDALGO-ROBATTO, B. M. et al. Pulsed laser deposition of copper and zinc doped hydroxyapatite coatings for biomedical applications. **Surface and Coatings Technology**, v. 333, p. 168–177, 2018.

HUANG, Y. et al. Antibacterial efficacy, corrosion resistance, and cytotoxicity studies of copper-substituted carbonated hydroxyapatite coating on titanium substrate. **Journal of Materials Science**, v. 50, n. 4, p. 1688–1700, 2015.

HUANG, Y. et al. Modification and evaluation of micro-nano structured porous bacterial cellulose scaffold for bone tissue engineering. **Materials Science and Engineering C**, v. 75, p. 1034–1041, 2017.

HUTCHENS, S. A. et al. Biomimetic synthesis of calcium-deficient hydroxyapatite in a natural hydrogel. **Biomaterials**, v. 27, p. 4661–4670, 2006.

ISO/EN10993-5. Biological evaluation of medical devices - Part 5: Tests for *in vitro* cytotoxicity. **International Organization for Standardization**, 2009.

JIN, H. H. et al. *In vivo* evaluation of porous hydroxyapatite/chitosan–alginate composite scaffolds for bone tissue engineering. **International Journal of Biological Macromolecules**, v. 51, n. 5, p. 1079–1085, 2012.

KIM, H. L. et al. Preparation and characterization of nano-sized hydroxyapatite/alginate/chitosan composite scaffolds for bone tissue engineering. **Materials science & engineering. C, Materials for biological applications**, v. 54, p. 20–25, 2015.

LIAN, M. et al. A multifunctional electrowritten bi-layered scaffold for guided bone regeneration. **Acta Biomaterialia**, v. 118, p. 83–99, 2020.

LIMA, L. R. et al. Nanocristais de celulose a partir de celulose bacteriana. **Química Nova**, v. 38, n. 9, p. 1140–1147, 2015.

LIN, B. et al. Preparation and characterization of dopamine-induced biomimetic hydroxyapatite coatings on the AZ31 magnesium alloy. **Surface and Coatings Technology**, v. 281, p. 82–88, 2015.

LIU, C. et al. Biodegradable Mg-Cu alloys with enhanced osteogenesis, angiogenesis, and long-lasting antibacterial effects. **Scientific Reports**, v. 6, n. 1, p. 27374, 2016.

LUZ, E. P. C. G. **Desenvolvimento de materiais híbridos à base de celulose bacteriana e/ou hidroxiapatita dopados com estrôncio**. [Dissertação de Mestrado] Universidade Federal do Ceará, 2016.

LUZ, E. P. C. G. et al. Strontium delivery systems based on bacterial cellulose and hydroxyapatite for guided bone regeneration. **Cellulose**, v. 25, n. 11, p. 6661–6679, 2018.

LUZ, E. P. C. G. et al. Resorbable bacterial cellulose membranes with strontium release for guided bone regeneration. **Materials Science and Engineering C**, v. 116, p. 111175, 2020.

MAIA, M. T. et al. Advances in bacterial cellulose/strontium apatite composites for bone applications. **Polymer Reviews**, v. 61, n. 14, p. 1–29, 2021.

NAM, P. T. et al. Synthesis, characterization and antimicrobial activity of copper doped hydroxyapatite. **Vietnam Journal of Chemistry**, v. 56, n. 6, p. 672–678, 2018.

NETO, J. DA S. R. **Efeitos da substituição iônica por estrôncio na morfologia de cristais de fosfatos de cálcio e no polimorfismo da hidroxiapatita hexagonal e monoclínica**. [Tese de Doutorado] Universidade Federal de Santa Catarina, 2015.

PANG, M. et al. Application of bacterial cellulose in skin and bone tissue engineering. **European Polymer Journal**, v. 122, p. 109365, 2020.

PEREIRA, H. F. et al. Scaffolds and coatings for bone regeneration. **Journal of Materials Science: Materials in Medicine**, v. 31, n. 3, p. 1 - 16, 2020.

PREDOI, D. et al. Synthesis, characterization, and antimicrobial activity of magnesium-doped hydroxyapatite suspensions. **Nanomaterials**, v. 9, n. 9, p. 1–20, 2019.

RANGASWAMY, B. E.; VANITHA, K. P.; HUNGUND, B. S. Microbial cellulose production from bacteria isolated from rotten fruit. **International Journal of Polymer Science**, v. 2015, p. 1 - 9, 2015.

RYNGAJŁŁO, M. et al. Comparative genomics of the Komagataeibacter strains—Efficient bionanocellulose producers. **MicrobiologyOpen**, v. 8, n. 5, p. 1–25, 2019.

SABET, A. S.; JABBARI, A. H.; SEDIGHI, M. Microstructural properties and mechanical behavior of magnesium/hydroxyapatite biocomposite under static and high cycle fatigue loading. **Journal of Composite Materials**, v. 52, n. 13, p. 1711–1722, 2018.

SASKA, S. et al. Bacterial cellulose-hydroxyapatite nanocomposites for bone regeneration. **International Journal of Biomaterials**, v. 2011, p. 1–8, 2011.

SHANMUGAM, S.; GOPAL, B. Antimicrobial and cytotoxicity evaluation of aliovalent substituted hydroxyapatite. **Applied Surface Science**, v. 303, p. 277–281, 2014.

SIMON, A. T. et al. Copper nanocluster-doped luminescent hydroxyapatite nanoparticles for antibacterial and antibiofilm applications. **ACS Omega**, v. 4, n. 3, p. 4697–4706, 2019.

TEIXEIRA, S. R. Z. et al. Biosynthesis and functionalization of bacterial cellulose membranes with cerium nitrate and silver nanoparticles. **Materials Research**, v. 22, n. 3, p. 1–13, 2019.

TORGBO, S.; SUKYAI, P. Fabrication of microporous bacterial cellulose embedded with magnetite and hydroxyapatite nanocomposite scaffold for bone tissue engineering. **Materials Chemistry and Physics**, v. 237, p. 121868, 2019.

TU, Y. et al. Fabrication of nano-hydroxyapatite/chitosan membrane with asymmetric structure and its applications in guided bone regeneration. **Bio-Medical Materials and Engineering**, v. 28, n. 3, p. 223–233, 2017.

VRANCEANU, D. M. et al. Magnesium doped hydroxyapatite-based coatings obtained by pulsed galvanostatic electrochemical deposition with adjustable electrochemical

behavior. **Coatings**, v. 10, n. 8, p. 1–15, 2020.

WAN, Y. et al. Preparation and mineralization of three-dimensional carbon nano fi bers from bacterial cellulose as potential scaffolds for bone tissue engineering. **Surface & Coatings Technology**, v. 205, n. 8–9, p. 2938–2946, 2011.

XU, T. et al. Effect of magnesium particle fraction on osteoinduction of hydroxyapatite sphere-based scaffolds. **Journal of Materials Chemistry B**, v. 7, n. 37, p. 5648–5660, 2019.

ZENG, X.; RUCKENSTEIN, E. Control of pore sizes in macroporous chitosan and chitin membranes. **Industrial and Engineering Chemistry Research**, v. 35, n. 11, p. 4169–4175, 1996.

ZOU, L. et al. Biomimetic mineralization on natural and synthetic polymers to prepare hybrid scaffolds for bone tissue engineering. **Colloids and Surfaces B: Biointerfaces**, v. 178, n. 523, p. 222–229, 2019.

4 CHAPTER: Based on the article submitted to the Journal Materials Research

Bacterial nanocellulose biocomposites and HAp with cationic substitution by Mg, Cu, Zn and Sr bioactivated in simulated body fluid for bone regeneration.

Bacterial nanocellulose membranes (BNC) have been used in tissue engineering because their structure is similar to the extracellular matrix. Hydroxyapatite (HAp) is the main constituent inorganic in natural bone. This work aims to produce BNC biocomposites with Mg^{2+}, Cu^{2+}, Zn^{2+} and Sr^{2+} apatites for application in Bone Tissue Engineering. Thus, biocomposites were produced in different concentrations and bioactivated in simulated body fluid. The samples were characterized by SEM/EDS, FTIR/ATR, DRX, TGA, and analysis cytotoxicity. SEM analysis showed the presence of HAp crystals distributed over the BNC nanofibrils, and EDS analysis detected Ca and P elements. FTIR also confirmed the presence of phosphates groups. XRD showed diffraction peaks characteristic of BNC and HAp. TGA analysis showed a high percentage of residue, confirming the deposition of HAp in the membrane, and the cytotoxicity analysis showed that the BNC/MgHAp, BNC/ZnHAp, and BNC/SrHAp biocomposites are suitable for biomedical applications.

Keywords: Bacterial Nanocellulose. Hydroxyapatite. Biocomposites. Osteogenesis. Bone Regeneration.

4.1 Introduction

Traumas caused by accidents or degenerative diseases can cause bone defects, affect people's quality of life, and often require surgical interventions. Among the most common practices in these cases are autologous grafts, allografts, demineralized heterologous bones, or even other materials as bone substitutes (SOFI et al., 2018).

Bone tissue engineering (BTE) emerges, bringing new solutions to this problem. The basic principle of these techniques is to create an isolated space using a barrier membrane – to prevent the invasion of rapidly growing fibrous tissue and other soft tissues from migrating to bone defects – thus allowing time for osteogenic cell populations from the host bone inhabiting the defective bone (TU et al., 2017). This procedure avoids the many disadvantages of traditional treatments, such as chronic

inflammation, complicated surgical procedures, and immunological rejection (ZHANG et al., 2017).

Materials play an essential role in this process. The combination of inorganic compounds, such as calcium phosphates (CaPs) (PINA et al., 2017) and biopolymers, has attracted much attention in tissue engineering. This mixture promotes materials with better mechanical properties (PINA et al., 2017) and stimulates the adhesion and proliferation of osteoblasts (TU et al., 2017).

In this context, bacterial nanocellulose (BNC) emerges as a polysaccharide secreted by several bacterial species (DU et al., 2016; INOUE et al., 2020; VOLOVA et al., 2018). With high purity, crystallinity, and porosity (AN et al., 2017a; BALDIKOVA et al., 2017; RECOUVREUX et al., 2011), in addition to being biocompatible, non-toxic, and non-allergenic (INOUE et al., 2020), BNC has a network structure with nanoscale fibrils that mimics the structure of the extracellular matrix of mammalian tissues. Added to this is the fact that it is approved by the US Food and Drug Administration (FDA) for biomedical applications (INOUE et al., 2020), such as dressings, tissue engineering, bio-capacitors and biobatteries (REBELO et al., 2018), essential characteristics for the regeneration of body organs.

Despite this, its use is still limited. Several studies seek to improve the mechanical properties of BNC (HUANG et al., 2017) and promote bioactivity and osteogenicity. Studies have been developed on production BNC bio-composites with hydroxyapatite (HAp) (HUANG et al., 2017; HUTCHENS et al., 2006). Combining a biopolymer such as BNC with HAp in the composite material can help overcome the disadvantages of each one alone (PINA et al., 2017), mainly by stimulating the adhesion and proliferation of osteoblasts by composing the inorganic portion of the natural bone tissue (INOUE et al., 2020).

The bioactivity and biodegradability of HAp are by themselves excellent properties for third-generation biomedical materials; however, studies have shown that the replacement of Ca and P sites in HAp can increase degradation kinetics, in addition to promoting even more cell growth, thus improving the interface between bioceramics and biological tissue (EHRET et al., 2017; ZHU et al., 2018).

This work intends to develop and characterize BNC biocomposites with hydroxyapatite and hydroxyapatite with replacement of Ca by Mg^{2+}, Cu^{2+}, Zn^{2+}, and Sr^{2+} bioactivated in SBF, aiming to application in Guided Bone Regeneration.

4.2 Materials and methods

4.2.1 Synthesis and purification of BNC membranes

The production of BNC membranes was carried out by the bacterium *Komagataeibacter hansenii* (ATCC 23769). The culture medium used was Mannitol Medium. The cultivation was carried out in Erlenmeyer flasks under the static condition at 30 °C for 9 days (TEIXEIRA et al., 2019) (Figure 4.1).

The BNC membranes formed on the surface of the culture medium were removed, washed and treated with 0.1 mol/L of NaOH at 80°C for 60 min in a thermostatic bath (Fisatom model 573). Afterward, they were washed with distilled water until reaching pH 7, autoclaved and stored in a refrigerator (TEIXEIRA et al., 2019) (Figure 4.1).

Figure 4.1: Illustrative schematic demonstrating the steps of the composites production process.

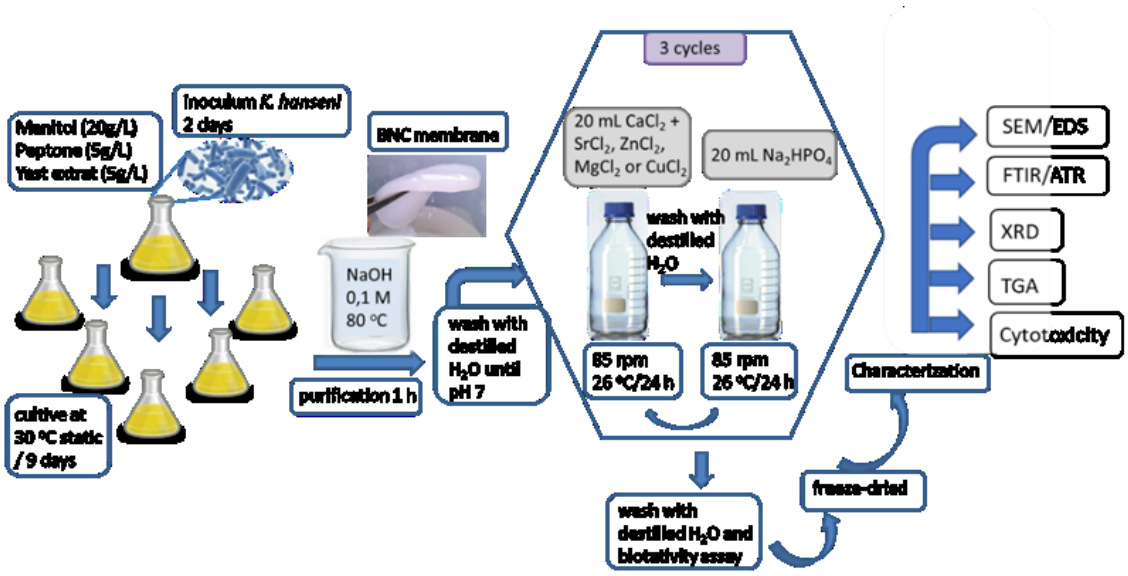

4.2.2 Production of biocomposites and bioactivation

The biocomposites were prepared by the immersion cycle method proposed by Hutchens et al. (2006), being immersed in: $CaCl_2$, $CaCl_2/MgCl_2$, $CaCl_2/CuCl_2$, $CaCl_2/ZnCl_2$, and $CaCl_2/SrCl_2$ solution, remaining for 24 h under agitation in an orbital shaker at 26 °C and 85 rpm. Subsequently washed to remove the residue and immersed in a solution of Na_2HPO_4 for another 24 h. Three immersion cycles were performed in each solution. The biocomposites formed were HAp, BNC/MgAp, BNC/CuAp, BNC/ZnAp, and BNC/SrAp (Figure 4.1).

BNC and biocomposites were lyophilized (Terroni LT 1000 Lyophilizer) and stored in a desiccator. The biocomposites were immersed in 5 mL of SBF (simulated body fluid) to induce apatite formation *in vitro*. The SBF solution was prepared, according to Kokubo et al. (1990), briefly (in $g \cdot L^{-1}$): 6,55 g NaCl, 2,27 g $NaHCO_3$, 0,37 g KCl, 0,18 g $Na_2HPO_4 \cdot 2H_2O$, 0,30 g $MgCl_2 \cdot 6H_2O$, 40 mL HCl 1M, 0,37 g $CaCl_2 \cdot 2H_2O$, 0,07 g Na_2SO_4 e 6,06 g de TRIS, with final pH 7.4. The polypropylene flasks containing the SBF and the membranes were conditioned at 37 °C, remaining for 14 days, and the PBS solution was changed every 4 days. Afterward, the samples were washed with distilled water, lyophilized, and characterized.

4.2.3 Characterization

4.2.3.1 Scanning electron microscopy with dispersive energy spectroscopy (SEM/EDS)

Scanning electron microscopy (SEM) was performed in a JEOL JSM-6390LV (JEOL, Tokyo, Japan) with a tungsten filament and an accelerated voltage of 10 kV. An electron beam bombarded the same samples, and the X-rays emitted from the samples were detected by a silicon solid-state detector device for a point elemental analysis of the sample.

4.2.3.2 Fourier transform infrared spectroscopy with attenuated total reflectance (FTIR/ATR)

The analyses were performed in Perkin-Elmer Spectrum equipment with 32 scans per sample in the range of 4000 to 500 cm^{-1}, resolution of 4 cm^{-1}, using the module attenuated total reflectance (ATR).

4.2.3.3 Wide-angle X-ray diffractometry (XRD)

X-ray diffraction was measured with an X-ray diffractometer (Bruker XRD 8 Advance), using CuKα radiation 1.5418 with 1000 W of power, 40 kV, 25 mA, and a digital detector with 160 channels. The angle 2θ covered the study range from 5° to 70° at 0.02 °/s.

4.2.3.4 Thermogravimetric analysis (TGA)

To know the thermal stability of the biocomposites produced, evaluate the incorporation of the mineral phase into the membrane, and quantify each phase present in the material (organic/inorganic), TGA analyzes were performed in the TGA-Q50 (TA Instruments) equipment. Samples between 5 and 10 mg will be heated from 25 °C to 600 °C at the flow rate of 10 °C/min in an oxidizing atmosphere.

4.3.4 Cytotoxicity assay

The cytotoxicity analysis was evaluated by measuring the metabolic activity of rat fibroblasts (L929) following the ISO 10993-5 (2009) using the MTS assays (Aguilar et al., 2021).

Data from in vitro cell culture were statistically analyzed using one-way repeated Analysis of Variance (ANOVA). The data represent the mean ± standard error from three independent assays in triplicates.

4.4 Results and discussion

4.4.1 Scanning electron microscopy with dispersive energy spectroscopy (SEM/EDS)

According to Durdu et al. (2017), the structure of bioactivated apatite in SBF, also called secondary apatite, represents the formation of apatite *in vivo*, which is an essential requirement for the binding of artificial material to living bone. A dense layer of HAp crystals, in the form of rosettes and lamellae, can be observed over the BNC/HAp bio-composite (Fig. 4.2A), indicating the effectiveness of biomimetic mineralization for HAp nucleation. It was possible to observe that the BNC nanofibrils promoted sites for secondary apatite nucleation after immersion in SBF (Fig. 4.2A and C). After the bioactivation test, the composites were analyzed by SEM-EDS, confirming the deposition of Ca and P-based material on the membrane surface (Fig. 4.2B) and (supplementary material-S1). According to Durdu et al.(2017) and Hutchens et al. (2006), this observed "rosette" structure demonstrates that apatite was nucleated from a distinct location and formed outward in a radial pattern.

Figure 4.2: Surface micrographs of the A) BNC/HAp biocomposite, B) EDS of the biocomposite, and C) BNC.

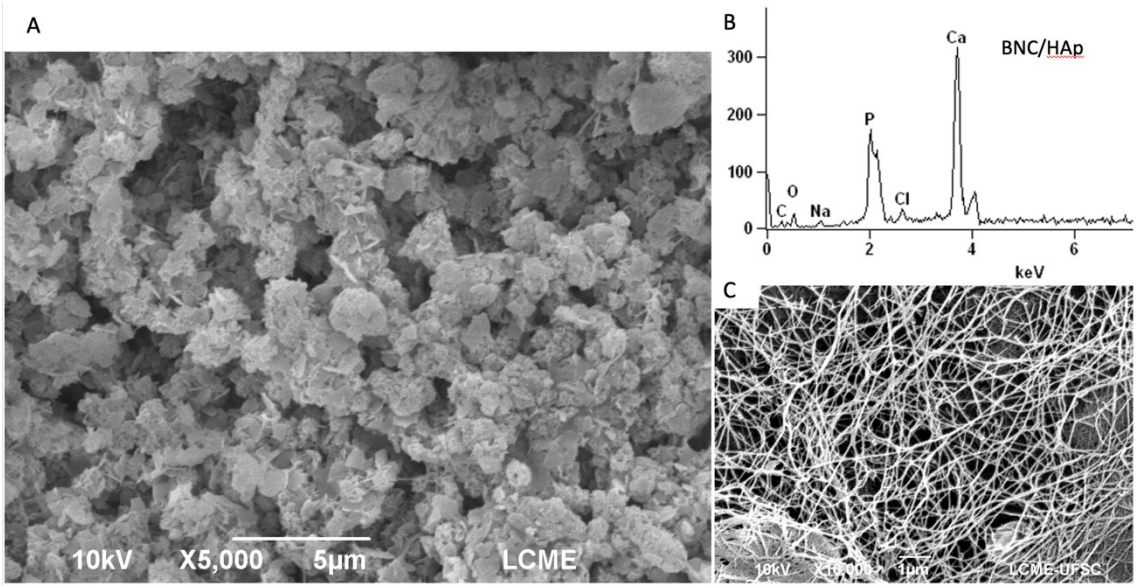

The replacement of Ca by Mg, Cu, Zn, and Sr ions in the biocomposite changed little the morphology of the crystals, showing a more change in their density (Fig. 4.3). Points with concentric aggregations (clusters) appeared, suggesting several nucleations in the same point of the nanofibril. Nagyné-Kovács et al. (2018) did not observe significant changes in the morphology of HAp crystals after doping with Sr.

The samples BCN/MgAp 5% and BCN/SrAp 1% (Figures 4.3C and J) showed more crystals in lamellar form. While the samples BCN/MgAp 1% and BCN/ZnAp 3% (Fig. 4.3A and H) also showed some crystal depositions in the form of flakes. The samples that incorporated Cu present a different behavior, with a dense formation covering the entire surface of the BNC, in all compositions (Fig. 4.3 D, E, F). This behavior affected the porosity of the biocomposite. Huang et al. (2015) also observed that the substitution of Cu in the HAp increased the density, generating a relatively minor porosity than the coating composed only of HAp.

Figure 4.3: Micrographs of the surface of incorporated biocomposites: A, B, C) BNC/MgAp 1, 3 and 5%; D, E, F) BNC/CuAp 1, 3 e 5%; G, H, I) BNC/ZnAp 1, 3 e 5%; J, K, L) BNC/SrAp 1, 3 e 5%.

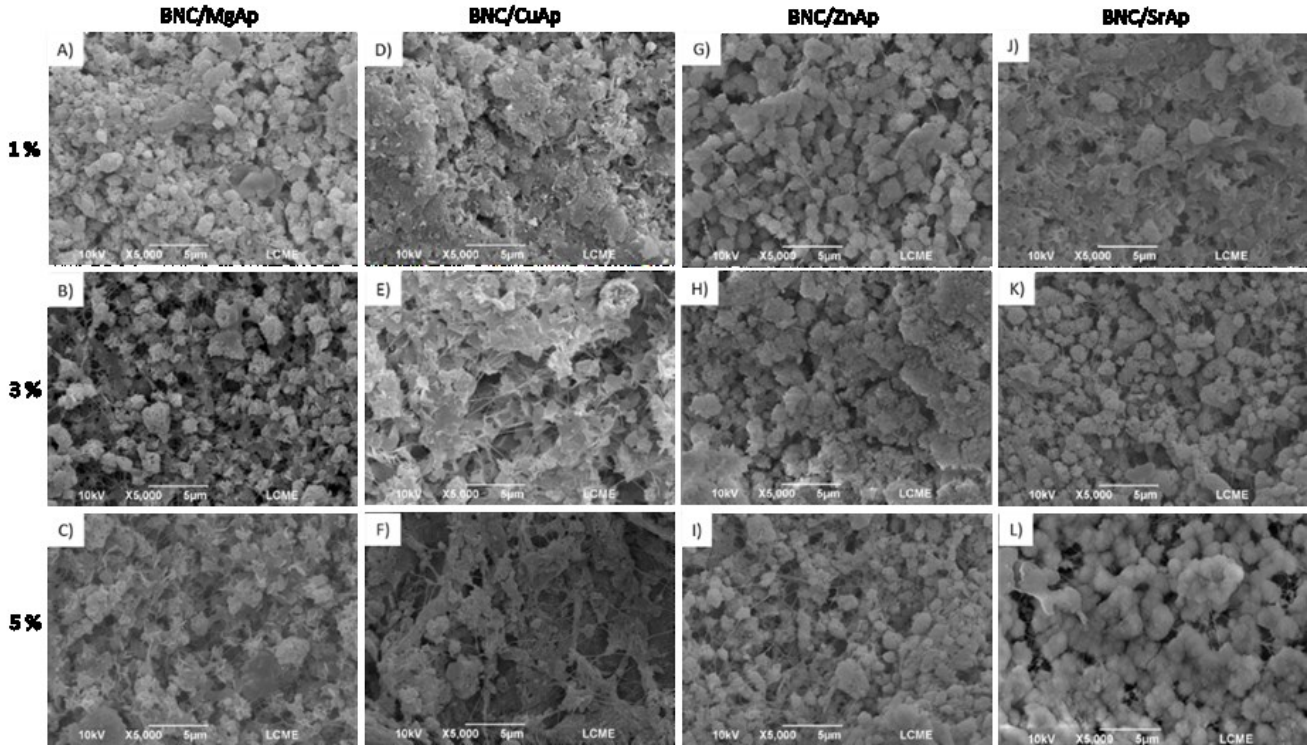

EDS analysis was used to detect Ca and P elements and verify the metallic ions added to the biocomposites (S1 – Supplementary material). Traces of chlorine, sodium, carbon, and oxygen were also observed in the spectra. The Cl and Na were attributed to residues of the reagents $CaCl_2$ and Na_2HPO_2 used in the mineralization process. The C and O peaks corroborate the results observed in the FTIR analysis, which indicated the presence of CO_3^2. Only the samples BNC/MgAp 3 and 5%, BNC/SrAp 3 and 5% were observed the presence of Mg and Sr ions in the biocomposite, which believed to be due to the low concentration of these elements. Predoi et al. (2019) highlight that this type of carbonation prevails in bone tissue and has superior biological performance compared to pure HAp.

4.4.2 Fourier transform infrared spectroscopy analysis with attenuated total reflectance (FTIR/ATR)

The FTIR spectra of the BNC/HAp composite are shown in Figure 4.4. The band in the 3500–3200 cm^{-1} region, attributed to the hydroxyl groups of cellulose, was observed in both samples. Furthermore, the slight shift observed in BNC/HAp towards the band attributed to intramolecular hydrogen bonding (~ 3500 cm^{-1}) confirms the strong interaction between the OH group and apatite. The chemical interaction between HAp and BNC stabilizes the composite to maintain the mechanical integrity necessary for bone replacement Saska et al. (2011).

Another feature that stands out in the biocomposites is the suppression of the bands at 1160 and 1050 cm^{-1} that corresponds to the C-O-C asymmetric elongation modes and C-O bond elongation of BNC, which also represents the presence of well-linked chemical groups of BNC and HAp improving the stabilization of the biocomposite (Grande et al., 2009). The bands observed for the BNC and biocomposites represented in Figure 4.4 are described in S2 (Supplementary material).

In all spectra, it can be observed that the predominance of bands at 1020 and 960 cm^{-1} correspond to the vibrational modes of the P–O bonds, demonstrating the presence of phosphate groups (Hutchens et al., 2006; Putrakumar et al., 2020). However, the 960 cm^{-1} bands appeared as a shoulder of the strongest band at 1020 cm^{-1}. In addition, the bands at 1418 and 872 cm^{-1} corresponding to the stretching

mode of the CO_3^2 ions suggest the absorption of atmospheric CO_2. Therefore, according to Saska et al. (2011), its analysis suggests the formation of a carbonate-containing apatite, similar to bone tissue apatite deposited on BNC nanofibers.

Predoi et al. (2019) attributed type B carbonation in their MgHAp samples to the presence of the 1461 and 1454 cm^{-1} bands. Popa et al. (2016) also observed the presence of the carbonate functional group in their Zn-doped HAp nanoparticles in the same bands. Durdu et al. (2017) produced steel materials with coating by deposition of bioactivated hydroxyapatite in SBF. Their samples also showed CO_3^{2-} absorption bands of characteristic elongation mode in slightly substituted carbonated HA of type A between 1460 and 1465 cm^{-1} and type B between 1420 and 1425 cm^{-1}.

Figure 4.4: FTIR/ATR spectra of BNC/HAp biocomposites (standard) and: A) BNC/MgAp; B) BNC/CuAp; C) BNC/ZnAp, and D) BNC/SrAp.

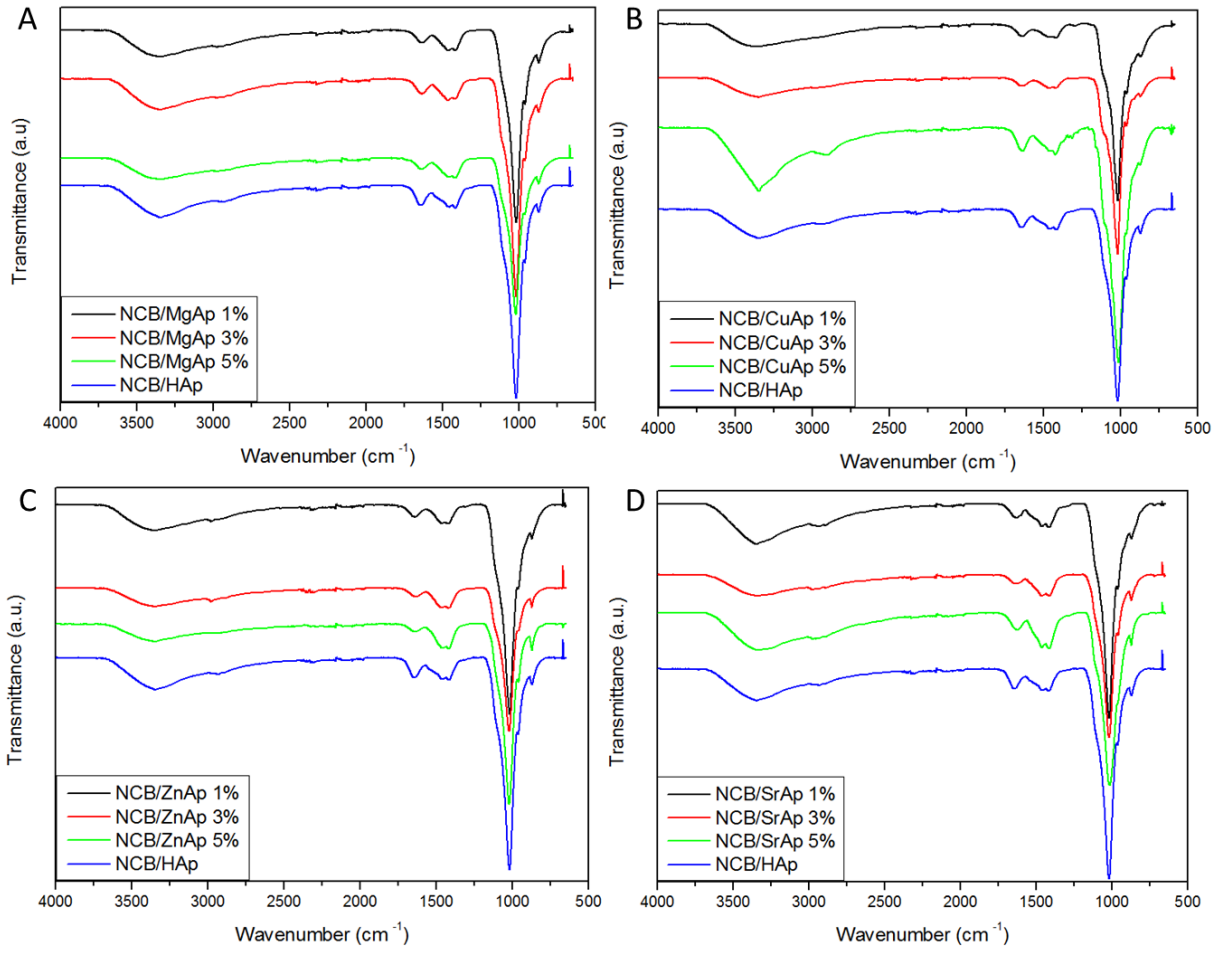

4.4.3 Wide-angle X-ray diffractometry (XRD)

Two very characteristic BNC diffraction peaks were observed at 2θ ≈ 14.5 and 22.6°, corresponding to the planes (1 0 1) and (0 0 2) (Casaburi et al., 2018 and Predoi et al., 2019) as well as two characteristic peaks of HAp demonstrated at 2 θ ≈ 26° (0 0 2) and 32° (2 1 1), other peaks equally characteristics of HAp that presented with less intensity were 33° (3 0 0), 40°(3 1 0), 46° (2 2 2) and 54°(0 0 4) (Grande et al., 2009; Nam et al., 2018; Wang et al. 2018) in all samples (Fig. 4.5), highlighting the incorporation between the material already observed in the FTIR analysis.

In the modified biocomposites, the intensity of the 2θ ≈ 26° and 31.8° peaks were observed concerning the standard BNC/HAp, representing an increase in the material's crystallinity. According to Giannoulatou et al. (2018), the gradual crystallization of a hydroxyapatite phase is confirmed by the progressive formation of peaks attributed to hydroxyapatite after 10 and 20 days of immersion in SBF. In this study, the samples were submitted for 14 days in SBF.

Putrakumar et al. (2020) observed in their samples of copper-modified hydroxyapatite, in addition to the peaks mentioned above, referring to HAp, the reflections at 2θ values of 35.57° and 38.67°, which were attributed to the appearance of a copper oxide phase with corresponding planes are (1 1 -1) and (1 1 1), respectively. In this case, the authors reported that the increase in peak intensity was proportional to the increase in Cu load, emphasizing that in samples with a content lower than 5%, these peaks were not visualized. However, this study observed these peaks subtly in NBC/CuAp 1 and 3% samples.

Giannoulatou et al. (2018) produced a magnesium calcium silicate bioactive glass doped with copper ions and highlighted the 2θ peaks of 27.74°, 30.89°, and 34.12° after 20 days of immersion in SBF. According to the authors, these peaks are associated with the crystalline phase of whitlockite ($Ca_{18}Mg_2H_2(PO_4)_{14}$), which results from a process in which calcium phosphate is replaced by small amounts of Mg instead of Ca. In this study, peaks around 2 θ ≈ 27.74° and 34.12° were observed, a very subtle, probably due to the low concentration used.

Wang et al. (2018) produced HAp scaffolds doped with Sr and Zn and found the presence of two new peaks at 31.7° and 34.7° were found for the materials doped

with Zn. The 31.7° peak was attributed to a small amount of tricalcium phosphate containing Zn, while the 34.7° peak was attributed to Zn-TCP formation after Zn-Hap (WANG et al., 2018). In this work, only the peak at 31.8° was verified, subtly, in the samples containing 1 and 3% of Zn.

Figure 4.5: X-ray diffractograms of BNC/HAp biocomposites (standart) and: A) BNC/MgAp; B) BNC/CuAp; C) BNC/ZnAp, and D) BNC/SrAp.

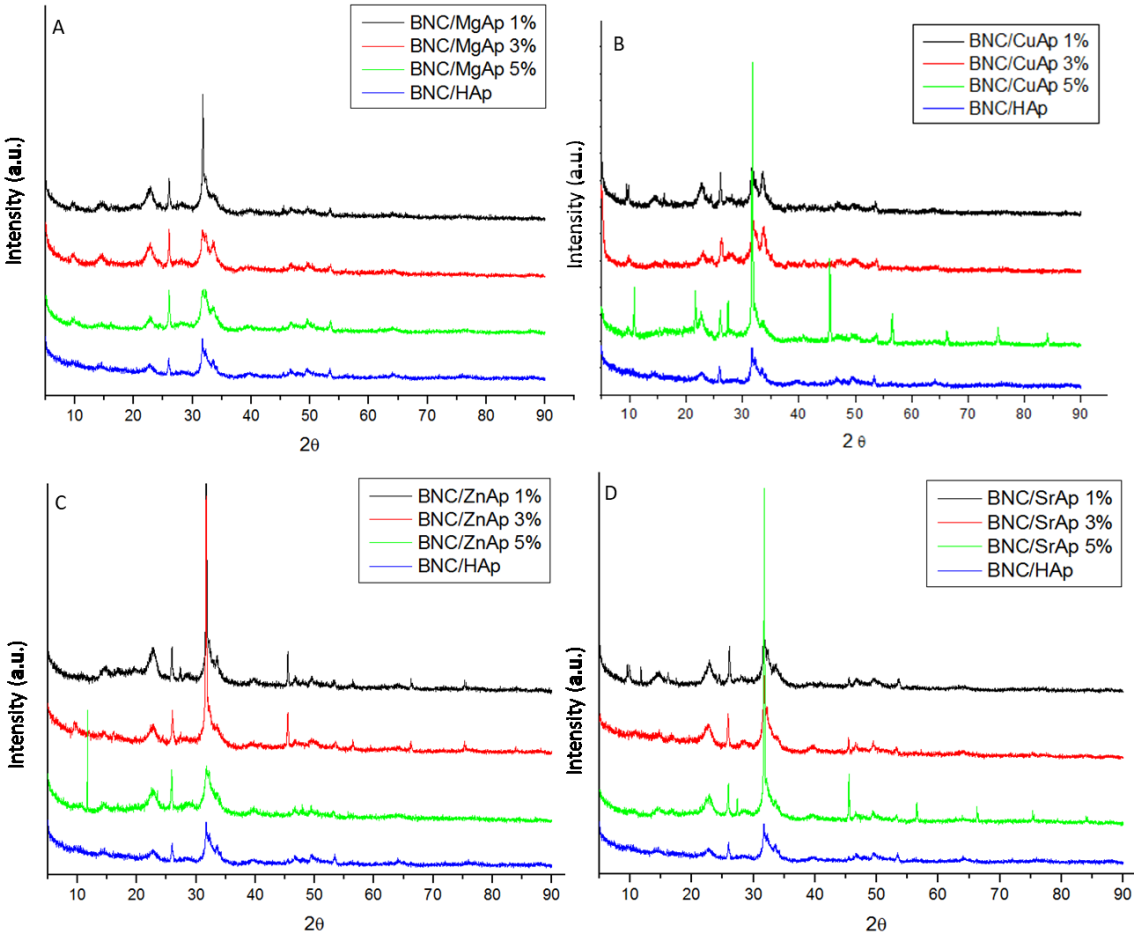

In samples containing Sr, a peak at 31.8° was observed and became sharper and more intense proportionally to the percentage of Sr in the samples. Sr doping of HAp was performed with different Sr/(Ca+Sr) molar ratios per Nagyné-Kovács et al., (2018). The authors also highlighted that there was no formation of new peaks related to Sr content; however, the peak positions slightly changed to lower diffraction angles

from 2θ ≈ 31.848° to 2θ 31.705°, from which the authors concluded that Sr ions were incorporated into the HAp unit cell, replacing Ca ions.

4.4.4 Thermogravimetric analysis (TGA)

The thermal degradation profile of BNC/HAp and the other biocomposites tested showed the occurrence of 6 stages of mass loss (Fig. 4.6). There was an initial loss of mass around 100 °C, referring to dehydration of the cellulose and a second stage that may result from the vaporization of hydroxyapatite crystallization water at around 120 °C (Saska et al. 2011). A very mild third stage at around 220 °C appeared for almost all samples, with mass losses of around (2.5% to 9.73%).

Cox et al. (2014) highlight that this may be associated with gradual later water loss. The fourth and most striking thermal event occurs at T_{max4} around 320 to 330 °C with a pronounced mass loss (17% to 28%). These refer to the cellulose degradation process, including depolymerization, dehydration, and decomposition of glycosyl units, followed by forming a carbonized residue (Jiang et al. 2018; Saska et al. 2011).

The fifth stage, around T_{max5} 412 °C to 452 °C, is due to the degradation of carbonaceous residues from the BNC (Nainggolan et al., 2013). In contrast, the sixth stage occurred at T_{max6} (702 and 856 °C), which, according to Zhang et al. (2009) is related to the mass loss of carbonated apatite. This result also agrees with the data observed by FTIR, which showed the decomposition of non-stoichiometric apatites into whitlockite; this event occurs above 600 °C (Cox et al. 2014). These data are organized in a table in the supplementary material S3.

It is also important to highlight that all samples had a high percentage of residues (51.9% to 65.6%), confirming that the deposition of HAp on the BNC membrane was around 50% (Saska et al., 2011).

Miyaji, Kono and Suyama (2005) reported in their work that the mass losses that occur between 750 and 850 °C are related to the decomposition of apatite to form tricalcium phosphate (TCP) ($Ca_3(PO_4)_2$), and this loss increases with the increasing percentage of Zn, that is, Zn can promote the transformation of apatite into TCP. The highest values in this temperature range were also found in this study for biocomposites containing Zn. In general, all biocomposites with the different metallic ions also showed this effect, raising the $Tmax_6$ in the biocomposite.

Figure 4.6: TG and DTG curves of BNC/HAp biocomposites (standard) and: A) BNC/MgAp; B) BNC/CuAp; C) BNC/ZnAp, and D) BNC/SrAp.

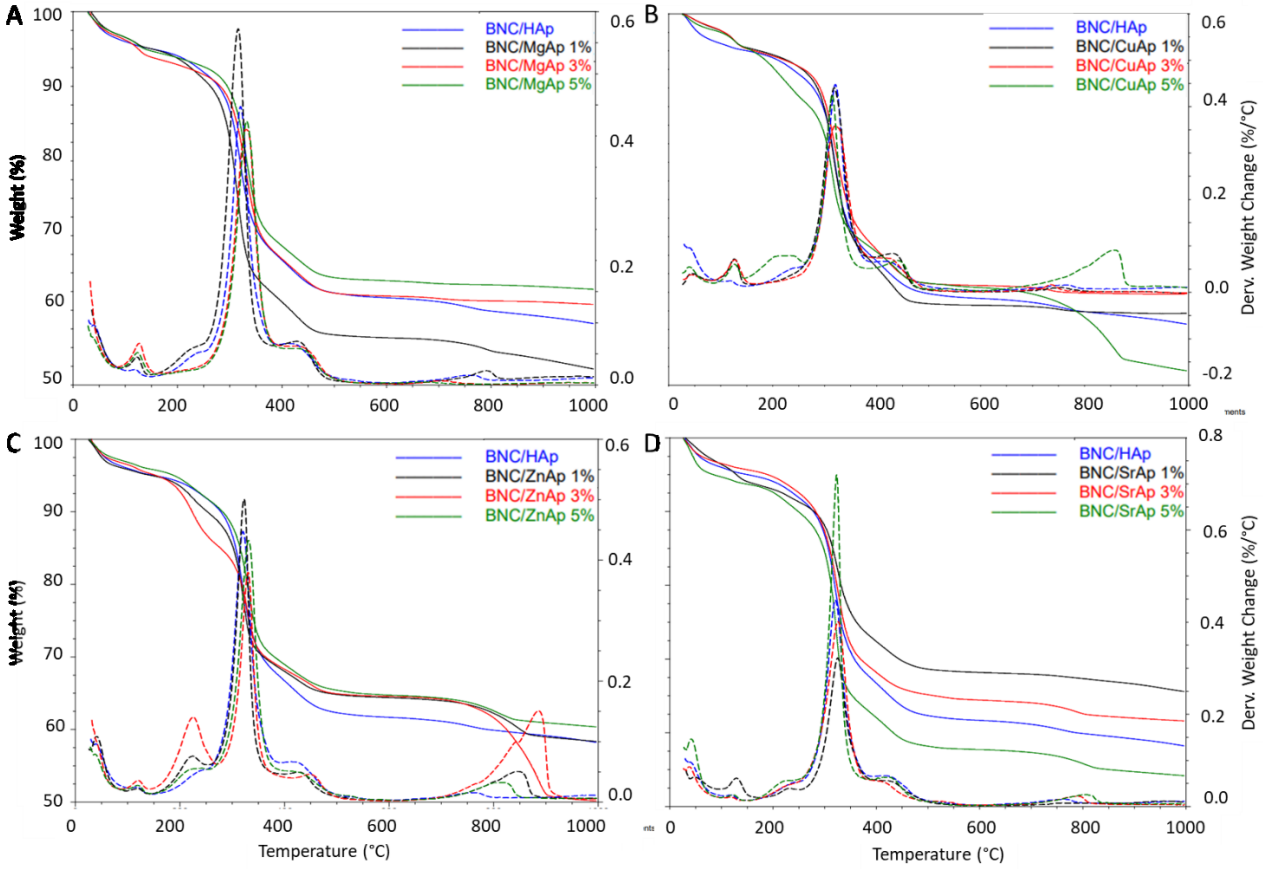

4.4.5 Cytotoxicity assay

The results of the MTS assay for cytotoxicity are shown in Fig. 4.7. It is important to note that lower cell viability values resulted in higher values of cytotoxic potential for the tested samples.

As shown, all samples containing Mg did not change compared to BNC/HAp during the analyzed period; this is a good result for the desired application. While samples containing Cu, all compositions showed a cytotoxic effect, reducing cellular metabolic activity to about 20%. The BNC/ZnAp 1% sample showed the best result keeping cells' metabolic activity at 90%. However, higher concentrations have caused a very intense reduction in the metabolic activity of the tested cells, leading to the belief that the cytotoxic effect is concentration-dependent. Stand out, the biocomposites containing Sr, the BNC/SrAp 1% sample presented a metabolic activity very close to

90%, and even at higher concentrations of 3 and 5%, the results were still higher than 70% about the metabolic activity, making this the best result for application as an implantable material. According to ISO 10993-5:2009, if cell viability is greater than 70% of the control group, the material is considered non-cytotoxic.

Favi et al. (2016) analyzed the cell viability of mesenchymal cells (hMSCs) in BNC samples and BNC/HAp biocomposite. The authors observed that the cells remained metabolically active even after 2 days in culture, thus confirming their viability.

Figure 4.7: Cytotoxicity assay of BNC/HAp, BNC/MgAp, BNC/CuAp, BNC/ZnAp and BNC/SrAp biocomposites, second the metabolic activity observed in 24h.

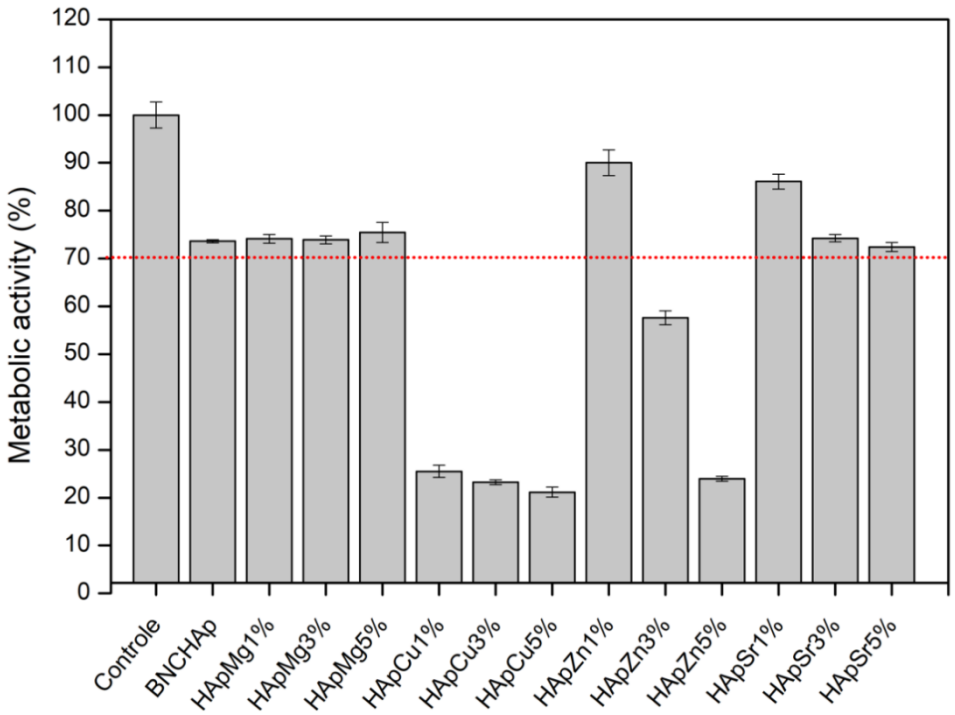

Kazimierczak et al. (2019) analyzed chitosan/agarose/HAp, chi/aga/MgAp, chi/aga/ZnAp, and chi/aga/Mg-ZnAp scaffolds containing 30% of HAp, 30% of metal ions separately or 15% of each when used together. The authors observed that after 24 h of exposure, the samples containing Mg^{2+} showed increased metabolic activity of the MC3T3-E1 cells compared to the other samples. The authors related this fact to

the ability of Mg^{2+} ions to increase osteoblast viability through increased intercellular communication.

Chi et al. (2019) produced CuAp microspheres by the ion exchange method and pneumatic impression. The cytotoxicity analysis was conducted with mesenchymal cells (BMMSCs). The authors also observed a significantly lower survival rate than the control group in the first 24 h and 72 h. According to the authors, the presence of the Cu ion has apparent cytotoxicity in the initial stage of the experiment, and the higher the concentration of copper ions, the more significant cytotoxicity.

Popa et al. (2016) produced ZnAp nanoparticles and analyzed their cytotoxicity toward HepG2 cells. The authors found that cell viability was only moderately affected (about 20%). In this case, the negative effect on cell viability was attributed to the size of the nanoparticles. According to the authors, increasing the concentration of Zn ion in HAp also reduces particle size. In contrast, in this study, the biomaterial formed was not in the form of nanoparticles, but the negative effect on cell viability observed was concentration-dependent, and only the concentration of 1% presented an excellent result.

Nguyen et al. (2019) studied the effect on the biocompatibility of Sr-doped calcium phosphate-coated titanium substrates. Cell viability was analyzed on rat osteoblast cells (MC3T3-E1). After 7 days, the highest viability compared to the control group was observed for samples containing Sr in higher concentrations (2.13%). The authors attributed it that Sr can act as a chemical activator and trigger the cellular response. The authors also highlighted that Sr might increase cell adhesion and proliferation, benefiting bone tissue growth and increasing implant anchorage to the bone.

4.5 Conclusion

BNC membranes presented as a good template for inserting metallic apatites, offering good porosity and available hydroxyls to make the bonds. SEM/EDS, FTIR/ATR, DRX, and TGA tests confirmed the presence of phosphate sources in the

analyzed biocomposites. The incorporation of metal ions in apatites was based on their known benefits in processes such as osteogenesis and neovascularization. However, at the concentrations tested, the addition of Cu still showed results pointing to cytotoxicity. While the biocomposites BNC/MgAp and BNC/SrAp at all concentrations and BNC/ZnAp 1% exerted less negative effect on the metabolic activity of the cells. Therefore, these biocomposites can be considered promising as implantable materials.

4.6 Acknowledgments

The authors are grateful for the financial support of FAPESC and FAP/UNIVILLE. Central Laboratory of Electronic Microscopy (LCME-UFSC) and Laboratory of Biological Engineering Laboratory (LiEB-UFSC) for the analysis.

4.7 References

AGUILAR, A. E. M., FAGUNDES, A. P., DOMINGOS, L. P. M, CESCA, K., PORTO, L. M., PADIN, N., SOARES, C., RIELLA, H. (2021). Green Synthesis of Nano Hydroxyapatite: morphology variation and its effect on cytotoxicity against fibroblast. **Materials Letters**, 284, part 2, 129013. https://doi.org/10.1016/j.matlet.2020.129013.

BALDIKOVA, E., POSPISKOVA, K., LADAKIS, D., KOOKOS, I. K., KOUTINAS, A. A., SAFARIKOVA, M., & SAFARIK, I. (2017). Magnetically modi fi ed bacterial cellulose: A promising carrier for immobilization of af fi nity ligands, enzymes, and cells. **Materials Science & Engineering C**, 71, 214–221. https://doi.org/10.1016/j.msec.2016.10.009

CASABURI, A., MONTOYA ROJO, Ú., CERRUTTI, P., VÁZQUEZ, A., & FORESTI, M. L. (2018). Carboxymethyl cellulose with tailored degree of substitution obtained from bacterial cellulose. **Food Hydrocolloids**, 75, 147–156. https://doi.org/10.1016/j.foodhyd.2017.09.002

CHI, W., ZOU, J., AI, F., LIN, Y., LI, W., CAO, C., YANG, K., & ZHOU, K. (2019). Research of Cu-doped hydroxyapatite microbeads fabricated by pneumatic extrusion printing. **Materials**, 12(11), 1–11. https://doi.org/10.3390/ma12111769

COX, S. C., JAMSHIDI, P., GROVER, L. M., & MALLICK, K. K. (2014). Preparation and characterisation of nanophase Sr, Mg, and Zn substituted hydroxyapatite by aqueous precipitation. **Materials Science and Engineering C**, 35(1), 106–114. https://doi.org/10.1016/j.msec.2013.10.015

DURDU, S., KORKMAZ, K., AKTUĞ, S. L., & ÇAKIR, A. (2017). Characterization and bioactivity of hydroxyapatite-based coatings formed on steel by electro-spark deposition and micro-arc oxidation. **Surface and Coatings Technology**, 326, 111–120. https://doi.org/10.1016/j.surfcoat.2017.07.039

EHRET, C., AID-LAUNAIS, R., SAGARDOY, T., SIADOUS, R., BAREILLE, R., REY, S., PECHEV, S., ETIENNE, L., KALISKY, J., DE MONES, E., LETOURNEUR, D., & AMEDEE VILAMITJANA, J. (2017). Strontium-doped hydroxyapatite polysaccharide materials effect on ectopic bone formation. **PLOS ONE**, 12(9), e0184663. https://doi.org/10.1371/journal.pone.0184663

FAVI, P. M., OSPINA, S. P., KACHOLE, M., GAO, M., ATEHORTUA, L., & WEBSTER, T. J. (2016). Preparation and characterization of biodegradable nano hydroxyapatite–bacterial cellulose composites with well-defined honeycomb pore arrays for bone tissue engineering applications. **Cellulose**, 23(2), 1263–1282. https://doi.org/10.1007/s10570-016-0867-4

GIANNOULATOU, V., THEODOROU, G. S., ZORBA, T., KONTONASAKI, E., PAPADOPOULOU, L., KANTIRANIS, N., CHRISSAFIS, K., ZACHARIADIS, G., & PARASKEVOPOULOS, K. M. (2018). Magnesium calcium silicate bioactive glass doped with copper ions; synthesis and *in vitro* bioactivity characterization. **Journal of Non-Crystalline Solids**, 500, 98–109. https://doi.org/10.1016/j.jnoncrysol.2018.06.037

GRANDE, C. J., TORRES, F. G., GOMEZ, C. M., & CARMEN BAÑÓ, M. (2009). Nanocomposites of bacterial cellulose/hydroxyapatite for biomedical applications. **Acta Biomaterialia**, 5(5), 1605–1615. https://doi.org/10.1016/j.actbio.2009.01.022

HUANG, YAN, WANG, J., YANG, F., SHAO, Y., ZHANG, X., & DAI, K. (2017). Modification and evaluation of micro-nano structured porous bacterial cellulose scaffold for bone tissue engineering. **Materials Science and Engineering C**, 75, 1034–1041. https://doi.org/10.1016/j.msec.2017.02.174

HUANG, YONG, ZHANG, X., ZHAO, R., MAO, H., YAN, Y., & PANG, X. (2015). Antibacterial efficacy, corrosion resistance, and cytotoxicity studies of copper-substituted carbonated hydroxyapatite coating on titanium substrate. **Journal of Materials Science**, 50(4), 1688–1700. https://doi.org/10.1007/s10853-014-8730-1

HUTCHENS, S. A., BENSON, R. S., EVANS, B. R., O'NEILL, H. M., & RAWN, C. J. (2006). Biomimetic synthesis of calcium-deficient hydroxyapatite in a natural hydrogel. **Biomaterials**, 27(26), 4661–4670. https://doi.org/10.1016/j.biomaterials.2006.04.032

INOUE, B. S., STREIT, S., SCHNEIDER, A. L. D. S, & MEIER, M. M. (2020). Bioactive bacterial cellulose membrane with prolonged release of chlorhexidine for dental medical application. **International Journal of Biological Macromolecules**, 148, 1098–1108. https://doi.org/10.1016/j.ijbiomac.2020.01.036

ISO/EN10993-5. (2009). Biological evaluation of medical devices - Part 5: Tests for in vitro cytotoxicity. **International Organization for Standardization**.

JIANG, P., RAN, J., YAN, P., ZHENG, L., SHEN, X., & TONG, H. (2018). Rational design of a high-strength bone scaffold platform based on in situ hybridization of bacterial cellulose/nano-hydroxyapatite framework and silk fibroin reinforcing phase. Journal of Biomaterials Science, **Polymer Edition**, 29(2), 107–124. https://doi.org/10.1080/09205063.2017.1403149

KAZIMIERCZAK, P., KOLMAS, J., & PRZEKORA, A. (2019). Biological Response to Macroporous Chitosan-Agarose Bone Scaffolds Comprising Mg- and Zn-Doped Nano-Hydroxyapatite. **International Journal of Molecular Sciences**, 20(15), 3835. https://doi.org/10.3390/ijms20153835

KOKUBO, T. (1990). Surface chemistry of bioactive glass-ceramics. **Jounal of Non-Cristalline Solids**, 120, 138 – 151.

LANGROUDI, M. M., SARAVANI, M., & NOURI, A. (2017). Surfactant-assisted synthesis of polyvinylpyrrolidone-hydroxyapatite composites as a bone filler. **Journal of Applied Biomaterials & Functional Materials**, 15(4), e334-e340. https://doi.org/10.5301/jabfm.5000348

MIYAJI, F., KONO, Y., SUYAMA, Y. (2005). Formation and structure or zinc-substituted calcium hydroxyapatite. **Mater. Res. Bull**, 40, 209-220. https:// doi:10.1016/j.materresbull.2004.10.020

NAGYNÉ-KOVÁCS, T., STUDNICKA, L., KINCSES, A., SPENGLER, G., MOLNÁR, M., TOLNER, M., LUKÁCS, I. E., SZILÁGYI, I. M., & POKOL, G. (2018). Synthesis and characterization of Sr and Mg-doped hydroxyapatite by a simple precipitation method. **Ceramics International**, 44(18), 22976–22982. https://doi.org/10.1016/j.ceramint.2018.09.096

NAINGGOLAN, H., GEA, S., BILOTTI, E., PEIJS, T., & HUTAGALUNG, S. D. (2013). Mechanical and thermal properties of bacterial-cellulose-fibre-reinforced Mater-Bi® bionanocomposite. **Beilstein Journal of Nanotechnology**, 4(1), 325–329. https://doi.org/10.3762/bjnano.4.37

NAM, P. T., THOM, N. T., PHUONG, N. T., XUYEN, N. T., HAI, N. S., ANH, N. T., DUNG, P. T., & THANH, D. T. M. (2018). Synthesis, characterization and antimicrobial activity of copper doped hydroxyapatite. **Vietnam Journal of Chemistry**, 56(6), 672–678. https://doi.org/10.1002/vjch.201800068

NGUYEN, T. D. T., JANG, Y. S., LEE, M. H., & BAE, T. S. (2019). Effect of strontium doping on the biocompatibility of calcium phosphate-coated titanium substrates. **Journal of Applied Biomaterials and Functional Materials**, 17(1). https://doi.org/10.1177/2280800019826517

PINA, S., CANADAS, R. F., JIMÉNEZ, G., PERÁN, M., MARCHAL, J. A., REIS, R. L., & OLIVEIRA, J. M. (2017). Biofunctional Ionic-Doped Calcium Phosphates: Silk Fibroin Composites for Bone Tissue Engineering Scaffolding. **Cells Tissues Organs**, 204(3–4), 150–163. https://doi.org/10.1159/000469703

POPA, C. L., DENIAUD, A., MICHAUD-SORET, I., GUÉGAN, R., MOTELICA-HEINO, M., & PREDOI, D. (2016). Structural and biological assessment of zinc doped

hydroxyapatite nanoparticles. **Journal of Nanomaterials**, 2016. https://doi.org/10.1155/2016/1062878

PREDOI, D., ICONARU, S. L., PREDOI, M. V., STAN, G. E., & BUTON, N. (2019). Synthesis, characterization, and antimicrobial activity of magnesium-doped hydroxyapatite suspensions. **Nanomaterials**, 9(9), 1–20. https://doi.org/10.3390/nano9091295

PUTRAKUMAR, B., SEELAM, P. K., SRINIVASARAO, G., RAJAN, K., RAJESH, R., RAMACHANDRA RAO, K., & LIANG, T. (2020). High performance and sustainable copper-modified hydroxyapatite catalysts for catalytic transfer hydrogenation of furfural. **Catalysts**, 10(9), 1–17. https://doi.org/10.3390/catal10091045

REBELO, A. R., ARCHER, A. J., CHEN, X., LIU, C., YANG, G., & LIU, Y. (2018). Dehydration of bacterial cellulose and the water content effects on its viscoelastic and electrochemical properties. **Science and Technology of Advanced Materials**, 19(1), 203–211. https://doi.org/10.1080/14686996.2018.1430981

SASKA, S., BARUD, H. S., GASPAR, A. M. M., MARCHETTO, R., RIBEIRO, S. J. L., & MESSADDEQ, Y. (2011). Bacterial Cellulose-Hydroxyapatite Nanocomposites for Bone Regeneration. **International Journal of Biomaterials**, 2011, 1–8. https://doi.org/10.1155/2011/175362

SOFI, H. S., ASHRAF, R., BEIGH, M. A., & SHEIKH, F. A. (2018). Scaffolds Fabricated from Natural Polymers/Composites by Electrospinning for Bone Tissue Regeneration. **Advances in Experimental Medicine and Biology**, 1078, 49–78. https://doi.org/10.1007/978-981-13-0950-2_4

TEIXEIRA, S. R. Z., REIS, E. M. D., APATI, G. P, MEIER, M. M., NOGUEIRA, A. L., GARCIA, M. C. F., SCHNEIDER, A. L. D. S., PEZZIN, A. P. T., Porto, L. M. (2019). Biosynthesis and Functionalization of Bacterial Cellulose Membranes with Cerium Nitrate and Silver Nanoparticles. **Materials Research**. 22, e20190054. http://dx.doi.org/10.1590/1980-5373-MR-2019-0054.

TU, Y., CHEN, C., LI, Y., HOU, Y., HUANG, M., & ZHANG, L. (2017). Fabrication of nano-hydroxyapatite/chitosan membrane with asymmetric structure and its

applications in guided bone regeneration. **Bio-Medical Materials and Engineering**, 28(3), 223–233. https://doi.org/10.3233/BME-171669

VOLOVA, T. G., PRUDNIKOVA, S. V., SUKOVATYI, A. G., & SHISHATSKAYA, E. I. (2018). Production and properties of bacterial cellulose by the strain *Komagataeibacter xylinus* B-12068. **Applied Microbiology and Biotechnology**, 102(17), 7417–7428. https://doi.org/10.1007/s00253-018-9198-8

WANG, Q., TANG, P., GE, X., LI, P., LV, C., WANG, M., WANG, K., FANG, L., & LU, X. (2018). Experimental and simulation studies of strontium/zinc-codoped hydroxyapatite porous scaffolds with excellent osteoinductivity and antibacterial activity. **Applied Surface Science**, 462, 118–126. https://doi.org/10.1016/j.apsusc.2018.08.068

WU, J., YIN, N., CHEN, S., WEIBEL, D. B., & WANG, H. (2019). Simultaneous 3D cell distribution and bioactivity enhancement of bacterial cellulose (BC) scaffold for articular cartilage tissue engineering. **Cellulose**, 26(4), 2513–2528. https://doi.org/10.1007/s10570-018-02240-9

ZHANG, M.-L., CHENG, J., XIAO, Y.-C., YIN, R.-F., & FENG, X. (2017). Raloxifene microsphere-embedded collagen/chitosan/β-tricalcium phosphate scaffold for effective bone tissue engineering. **International Journal of Pharmaceutics**, 518(1–2), 80–85. https://doi.org/10.1016/j.ijpharm.2016.12.031

ZHANG, S., XIONG, G., HE, F., HUANG, Y., WANG, Y., & WAN, Y. (2009). Characterisation of Hydroxyapatite/Bacterial Cellulose Nanocomposites. **Polymers and Polymer Composites**, 17(6), 353–358. https://doi.org/10.1177/096739110901700602

ZHU, H., GUO, D., SUN, L., LI, H., HANAOR, D. A. H., SCHMIDT, F., & XU, K. (2018). Nanostructural insights into the dissolution behavior of Sr-doped hydroxyapatite. **Journal of the European Ceramic Society**, 38(16), 5554–5562. https://doi.org/10.1016/j.jeurceramsoc.2018.07.056.

4.8 Supplementary material

S1. Result of EDS surface analysis of biocomposites: BNC/MgAp; BNC/CuAp; BNC/ZnAp and BNC/SrAp in compositions 1, 3 and 5%.

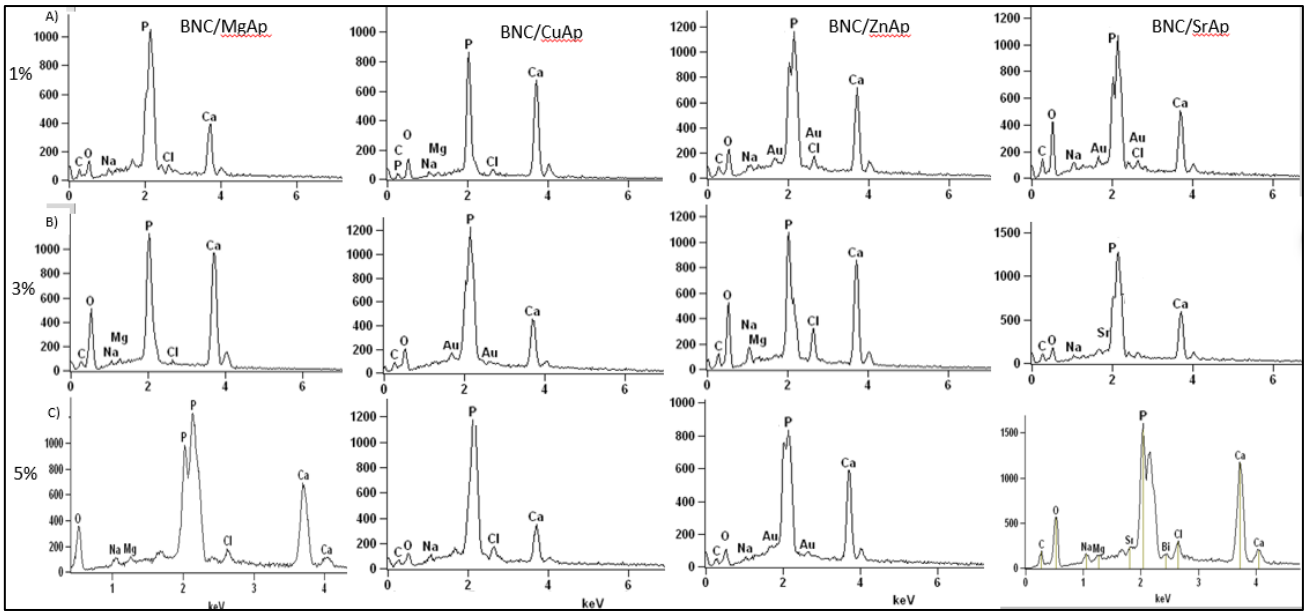

S2. Data obtained from FTIR analysis for BNC membranes and biocomposites BNC/HAp (standard), BNC/MgAp, BNC/CuAp, BNC/ZnAp, and BNC/SrAp.

Vibrational frequencies	**BNC**	**BNC/HAp**	**BNC/ MgAp 1%**	**BNC/ MgAp 3%**	**BNC/ MgAp 5%**	**BNC/ CuAp 1%**	**BNC/ CuAp 3%**	**BNC/ CuAp 5%**	**BNC/ ZnAp 1%**	**BNC/ ZnAp 3%**	**BNC/ ZnAp 5%**	**BNC/ SrAp 1%**	**BNC/ SrAp 3%**	**BNC/ SrAp 5%**	Ref.
OH stretching	3338	3344	3453	3349	3454	3351	3347	3450	3350	3347	3350	3350	3344	3341	(Saska et al.2011)
Water OH bending	1635	1644	1639	1640	1641	1640	1638	1639	1641	1638	1648	1635	1639	1630	(Casaburi et al. 2018)
Stretching mode of CO_3^2	---	1415	1415	1415	1418	1418	1418	---	---	---	1418	1418	1416	1418	(Popa et al., 2016, Giannoulatou et al. 2018)
Antisymmetric bridge C–O–C stretching	1163	1142	---	---	---	1176	1196	1158	1158	1149	1162	---	1145	1147	(Grande et al. 2009)
C–O C-C strecthing	1057	---	---	---	---	1078	---	---	1065	---	---	---	---	---	(Grande et al. 2009)
Asymmetric stretching vibration of P–O bond	---	1020	1020	1019	1020	1022	1017	1012	1021	1021	1023	1020	1020	1014	(Hutchens et al. 2006)
		958	963	961	960	962	960	957	961	962	960	963	960	960	(Putrakumar et al. 2020, Popa et al. 2016)
Stretching mode of CO_3^2	873	871	871	872	868	872	871	869	872	872	869	871	871	871	(Popa et al. 2016; Casaburiet al. 2018)

S3. Table with maximum degradation temperature (T_{max}) and percentage of mass loss (M%) data obtained from the TG and DTG curves of BNC/HAp biocomposites (standard) and BNC/MgAp, BNC/CuAp, BNC/ZnAp, BNC/SrAp.

	M_1 (%)	$T_{máx2}$ (°C)	M_2 (%)	$T_{máx3}$ (°C)	M_3 (%)	$T_{máx4}$ (°C)	M_4 (%)	$T_{máx5}$ (°C)	M_5 (%)	$T_{máx6}$ (°C)	M_6 (%)	Residue (%)
BNC/HAp	3.78	119	1,02	232	3,28	320	24,46	412	5,51	763	1,6	58,23
BNC/MgAp 1%	3.08	122	1,76	220	4,09	315	28,78	435	5,65	791	1,95	52,14
BNC/MgAp 3%	3.33	126	2,91	-	-	330	26,72	443	5,02	702	0,56	60,79
BNC/MgAp 5%	2.95	123	2,39	-	-	332	25,73	444	4,77	-	-	62,82
BNC/CuAp 1%	1.78	125	2,81	-	-	317	27,54	437	6,5	754	0,66	59,67
BNC/CuAp 3%	1.5	126	3,38	-	-	319	26,27	428	5,2	735	0,86	62,29
BNC/CuAp 5%	2.14	126	2,36	234	7,34	314	19,15	444	5,15	856	10	51,96
BNC/ZnAp 1%	4.05	120	0,92	220	4,93	322	21,34	432	4,21	844	5,23	58,36
BNC/ZnAp 3%	3.2	119	1,53	224	9,73	330	17,4	452	3,31	885	13,98	50,16
BNC/ZnAp 5%	2.87	119	1,22	218	4,17	331	22,63	434	3,73	818	3,41	60,36
BNC/SrAp 1%	3.24	129	3,02	228	2,51	325	19,3	432	3,52	-	-	65,60
BNC/SrAp 3%	4.46	119	0,67	225	2,31	325	23,8	417	3,81	788	1,8	61,60
BNC/SrAp 5%	5.03	124	0,13	219	3,23	323	26,83	428	5,25	801	2,4	54,17

5 CHAPTER: Unpublished results

Cytocompatibility study and enzymatic biodegradation of BNC/HAp biocomposites, BNC/MgAp, BNC/ZnAp and BNC/SrAp

The use of biocomposites in regeneration has been explored, seeking biomimetic properties. In this context, biocomposites emerge that add bacterial nanocellulose (BNC) with a unique nanofibrillar network morphology, similar to collagen fibers and hydroxyapatite (HAp) chemical and crystalline structure similar to natural bone apatite, in addition to the incorporation of trace elements existing in bones, such as Na^{+}, Sr^{2+} and Mg^{2+} can increase osteogenesis and neovascularization. However, the lack of metabolic processes for the degradation of BNC in the body is still challenging. In this context, this work aims to study the cellulase-mediated degradation of NBC/HAp biocomposites partially replaced by Mg, Zn and Sr cations, in addition to a study of cell adhesion aiming at its application as an implantable biomaterial. Therefore, the biocomposites were first characterized by Raman and then subjected to cell adhesion assay with osteoblasts MC3T3-E1 and enzyme biodegradation assay in the presence of cellulases. No new bands were observed in the Raman spectra due to the low concentration of ions, but some band shifts suggest their incorporation. However, at all observed times, cell growth was significantly higher in the biocomposites than in the BNC/HAp control. While the cellulases were able to affect the structure of BNC in the biocomposites, producing only a precipitate of cellulosic crystals at the end of the assay.

Keywords: Bacterial Nanocellulose. Cellulase. Biodegradation. Hydroxyapatite. Biocomposites.

5.1 Introduction

Three-dimensional (3D) scaffolds are highly efficient as they provide a physical environment for remodeling tissue structures (ESLAMI-ARSHAGHI; VAKILIAN; SEYEDJAFARI, 2016). It is important to emphasize that in a living organism, the cell microenvironment is inherently three-dimensional; this environment, represented by the Extracellular Matrix (ECM), is crucial for cell development and behavior, such as growth, proliferation, migration and its normal metabolism (DA ROCHA; PORTO; RAMBO, 2014).

In order to imitate the ECM, the development of 3D scaffolds should be able to serve as a substrate to interact with cells, support newly graduated tissues, provide nutrients and promote cell invasion (WU et al., 2019).

Hydrogels, composed of cross-linked hydrophilic polymeric networks, provide an ideal platform to mimic key in vivo characteristics of the microenvironments surrounding cells (HILDERBRAND et al., 2016). In this sense, bacterial nanocellulose (BNC) hydrogels stand out for their high purity and architecture composed of randomly organized nanofibrils, building a highly porous structure, similar to natural ECM (DA ROCHA; PORTO; RAMBO, 2014).

The BNC presents itself as a basic nanofibrils structure consisting of a β(1-4) glucan chain, with the molecular formula $(C_6H_{10}O_5)_n$. It has high purity, high crystallinity, high porosity, high water holding capacity and excellent biocompatibility (AN et al., 2017; BALDIKOVA et al., 2017; RECOUVREUX et al., 2011).

Different types of biomaterials, based on calcium phosphate, have been extensively studied, aiming at the application in bone regeneration, emphasizing hydroxyapatite (HAp), an essential bioactive component present in bones, which facilitates the differentiation and growth of cells of this tissue (WU et al., 2019).

Nanostructures based on nanofibers were designed to enhance the mechanical properties of scaffolds to mimic natural bone. Nanocomposites have been applied to produce osteoinductive structures by increasing surface area and volume proportions, improving surface roughness and changing nano-topography (SHI et al., 2019). In this sense, BNC/HAp biocomposites have also been extensively studied for bone regeneration applications (WU et al., 2019).

Furthermore, it is essential to emphasize that bone tissue is naturally a composite, composed not only of calcium phosphate but also other elements such as Na^+, Mg^{2+} or Sr^{2+} in the form of trace elements. These trace elements play a vital role in bone growth and repair. They can control degradation, increase the mechanical strength of materials and upregulate their bioactive properties, such as osteoconduction (EHRET et al., 2017).

However, the lack of biochemical processes that promote the biodegradability of BNC in the human organism making it a bioabsorbable biomaterial, still represents an obstacle to be overcome (WANG et al., 2016).

In the search for solutions, some research has been carried out in the sense of partial pre-oxidation using chemical agents such as sodium metaperiodate (CALVINI, et al., 2006), TEMPO (2,2,6,6-tetrametil-1-piperidinoxilo) (CHITBANYONG; PISUTPICHED; KHANTAYANUWONG, 2020) or the use of 2,3-dialdehyde BC (DABC) as an alternative to improve the degradability of BNC; however, it is essential to note that chemical modification damages the mechanical properties of BNC which may limit its application for specific tissue repair (WANG et al., 2016). In addition to studying the enzymatic degradation of regenerated cellulose (RCS) with cellulases and lysozyme (ARAÚJO et al., 2016).

Cellulases can quickly degrade cellulose under appropriate conditions (WANG et al., 2016). Cellulases are enzymes from fungi such as *Trichoderma sp*, *Aspergillus sp* and *Penicillium sp.* Therefore, their optimal activity is usually close to pH 5 (MIAO et al., 2016). However, considering the metabolic processes of bone regeneration and having alkaline phosphatase as the primary indicator of this process, with an optimal pH between 8.5 and 9.5 (MAZORRA; RUBIO; BLASCO, 2002) (BARBIERI, 2006), and the physiological pH of the human body around 7.4 (HOPKINS; SANVICTORES; SHARMA, 2022) cellulase activity can be inhibited at these pH values.

In this context, this work aims to study cellulase-mediated degradation of NBC/HAp biocomposites partially replaced by Mg, Zn and Sr cations at pH 8.5 and perform a cell adhesion study aiming at the application as an implantable biomaterial.

5.2 Material and methods

5.2.1 Raman spectroscopy

According to Al-Wafi et al. (2017), Raman spectroscopy is essential in analyzing information about the prepared material's chemical bond, especially in observing the behavior of PO_4^{3} ions, which are the basic units of HAp structures. Raman spectroscopy was performed using Anton Paar Cora 5200 Raman

equipment, in the spectral range of 100 to 2000 cm^{-1}, with laser power at 450 mW and a single wavelength at 785 nm (PEREIRA et al., 2021).

5.2.2 Cell adhesion assay

For the cell adhesion assay, osteoblasts of the MC3T3-E1 lineage were used, according to Santos et al. (2020). Cells were cultured in α-MEM medium (α-Modified Eagle's Medium, M0644-Sigma®) supplemented with 1% penicillin/streptomycin (SigmaAldrich®) and 10% fetal bovine serum (FBS, Sigma-Aldrich®). After activation and growth with 80% confluence of plate filling, the cells were detached using trypsin TrypLE Express Enzyme, Thermo Fisher Scientific®) and then centrifuged for 2 min at 5000 rpm to remove it. Osteoblasts were resuspended in the medium and culture and quantified in a Neubauer chamber (SP Labor, Brazil).

The previously sterilized biocomposites were deposited in 96-well tissue culture plates and hydrated with a culture medium for 24 h. After this period, the culture medium was removed, and the cells were seeded on the samples at a density of $1.5 \cdot 10^5$ cells/cm^2 for each biomaterial.

BNC/HAp biocomposites were used as controls. The assay was conducted for 21 days, with samples taken at 1, 7, 14 and 21 days. After these periods, the biocomposites were washed with PBS. The MTS assay was used to quantify the activity of metabolically active adherent cells.

This assay was carried out in octoplicate only with samples of BNC/HAp, BNC/MgAp, BNC/ZnAp and BNC/SrAp biocomposites at a concentration of 1%, these being the samples that showed a less adverse effect on the metabolic activity of the tested cells.

The cell growth data obtained were statistically analyzed and submitted to the Shapiro-Wilk Normality Test with a significance of 0.05 (95% confidence). Considering that p-value < 0.05 means that the samples do not follow a normal distribution but a non-parametric distribution which, according to Pérez (2019), refers to the fact that there are no parameters involved in the traditional sense of the term parameter used, being applied in situations where standard theoretical procedures cannot be used.

Thus, for data with non-normal distribution, the Kruskal-Wallis test was applied with 95% confidence (significance of 0.05), which according to Pires et al. (2018), allows the comparison of more than two groups in independent samples, where the following hypotheses were tested: null hypothesis (which suggests that there is no difference between doping) and alternative hypothesis (there is a significant difference between doping). When $p > 0.05$, there is no significant difference, and when $p < 0.05$, there is a significant difference between the dopings. To compare each doping with the Ca standard, the non-parametric Mann-Whitney test was used.

5.2.3. Total cellulase assay

According to Zhang, Hong and Ye (2009), a total cellulase system consists of three enzymatic activities: endoglucanases, exoglucanases and β-D-glucosidases. Therefore, total cellulase activity should be measured using insoluble cellulosic substrates such as Whatman No. 1, cotton, CMC, and bacterial cellulose, among others.

Thus, the enzyme activity was measured by the filter paper method (FPA) according to the changes methodology of Zhang, Hong and Ye (2009). Whatman No. 1 was cut into 1.0 x 6.0 cm strips (about 50 mg) and placed in test tubes to which 1 mL 50 mM citrate buffer (pH 4.8) and 1 mL of the extract were added enzyme (diluted when necessary) and incubated in a thermostatic bath at 50 °C for 60 minutes.

The product of this reaction was analyzed by the DNS colorimetric method (Miller, 1959). Briefly, 1 mL of this reaction solution was added to 1 mL of DNS reagent, and the reaction took place in a thermostatic bath (100 °C) for 5 minutes. Afterward, the mixture was cooled in an ice bath, and 10 mL of deionized water was added. The absorbance was read at 540 nm in a UV-Vis spectrophotometer, and the enzymatic activity was calculated simultaneously.

The method was previously standardized by a glucose calibration curve (0.25 to 2.0 $mg.mL^{-1}$). The absorbance reading was performed in a spectrophotometer (LKB Biochron – Novaspec II) at 540 nm, using disposable

cuvettes. The absorbance values were converted to reducing sugars concentration values (μmol.mL^{-1}) by interpolation in the standard curve.

Thus, after the previous analytical determinations, the enzyme concentrations (IU. mL^{-1}) were calculated according to the equation (1):

$$[enzyme] = [RS] \times V_{mixture} \times (t_{reaction})^{-1} \quad (1)$$

Where:
[RS] = concentration of reducing sugars produced (μmol.mL^{-1})
V = volume of the reaction mixture (mL)
reaction = enzymatic reaction time (min)

5.2.4 Preliminary study of BNC degradation in enzymatic solution evaluating the influence of pH

The BNC degradation assays followed the methodology (OLIVEIRA; RAMBO; PORTO, 2013) with adaptations. BNC discs about 0.5 cm in diameter were placed in test tubes containing phosphate buffer solutions at pH 7 and 8.5. These were autoclaved and added with 100 μL of a cellulase solution (145.27 UI. mL^{-1}) (Blend Cellulase SAE 0020, Sigma) and then incubated at 37 °C in a thermostatic bath.

Samples were collected at different times to monitor the degradation process and accompanied by visual analysis through images, analysis of glucose concentration (degradation product) by the colorimetric method of 3-5-dinitro salicylic acid DNS (MILLER, 1959) and determination of absorbance, was read at 540 nm which was read in a spectrophotometer (LKB Biochron – Novaspec II). The assay was performed in triplicate.

5.2.5 Degradation assay of biocomposites in an enzymatic solution

The enzymatic degradation assay of the biocomposites followed the methodology established from item 5.2.3. However, this assay was conducted only at pH 8.5. During the test, the samples were accompanied by visual analysis through images. Afterward, the samples were centrifuged at 3800 rpm for 10 min, and the supernatant was collected to determine the concentration of the reducing sugar by DNS and how enzymatic degradation product. After 12 h of biodegradation, the precipitated material was analyzed by XRD for comparison with samples without degradation.

5.2.5.1 Wide-angle X-ray diffractometry (XRD)

X-ray diffraction was measured with an X-ray diffractometer (Bruker XRD 8 Advance), using CuKα radiation 1.5418 with 1000 W of power, 40 kV, 25 mA, and a digital detector with 160 channels. The angle 2θ covered the study range from 5° to 70° at 0.02 °/s.

5.3 Results and discussion

5.3.1 Raman spectroscopy

The Raman spectra for all samples are shown in Figure 5.1 and summarized in Table 5.1. It was possible to observe, for all samples, an intense band around ~960 cm^{-1} corresponding to the symmetrical axial deformation (υ 1) of the PO_4 group and the other three bands of lower intensity around ~1046, ~589 and ~431 cm^{-1} relative to asymmetric axial strain (υ 3), symmetric angular strain (υ 4) and asymmetric angular strain (υ 2) of PO_4 respectively (AINA et al., 2013; AL-WAFI et al., 2017; BORGES, 2018).

Aina et al. (2013) discussed in their work that the ~1050 band was consistent with network modes υ3 of (PO_4^{-3}) and network modes υ1 of (HPO_4^{-2}) and mode υ3 of (CO_3^{-2}). While the band at ~1080 cm^{-1} was attributed to the υ1 mode of (CO_3^{-2}), it characterized the formation of type A carboapatite. It is

noteworthy that, in this work, the band ~1080 cm^{-1} appeared only in the biocomposites added of metals with different intensities and different displacements as a function of the ion (1082 – 1098 cm^{-1}). This data agrees with what was previously observed in the FT-IR analyses.

Figure 5.1: Raman spectra of BNC/HAp biocomposites (standard) and: A) BNC/MgAp; B) BNC/CuAp; C) BNC/ZnAp, and D) BNC/SrAp.

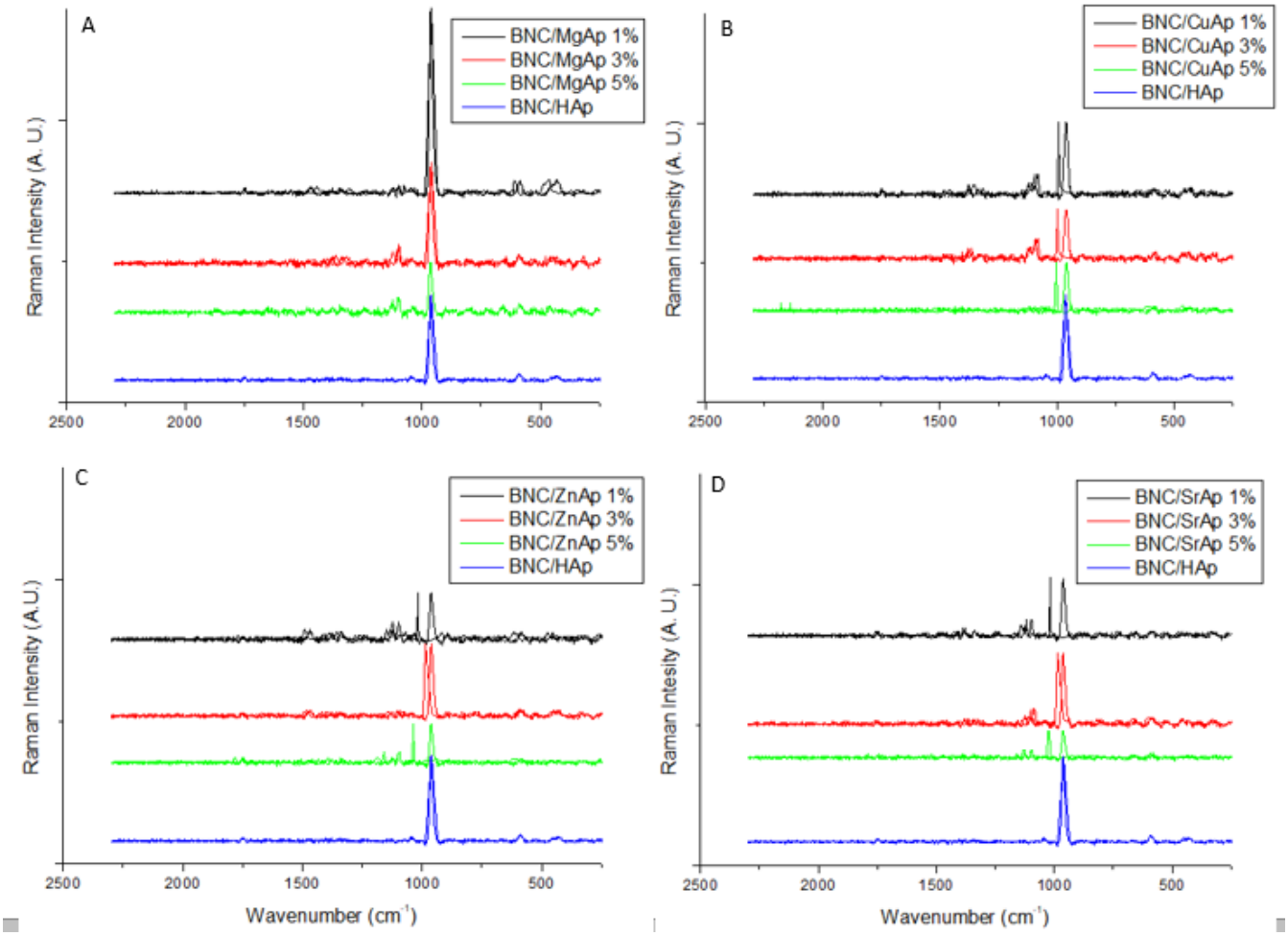

Table 5.1: Data obtained from Raman analysis for BNC/HAp (standard) and the biocomposites BNC/MgAp, BNC/CuAp, BNC/ZnAp, and BNC/SrAp, compared with the literature references.

Wavenumber (cm^{-1})	HAp (ref)	BNC/HAp	BNC/ MgHAp 1%	BNC/ MgHAp 3%	BNC/ MgHAp 5%	BNC/ CuHAp 1%	BNC/ CuHAp 3%	BNC/ CuHAp 5%	BNC/ ZnHAp 1%	BNC/ ZnHAp 3%	BNC/ ZnHAp 5%	BNC/ SrHAp 1%	BNC/ SrHAp 3%	BNC/ SrHAp 5%	Ref.
Asymmetric angular deformation (υ3) PO_4^{3-}	1050	1046	1046	1046	1046	1042	1042	1042	---	---	1034	1018	---	1022	(Aina et al., 2013) Borges (2018)
Asymmetric angular deformation (υ3) CO_3^{2-}	1080	---	1095	1095	1095	1086	1082	---	1098	1098	1098	1098	1086	1098	(Aina et al., 2013) Borges (2018)
Symmetrical angular deformation (υ1) PO_4^{3-}	960	963	963	963	963	959	959	959	959	959	959	963	963	959	(Aina et al., 2013) Borges (2018)
Symmetrical angular deformation (υ4) CO_3^{2-}	766	---	---	---	---	---	---	---	---	---	---	727	727	---	(Aina et al., 2013) Borges (2018)
Symmetrical angular deformation (υ4) PO_4^{3-}	580	589	585	589	589	589	589	589	585	585	---	589	589	589	(Aina et al., 2013) Borges (2018)
Asymmetric angular deformation (υ2) PO_4^{3-}	430	431	431	---	---	431	431	431	---	443	---	431	431	431	(Aina et al., 2013) Borges (2018)

No new bands appeared in the biocomposites, but it was observed that the main analytical Raman band of (PO_4^{3-}) at 960 cm^{-1} suffered some small displacements (959 to 963 cm^{-1}). Aina et al. (2013) observed, in their work with Sr-substituted hydroxyapatites, that the displacement of this band and the reduction of its amplitude were related to the greater mass of Sr concerning Ca. This work was observed for the BNC/CuAp, BNC/ZnAp and BNC/SrAp biocomposites, although for the last two, the samples containing 3% showed more intense peaks than the others. For the BNC/MgAp samples, this same peak seems to have been intensified in BNC/MgAp 1%, reducing the intensity as the Mg content in the sample was high.

5.3.2 Cell adhesion assay

In Fig. 5.2, data on the metabolic activity of osteoblasts on the biocomposites BNC/HAp, BNC/MgHAp, BNC/ZnHAp and BNC/SrHAp in the periods of 1, 7, 14 and 21 days are presented.

Figure 5.2: Cell adhesion assay with osteoblasts MC3T3 on the biocomposites BNC/HAp 1%, BNC/MgHAp 1%, BNC/ZnHAp 1% and BNC/SrHAp 1% in the periods of 1, 7, 14 and 21 days.

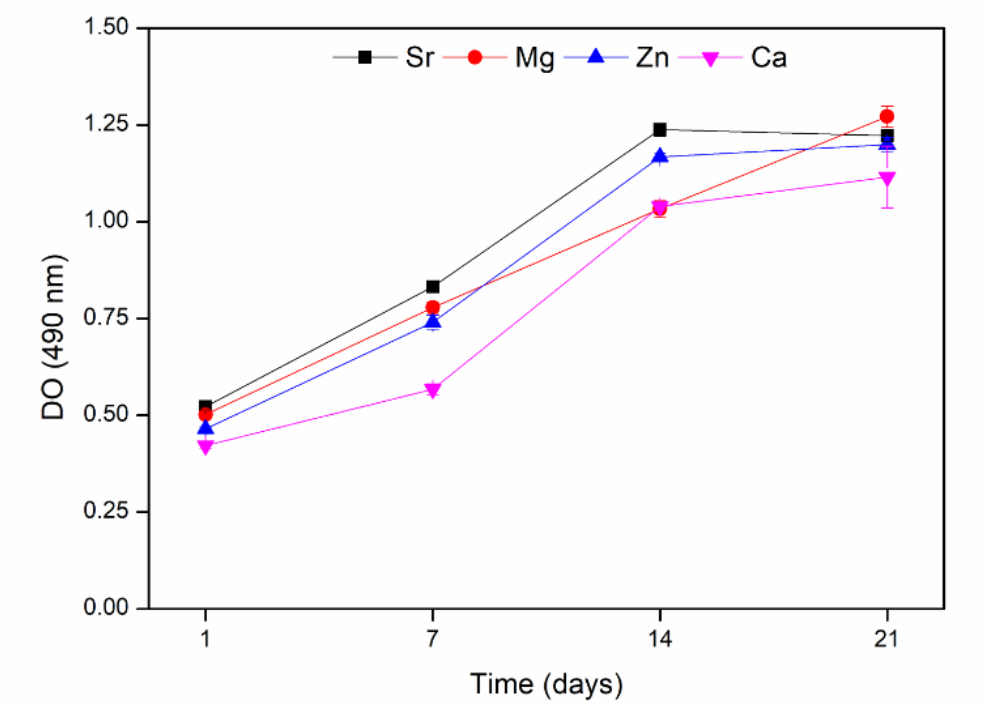

This result demonstrated more significant cell growth after seven days of all biocomposites compared to the control, which, according to Santos et al. (2020) (SANTOS et al., 2020) may be related to a good interaction of cells with these biomaterials, demonstrating a preference for adhesion in the first days. Over time, however, the behavior of cells on the biocomposites changes, highlighting the biocomposites BNC/SrAp 1% and BNC/ZnAp 1% as being more favorable to cell growth in 14 days.

At 21 days, although the behavior of the cells concerning the BNC/SrAp 1% and BNC/ZnAp 1% biocomposites did not undergo significant changes in the result presented at 14 days, the BNC/MgAp 1% sample was the only one that highlighted both about the control and with the other samples. It is also noteworthy that the 1% BNC/MgAp sample was the only one that maintained an increasing result throughout the entire trial.

These findings may be related to the oligodynamic property highlighted by Ehret et al. (2017). According to the authors, these elements play a vital role in bone growth and repair, controlling degradation and positively regulating their bioactive properties, such as osteoconduction.

This positive influence on the cell growth of the biocomposites about the standard can also be seen in the analysis of the distribution of the medians considering the entire assay about the BNC/HAp standard (Figure 5.3).

The Mann-Whitney test was used to compare the effect on cell growth of each biocomposite in each period compared to the BNC/HAp standard. Thus, it was possible to observe that there was a significant difference in all samples in reaction to the BNC/HAp control in all analysis periods with $p < 0.05$ ($p = 0.0001554$). Only the BNC/MgAp 1% sample in 14 days of analysis differed from this pattern, with no significant difference from the control ($p = 0.573737$). This result is still considered positive due to the general behavior over time and because of, in this case, being on an equal footing with the control.

Figure 5.3: Distribution of medians of cell growth data referring to cell adhesion assay with osteoblasts MC3T3 on the biocomposites BNC/HAp 1%, BNC/MgAp 1%, BNC/ZnAp 1% and BNC/SrAp 1%.

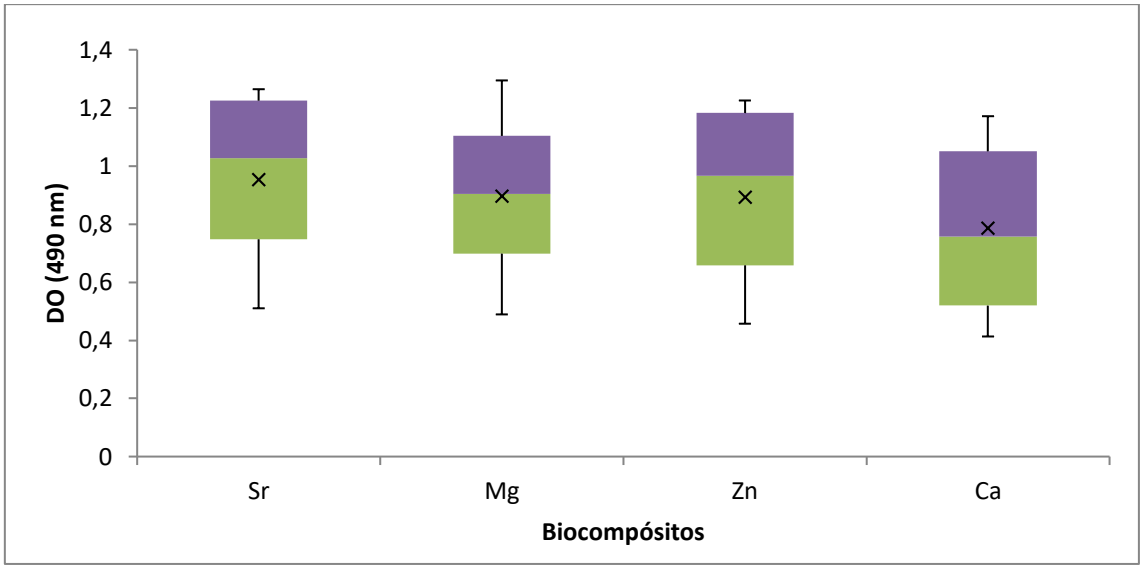

The results indicate that the cellular viability of the biocomposites was higher than those of the control group at different time points, demonstrating good cytocompatibility. According to (ZHANG et al., 2020) Zhang et al. (2020), cell viability is essential for tissue regeneration and the entire trauma repair process.

5.3.3. Preliminary study of BNC degradation in enzyme solution

Considering the optimal pH for alkaline phosphatase activity between 8.5 and 9.5 (MAZORRA; RUBIO; BLASCO, 2002), which, in this work, is being considered as an indicator of bone formation (BARBIERI, 2006), and the physiological pH of the body around 7.4 (HOPKINS; SANVICTORES; SHARMA, 2022) was carrying out a preliminary assay to verify the degradation of pure BNC using a cellulase enzymatic solution to verify the influence of these pHs on the cellulase enzymatic activity. Cellulase is an enzyme produced mainly from fungi such as *Trichoderma sp*, *Aspergillus sp* and *Penicillium sp*. Therefore, its optimal activity is usually close to pH 5 (MIAO et al., 2016).

Figure 5.4 shows the images of the BNC samples submitted to the enzymatic biodegradation test in phosphate buffer at pH 7.5 and 8.5. According

to the images, it is possible to observe that at pH 7.5, in just 2 h, the membrane showed signs of fragmentation. After 6 h, observing small fragments in suspension was only possible. These fragments remained until the end of the assay (48 h). While at pH 8.5, in 2 h of an assay, the membranes were completely intact; in 6 h, they presented the first crack and only in 12 h did more intense signs of fragmentation appear and only after 24 h the membrane had been completely fragmented, showing only material suspended in the test tube. As in the pH 7.5 assay, these suspended fragments remained until 48 h when the assay was completed.

According to Penttilä et al. (2018), the mechanism of degradation of BNC by cellulolytic enzymes occurs by the process of fibrillation of BNC strands into thinner cellulose microfibril (CMF) bundles through longitudinal cracks and, after the hydrolysis of this CMF proceeds faster, while some more substantial beams will retain their morphology even at higher degrees of hydrolysis. The authors verified by SEM and SAXS (Small-angle X-ray scattering) that after 4 h, despite the general appearance of the fragmented sample, there were still CMF bundles and strips practically intact, which was also reflected in a low change in the degree of crystallinity of the samples.

Figure 5.5 presents data on reducing sugars concentration as a function of time as a product of BNC degradation by cellulases. The results show that the sugar concentration in the reaction medium increased due to this treatment. It was possible to observe that the enzymatic biodegradation process occurred more intensely in the first 6 h, with few changes concerning glucose production after 12 h at both tested pHs. This result differs from what was observed in the visual analysis (Fig 5.4).

Figure 5.4: Visual analysis of the enzymatic biodegradation process of BNC at pH 7.5 and 8.5.

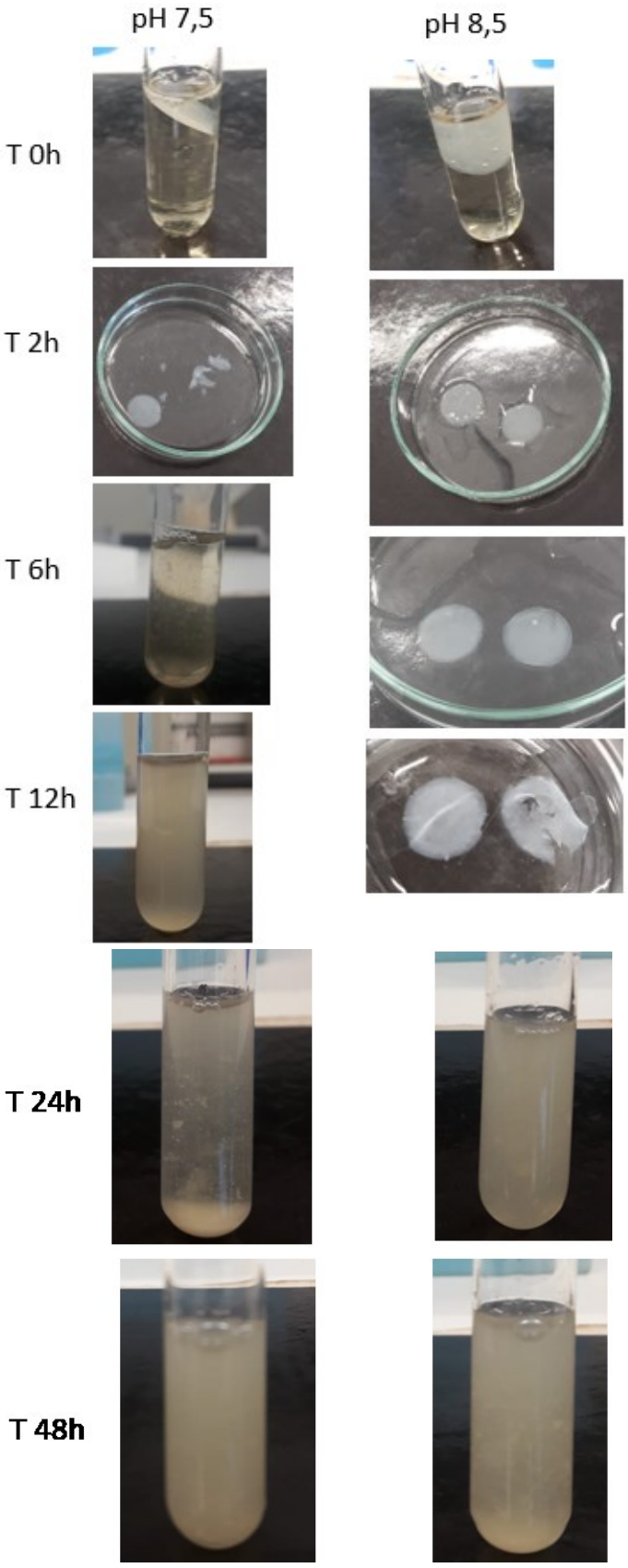

Figure 5.5: BNC biodegradation assay compared at pH 7.5 and 8.5, analysis of sugar production as a function of the enzymatic attack.

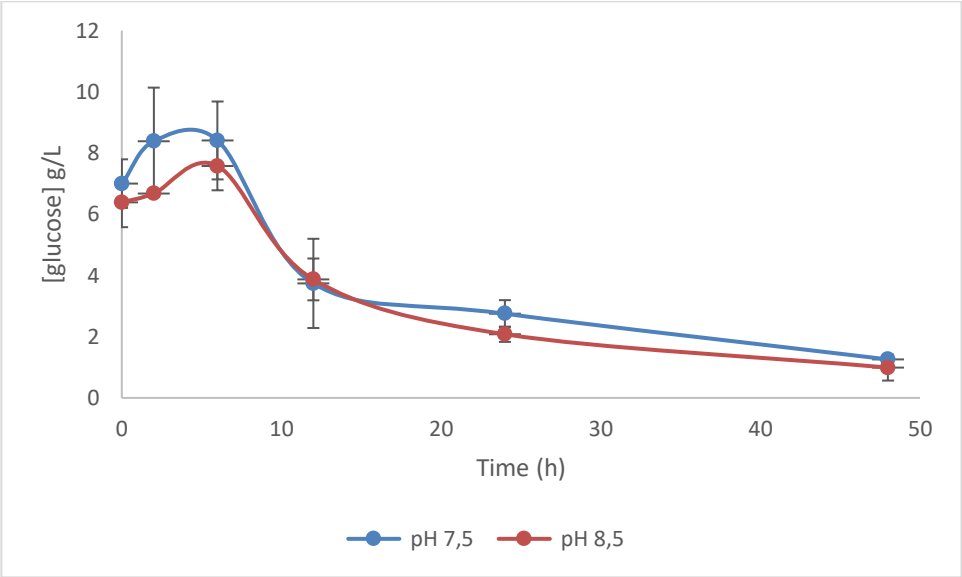

Pentilä et al. (2018), in their studies, analyzed the enzymatic hydrolysis of bacterial cellulose-hemicellulose composites from a commercial cellulase mixture (Celluclast). The authors observed the increasing formation of glucose during the first 10 h of the assay. Also, considering other assays such as GC, XRD and SEM, it is suggested that the least ordered part initiated the degradation of BNC. In addition to the formation of glucose, the authors also identified the formation of other sugars in lower concentrations, such as xylose, mannose, galactose, rhamnose, and arabinose.

A point that drew attention was the reduction in glucose concentration over time, considering that reaction volumes were not removed during the assay. Pentilä et al. (2018) also mention a reduction in the “shoulder” characteristic of the graph after ten h of testing. Two propositions can be made regarding this behavior: As the enzyme solution used was a “blend”, endoglucanases and exoglucanases in addition to β-glucosidase may also be present, and although their synergistic effect is well seen on the breaking of bonds in the BNC, Ribeiro (2020) highlights that the hydrolysis product can inhibit exoglucanases. Furthermore, according to the findings of Penttilä et al. (2018), already mentioned in this work, the mechanism of enzymatic degradation of BNC occurs by the

fibrillation of NBC strands in bundles of more resistant cellulose microfibrils, reducing the access or effectiveness of enzymes on these bundles.

Another factor that stands out, although on average, biodegradation at pH 7.5 was more intense in this first 6 h compared to pH 8.5, it can be seen from the standard deviations that the behavior was very similar for both the tested pHs. Based on these results and considering the pH of alkaline phosphatase as an indicator of bone regeneration, the assay with the biocomposites was conducted only at pH 8.5.

5.3.5 Degradation assay of biocomposites in an enzymatic solution

The enzymatic biodegradation process of the composites underwent little change about what has already been observed for pure BNC; it was possible to observe that it occurred more slowly initially, which may be due to the coating of BNC microfibrils by apatites.

Figure 5.6 shows photographs of samples of BNC/HAp, BNC/MgHAp, BNC/ZnHAp and BNC/SrHAp submitted to the enzymatic biodegradation assay in phosphate buffer at pH 8.5. The images allowed observing a behavior trend like that of pure BNC at pH 8.5. The first signs of fragility were detected only after 12 h of testing. However, interestingly, even after 24 h of testing, the BNC/ZnHAp and BNC/SrHAp samples were still intact, but after 48 h, all samples were similarly fragmented.

Figure 5.7 presents sugar production data as a function of enzymatic degradation time at pH 8.5. In the enlarged portion of the graph, it can be observed that the BNC/MgHAp and BNC/HAp biocomposites showed higher sugar formation in the first two h of the test. After 6 h, the BNC/MgHAp sample still showed high concentrations, while the BNC/HAp sample started to show lower values. The BNC/SrHAp sample showed higher sugar values only at 6 h, while the BNC/ZnHAp sample showed little change. These results agree with what was observed in the visual analysis.

Figure 5.6: Visual analysis of BNC/HAp, BNC/MgHAp, BNC/ZnHAp and BNC/SrHAp biocomposites subjected to enzymatic degradation in phosphate buffer pH 8.5 as a function of time.

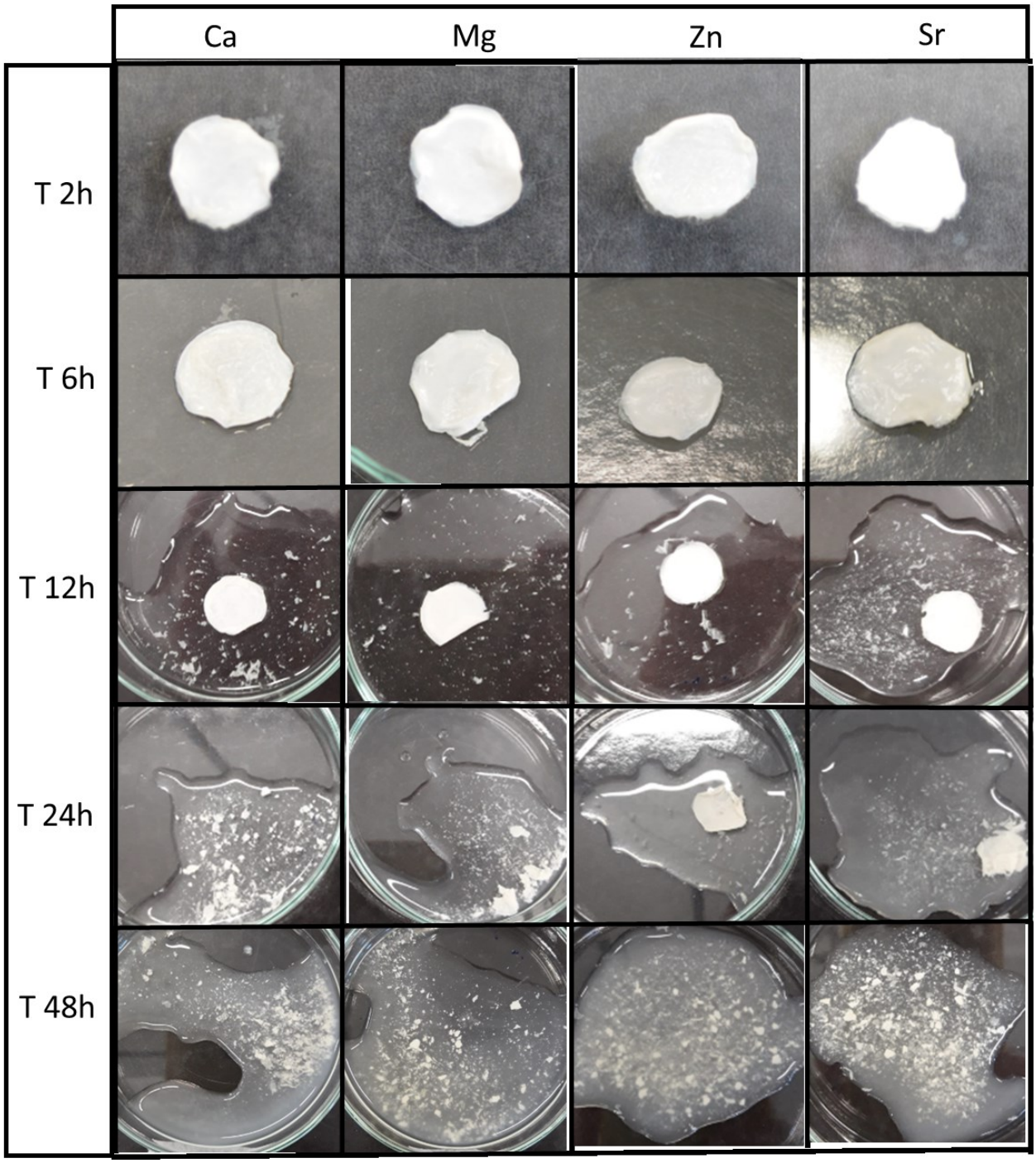

Figure 5.7: Analysis of sugar production as a function of enzymatic attack on BNC/HAp, BNC/MgHAp, BNC/ZnHAp and BNC/SrHAp biocomposites in pH 8.5 phosphate buffer as a function of time.

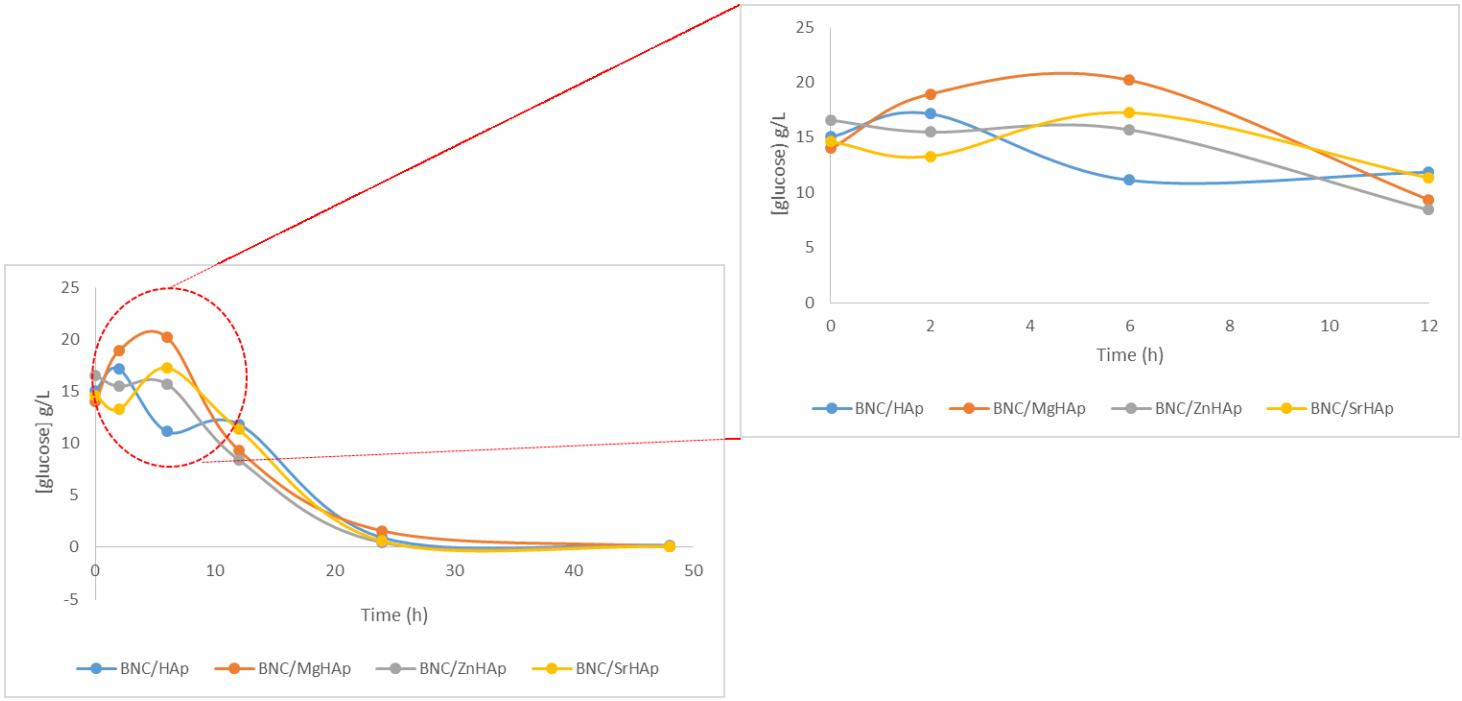

In the case of biocomposites, unlike the test with pure BNC, the variable is the addition of partially substituted apatites containing Mg^{2+}, Zn^{2+} and Sr^{2+} ions in addition to Ca^{2+} as a standard, which, when released in an aqueous solution over time may play some inhibitory property on enzyme activity.

Costa (2013), in his studies, isolated two β-glycosidases from the fungus *P. chrysogenum*. In addition to the various analyzes of enzymatic characterizations studied, the authors also analyzed the effect of different ions on the hydrolytic capacity of the enzymes. The author observed that Fe^{3+}, Pb^{+} and Ba^{2+} ions had a more substantial adverse effect on the enzymes, and to a lesser extent, Cu^{+2} > Hg^{+} > Mn^{2+} > Co^{2+} > Ca^{2+} > Zn^{2+} ions, Mg^{2+} showed inhibitory activity on only one of the two enzymes and with a similar effect to Zn^{2+}. According to the author, these ions can cause changes in the enzyme's thiol groups, which are related to the catalytic center of the enzyme and to the maintenance of its tertiary structure, which can cause the inhibition of the hydrolytic process and, in comparison with this study, may be related to with the different behaviors among the tested biocomposites.

5.3.5.1 Wide-angle X-ray Diffractometry (XRD)

Figure 5.8 shows the diffractograms of the biocomposite samples before and after 12 h of the in vitro biodegradation process. The peaks highlighted in red (2 θ ≈ 14.5° and 22.6°) are characteristic of the BNC (Casaburi et al., 2018; Predoi et al., 2019), and the peaks indicated with blue arrows are characteristic of HAp (2 θ ≈ 26°, 32°, 33° , 40°, 46° and 54°) (Nam et al., 2018; Wang et al. 2018). All are present in the non-degraded samples.

Figure 5.8: X-ray diffractograms of biocomposites after enzymatic biodegradation. Comparison of samples before and after the degradation process: A) BNC/HAp(standard); B) BNC/MgHAp; C) BNC/ZnHAp and D) BNC/SrHAp.

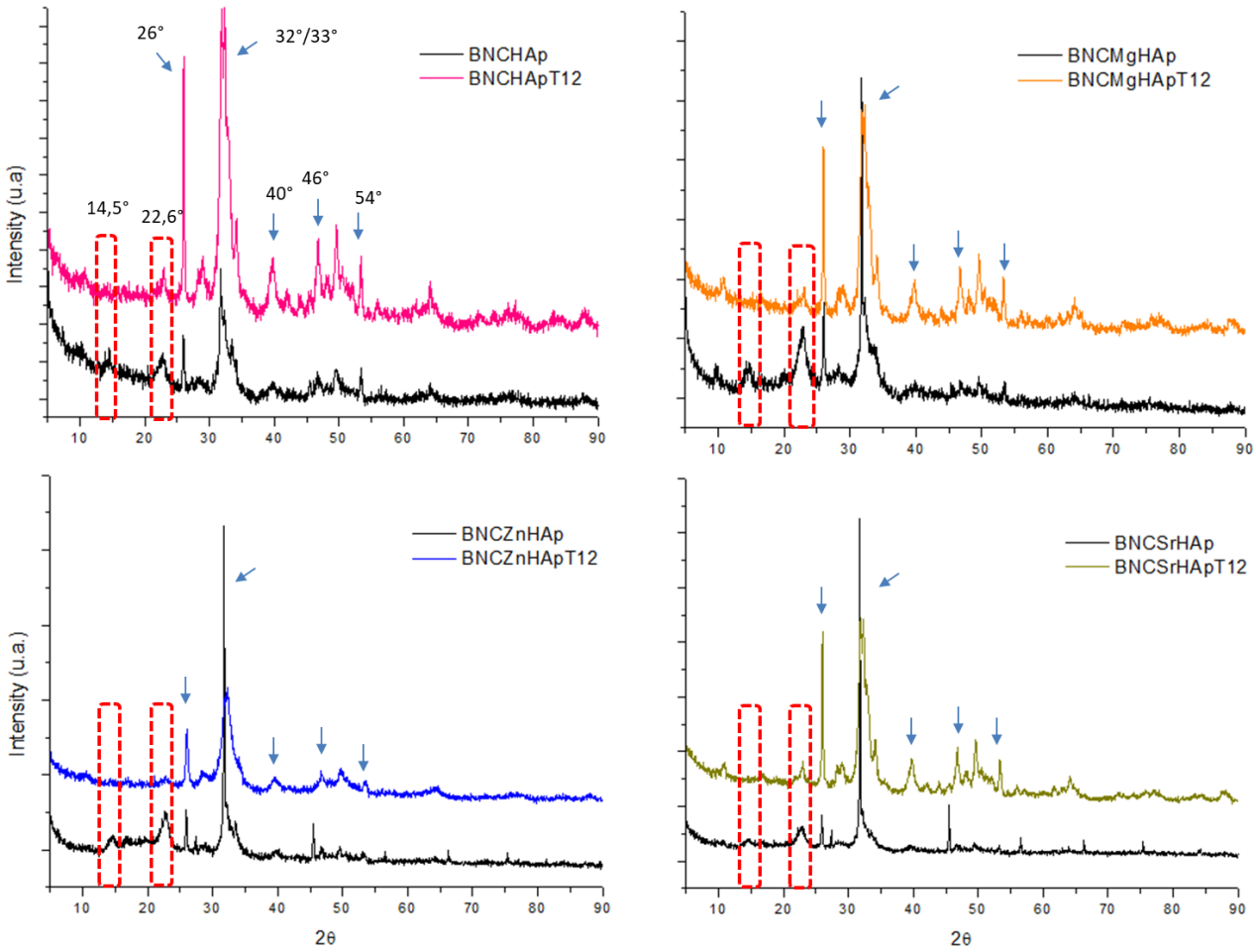

However, after the biodegradation process, the peaks referring to BNC were attenuated with different intensities for the different biocomposites. In the

BNC/HAp biocomposites, a marked attenuation is observed at the intensity of the peak 2 θ ≈ 14.5° and a subtler attenuation at the peak 2 θ ≈ 22.6°. For the other BNC/MgHAp, BNC/ZnHAp and BNC/SrHAp biocomposites, the peak of 2 θ ≈ 14.5° was not visualized. In contrast, the behavior concerning the peak at 2 θ ≈ 22.6° was quite different for the other biocomposites. For the BNC/ZnHAp sample, the attenuation was more intense, followed by the BNC/MgHAp sample and finally the BNC/SrHAp sample, which showed a very subtle attenuation, similar to what happened with BNC/HAp. It is important to highlight that according to the results presented in Figure 5.7, reducing sugar conversion also ceases after 12 h.

Wang et al. (2016) studied the in vitro biodegradation of BNC incorporated with different levels of cellulases in FBS at pH 7.4 over 24 weeks. They identified a reduction in the intensity of the characteristic peaks of BNC as soon as the cellulases were introduced; however, even after 10 weeks of biodegradation, the peak at 2 θ ≈ 22.6° could still be observed subtly. According to the authors, this occurs because the cellulose chains were broken randomly by endo-1,4-β-D-glucanase and the crystalline region gradually transformed into an amorphous region, leading to a decrease in the degree of crystallinity and the intensity of the peaks.

Calvini et al. (2006) studied the degradation of cellulose (Whatman No. 1 filter paper) by oxidation in sodium metaperiodate. The authors also observed a more significant reduction in the intensity of the peak 2 θ ≈ 14.5° and a lower intensity of the peak 2 θ ≈ 22.6° over 10 days. They concluded that metaperiodate more easily oxidizes the crystalline regions of cellulose.

Pentilä et al. (2018) studied the enzymatic hydrolysis of a cellulose-hemicellulose composite; the tests were conducted at pH 5.4 and incubated at 26 °C. The biodegradation process was followed by Small-angle X-ray scattering, among other analyses. In this study, a general intensity was also observed, attributed to the gradual conversion of the substrate into soluble sugars.

It is essential to highlight that after exposure to enzymatic biodegradation, the HAp peaks remained and were more intense. Luz et al. (2020) studied the in vitro degradation of a BNC/HAp composite using a BNC oxidized in KCl–HCl (pH 1) for 12 h. Also, they observed a decrease in the intensity of the peaks referring to the BNC and the maintenance of the peaks referring to HAp,

indicating that HAp became the dominant component in the composite. Thus, in this work, it is possible to state that HAp and metallic apatites became the predominant material of the precipitate after the enzymatic biodegradation process.

5.4 Conclusions

The cationic substitution of the biocomposites produced showed an optimized property concerning the control sample BNC/HAp, demonstrated by the significantly higher cell growth of the osteoblasts tested.

The cellulases promoted the desired hydrolytic attack even in extreme conditions such as pH 8.5, which was selected in this work as related to the alkaline phosphatase activity and, therefore, possible physiological pH found at the time of bone regeneration.

Enzymatic hydrolysis also occurred in the biocomposites, with little change compared to pure BNC, even considering the coating of BNC nanofibrils by metallic apatites, which only delayed the process by a few hours. The degradation of cellulosic material with reducing sugars formation occurred more intensely in the first 12 h for all materials. However, after this process, for the following 24 and 48 h, the biocomposites continued to undergo intense fragmentation.

These results were corroborated by the XRD analysis, which showed a reduction in the intensity of the peaks referring to BNC to an increase in the intensity of the HAp peaks, showing that this became the dominant material present in the precipitate after enzymatic biodegradation.

Finally, adding cellulases to make the biocomposite bioabsorbable proved very promising. More in-depth studies are still needed in this regard. However, the results obtained so far present an important perspective for future studies aimed at producing biomaterials with 4D characteristics.

5.5 References

AINA, V. et al. Sr-containing hydroxyapatite : morphologies of HA crystals and bioactivity on osteoblast cells. **Materials Science & Engineering C**, v. 33, n. 3, p. 1132–1142, 2013.

AL-WAFI, R. et al. Fast and easy synthesis of novel Strontium apatite nanostructured phase : structure , spectroscopy , and dielectric analysis. **Ceramics International**, v. 43, p. 17153–17159, 2017.

AN, S.-J. et al. Preparation and characterization of resorbable bacterial cellulose membranes treated by electron beam irradiation for guided bone regeneration. **International Journal of Molecular Sciences**, v. 18, n. 11, p. 2236, 25 out. 2017.

ARAÚJO, A. M. DE et al. Regenerated cellulose scaffolds : Preparation , characterization and toxicological evaluation. **Carbohydrate Polymers j**, v. 136, p. 892–898, 2016.

BALDIKOVA, E. et al. Magnetically modified bacterial cellulose : A promising carrier for immobilization of affinity ligands , enzymes , and cells. **Materials Science & Engineering C**, v. 71, p. 214–221, 2017.

BARBIERI, C. M. D. O. Efeito do fator de crescimento derivado de plaquetas humanas (PDGF) sobre o processo de regeneração óssea em tíbias de ratos. Tese (Faculdade de Ciências Farmacêuticas) UNESP - Araraquara, 2006.

BORGES, E. B. **Síntese e caracterização de hidroxiapatita dopada com metal de transição**. Niterói. Universidade Federal Fluminense, 2018.

CASABURI, A. et al. Carboxymethyl cellulose with tailored degree of substitution obtained from bacterial cellulose. **Food Hydrocoll**, v. 75, p.147–56, 2018.

CALVINI, P. et al. FTIR and WAXS analysis of periodate oxycellulose:

Evidence for a cluster mechanism of oxidation. **Vibrational Spectroscopy**, v. 40, p. 177–183, 2006.

CHITBANYONG, K.; PISUTPICHED, S.; KHANTAYANUWONG, S. TEMPO-oxidized cellulose nano fibril film from nano-structured bacterial cellulose derived

from the recently developed thermotolerant *Komagataeibacter xylinus* C30 and *Komagataeibacter oboediens*. **International Journal of Biological Macromolecules**, v. 163, p. 1908–1914, 2020.

COSTA, S. G. DA. Purificação e caracterização bioquímica de β-glicosidases de *Penicillium chrysogenum* e sua aplicação na suplementação de coquetéis enzimáticos para a hidrólise de biomassas. [Minas Gerais] Universidade Federal de Viçosa, 2013.

DA ROCHA, E. L.; PORTO, L. M.; RAMBO, C. R. Nanotechnology meets 3D in vitro models: Tissue engineered tumors and cancer therapies. **Materials Science and Engineering C**, v. 34, n. 1, p. 270–279, 2014.

ESLAMI-ARSHAGHI, T.; VAKILIAN, S.; SEYEDJAFARI, E. Primordial germ cell differentiation of nuclear transfer embryonic stem cells using surface modified electroconductive scaffolds. **In Vitro Cellular & Developmental Biology - Animal**, 2016.

HILDERBRAND, A. M. et al. Biomaterials for 4D stem cell culture. **Current Opinion in Solid State & Materials Science**, v. 20, n. 4, p. 212–224, 2016.

HOPKINS E, SANVICTORES T, SHARMA S. **Physiology, Acid Base Balance**. [Updated 2021 Sep 14]. In: StatPearls [Internet]. Treasure Island (FL): StatPearls Publishing; 2022 Jan-. Available from: https://www.ncbi.nlm.nih.gov/books/NBK507807/

LUZ, E. P. et al. *In vitro* degradability and bioactivity of oxidized bacterial cellulosehydroxyapatite composites. **Carbohydrate Polymers**, v. 237, p 116174e, 2020.

MAZORRA, M. T.; RUBIO, J. A.; BLASCO, J. Acid and alkaline phosphatase activities in the clam Scrobicularia plana : kinetic characteristics and effects of heavy metals. **Comparative Biochemistry and Physiology Part B: Biochemistry and Molecular Biology**, v. 131, p. 241–249, 2002.

MIAO, X. et al. Application and characterization of magnetic chitosan microspheres for enhanced immobilization of cellulase. **Biocatalysis and Biotransformation**, v. 34, n. 6, p. 272–282, 2016.

MILLER, G. L. Use of dinitrosalicylic acid reagent for determination of reducing

sugar. **Analytical Chemistry**, Washington, v. 31, n. 3, p. 426-428, 1959.

NAM, P. T., et al. Synthesis, characterization and antimicrobial activity of copper doped hydroxyapatite. **Vietnam Journal of Chemistry**, v. 56, n. 6, p. 672–678, 2018.

OLIVEIRA, V. A.; RAMBO, C. R.; PORTO, L. M. Production and in vitro degradation of Bacterial Cellulose tubular structures. **Polímeros**, v. 23, n. 4, p. 559–564, 2013.

PENTTILÄ, P. A. et al. Enzymatic hydrolysis of biomimetic bacterial cellulose – hemicellulose composites. **Carbohydrate Polymers**, v. 190, p. 95–102, 2018.

PEREIRA, G. N. et al. Non-thermal plasma as an innovative pretreatment technology in delignification of brewery by-product. **Innovative Food Science and Emerging Technologies**, v. 74, n. May, p. e-102827, 2021.

PÉREZ, Fernando L. Estatística Não Paramétrica. 2019. Disponível em: <http://leg.ufpr.br/~lucambio/Nonparam/Nparam.html> Acesso em 08 de maio de 2020.

PIRES, M. C. et al. Estatística não paramétrica básica no software R: uma abordagem por resolução de problemas. Universidade Federal de Minas Gerais, Minas Gerais, 2018.

PREDOI, D. et al. Synthesis, characterization, and antimicrobial activity of magnesium-doped hydroxyapatite suspensions. **Nanomaterials**, v. 9, n. 9, p. 1–20, 2019

RIBEIRO, B. F. Purificação e caracterização de celulase produzida por *Streptomyces sp* . S5 , e sua aplicação na panificação [Goiania] Universidade Federal de Goiás, 2020.

RECOUVREUX, D. O. S. et al. Novel three-dimensional cocoon-like hydrogels for soft tissue regeneration. **Materials Science and Engineering: C**, v. 31, n. 2, p. 151–157, 2011.

SANTOS, V. I. D et al. In fl uence of calcium phosphates incorporation into poly (lactic-co-glycolic acid) electrospun membranes for guided bone regeneration Vivian In e. v. 179, p. 109253 Contents, 2020.

SHI, R. et al. Current advances for bone regeneration based on tissue engineering strategies. **Front. Med.**, v. 13, n. 2, p. 160–188, 2019.

WANG, B. et al. In vitro biodegradability of bacterial cellulose by cellulase in simulated body fluid and compatibility in vivo. **Cellulose**, v. 23, n. 5, p. 3187–3198, 2016.

WANG, Q., et al. Experimental and simulation studies of strontium/zinc-codoped hydroxyapatite porous scaffolds with excellent osteoinductivity and antibacterial activity. **Applied Surface Science**, v. 462, p.118–126, 2018.

WU, J. et al. Simultaneous 3D cell distribution and bioactivity enhancement of bacterial cellulose (BC) scaffold for articular cartilage tissue engineering. **Cellulose**, v. 26, n. 4, p. 2513–2528, 2019.

ZHANG, Y. H. P.; HONG, J.; YE, X. Chapter 14 Cellulase Assays. In: MIELENZ, J. R. (Ed.). . Biofuels: Methods and Protocols, Methods in Molecular Biology. Humana Press, 2009. p. 213–231.

ZHANG, L. et al. Materials Science & Engineering C Potentials of sandwich-like chitosan / polycaprolactone / gelatin sca ff olds for guided tissue regeneration membrane. Materials Science & Engineering C, v. 109, n. February 2019, p. 110618, 2020.

6 CONCLUSIONS AND FUTURE PERSPECTIVES

The initial motivation of this work was to produce a biomaterial for a possible application for bone regeneration and, through a partial cationic substitution, to promote properties such as antimicrobial activity, non-cytotoxic with optimized osteogenic properties.

Thus, for the first materials formulated and presented in chapter 3, it was possible to conclude that the BNC membrane presented itself as a good template for incorporating metallic apatites with good porosity and hydroxyl groups available for bonding. The characterization tests confirmed the presence of phosphate sources in the analyzed biocomposites. Moreover, incorporation of Cu^{+2} in apatites promoted the desired antimicrobial action, but this element was cytotoxic at the concentrations tested.

These results produced new formulations, giving rise to the study presented in chapter 4 of this work. However, the biocomposites containing Cu^{+2} were still cytotoxic even at the new concentrations. Therefore, the efforts of this work were directed only toward the biocomposites BNC/MgAp, BNC/ZnAp and BNC/SrAp, which were considered promising as implantable materials.

As for the properties of biocomposites, in general, the new biocomposites presented structural characteristics similar to the previous ones, but, at this stage, XRD (chapter 4) and Raman (chapter 5) analyzes were proposed seeking variations in the biocomposites to indicate the presence of cations added to the biocomposites apatites, in the new formulations, however, the results were very subtle, probably due to the low concentration used.

Based on the results for all biocomposites produced and considering the best performance on metabolic activity, only the compositions BNC/MgAp 1%, BNC/ZnAp 1% and BNC/SrAp 1% were selected for subsequent assays.

The results obtained from the tests presented in chapter 5, allowed us to conclude that the proposed biocomposites presented an optimized property concerning the control sample, demonstrated by the significantly greater cell growth of the osteoblasts tested.

The enzymes promoted the desired hydrolytic attack even in the biocomposites, in which metallic apatites covered the BNC nanofibrils. The

degradation of cellulosic material with glucose formation occurred more intensely in the first 12 h for all materials. However, after this process, for the following 24 and 48 h, the biocomposites continued to undergo intense fragmentation. These results were corroborated by the XRD analysis, which showed that the HAp became the dominant material present in the precipitate after enzymatic biodegradation.

Thus, for future works, studies with different combinations of cationic substitution are suggested, in addition to deepening studies in the direction of enzymatic degradation, with different concentrations of the enzymatic solution, encapsulation of enzymes, a degradation study in a batch system fed with product withdrawals and enzyme solution pulses, seeking to simulate a behavior more similar to what happened in the organism.

However, as a scientific contribution of this thesis so far, considering the characterization results for all the compositions tested in this study, we can point out the BNC/MgHAp biocomposite as the biomaterial with the best performance as an implantable material in the bone regeneration process. In addition, although further studies are still needed, the addition of cellulases proved promising, representing an important perspective for future studies aimed at producing biomaterials with 4D characteristics.